Doctoral Dissertation

Development of Lensless Imaging Device with Hybrid Filter for Dual-color Fluorescence and Time-lapse Cell Observation

2色蛍光とタイムラプス細胞観察のための ハイブリッドフィルタ搭載レンズレス撮像デバイスの開発

Natcha Kulmala

September 2023

Division of Materials Science
Graduate School of Science and Technology
Nara Institute of Science and Technology

Abstract

Microscopy technology has been a crucial visualization tool for centuries in biological science, materials science, and other research fields. It enables visualization in different scales and has been widely used to study structure and function in biological research. Lensless imaging is an emerging technology that allows image acquisition without the use of lenses. It can compensate for the difficulties of using a conventional microscope in the matter of its bulky size, provides a wider field of view, and can be miniaturized for various applications. Fluorescence imaging has been commonly used in biological processes for visualizing fluorescent labeling molecules. However, sensitivity performance has been lower than using a conventional fluorescence microscope. The emission filter performance was insufficient to reject the excitation light. By taking advantage of the lensless features, this research proposes implementing a lensless imaging device with a hybrid filter for dual-color fluorescence and time-lapse cell observation.

This thesis proposed a lensless imaging device that employs the hybrid filter to selectively transmit the wavelengths of fluorescent targets and eliminate excitation light. The hybrid filter is assembled with an image sensor to visualize green and red fluorescence components. These fluorescent targets are excited by blue and yellow excitation lights. In the hybrid filter configuration, a fiber optic plate (FOP) was utilized to form a bandpass characteristic by attaching a longpass interference filter on the top side and a notch interference filter on the other. Then, yellow and blue absorption filters were added, respectively, to absorb the scattered components and transmit light at specific wavelengths to attain the dual-band characteristic. The arrangement of these filters was attentively considered and optimized to achieve high rejection performance for the excitation light and to avoid autofluorescence.

Furthermore, a lensless imaging device was proposed for time-lapse imaging for real-time cell observation. The proposed device was placed in the CO_2 incubator throughout the experiment to monitor the cell behavior for several hours. However, real-time cell imaging requires careful handling of cells in the appropriate conditions, as the heat generated by the imaging device can cause cell death. To solve the problem of the heat generated by the imaging device, a prototype time-lapse imaging system was demonstrated, incorporating a power control system for the imaging device.

The proposed lensless imaging device implemented with a hybrid filter for dual-color fluorescence and time-lapse systems for cell observation was demonstrated. It is possible to confirm that the proposed lensless imaging device with a hybrid filter can realize dual-color wavelength bands and can be used for time-lapse imaging in cultured cells through the consequence evaluation and experiment results described in the thesis.

Acknowledgment

I would like to express my heartfelt gratitude and appreciation to the individuals who have played an important role in successfully completing my research and thesis. Their support, guidance, and contributions have been helpful throughout this journey, and I sincerely thank each of them.

First and foremost, I would like to express my deep gratitude to Professor Jun Ohta for his belief in my abilities and the opportunity he provided me to continuously pursue my doctoral degree at Nara Institute of Science and Technology. His support, guidance, and advice have significantly contributed to my academic and personal development. Besides, I extend my gratitude to his wife, Dr. Yasumi Ohta, for her carefulness and always cheering me up. I also sincerely appreciate her support. These things have been genuinely respectable.

My sincere thanks to my supervisor and committee members, Professor Yoichiroh Hosokawa and Professor Hiroharu Ajiro, who provided their expertise and insightful suggestions during the various stages of this research. Their valuable feedback and constructive criticism have significantly enhanced the quality of this work. I am especially grateful to Associate Professor Kiyotaka Sasagawa for his invaluable contributions to this research. With his guidance, I have been able to overstep my limitations and strive for continuous improvement.

I would like to thank you for the mentorship provided by Associate Professor Hiroyuki Tashiro, Assistant Professor Makito Haruta, and Assistant Professor Hironari Takehara. Their extensive knowledge and constructive feedback have been invaluable in identifying areas for improvement and enhancing the quality of my research. I am extending my appreciation for the caring support from Mrs. Ryoko Fukuzawa and all laboratory members.

My heartfelt thanks go to my beloved family, who have been my greatest supporters since the very beginning and hold a special place in my life. Their support has been important in my journey. Their encouragement and loving care have shaped me into the person I am today, enabling me to face challenges and pursue my dreams with pride.

I am also thankful to Barbara, Izzat, Putter, Pai, my batchmate Latiful, and all my labmates for their support during difficult moments in my research. I am truly grateful for our friendship and look forward to more fruitful collaborations.

Special thanks to Risa Sato, Thanaree Treepetchkul (Yves), and Joshua Olorocisimo, my sisters and brother-in-crime, for always being by my side, ready to listen and share joyful moments together. Thanks a million to Shintaro Yokoyama, your friendship means the world to me, and I am forever thankful for the amazing times and support we shared. I treasure the moments we spent together.

Lastly, I wholeheartedly thank my loveliest boyfriend, Bunyapon Usawalertkamol, for his boundless love, patience, and support. Our journey together has been an extraordinary adventure of growth and learning. I am grateful for always believing in me. Our bond fills my heart with joy and gratitude.

Dedication

To myself, my beloved family, and all who contributed to my research, your unwavering support and guidance have been invaluable. This dissertation is a witness to our collective efforts and the profound impact you have had on my journey. お疲れ様でした。

In loving memory of my dearest mom, this dedication is a heartfelt tribute. Her presence is deeply missed and continues to resonate in my journey, and her love will forever reside within my heart.

Contents

List of Figures

List of Tables

Chapter 1

Introduction

1.1 Microscopy Technology in Biological Research

Microscopy technology has been a crucial visualization tool for centuries in biological science, materials science, and other research fields. It enables visualization in different scales, from individual cells and molecules to whole organisms. Thus, it has been widely used to study structure and function in biological research; cell biology is a branch of the biological discipline that studies cell structure, function, and behavior. Since the cell is the basic unit of all living organisms, it is essential to understand the properties of cells intensively [1]. There are various techniques have been improved to be able to see details and activities within cells. For example, fluorescence microscopy can be used to see the interaction of proteins or other molecules within cells, time-lapse microscopy can be used to track the movement and differentiation of cells, and optogenetics can be used to study the activity of neurons [2]–[4].

Many types of microscopes have been developed to study and operate biological processes, for example, light, electron, confocal, super-resolution, and lensless microscopes, each with advantages and limitations [2], [5], [6]. As microscope technology has progressed, there have been various technical difficulties that need to be resolved to continue making further improvements.

This thesis focuses on the miniaturized microscope utilizing a lensless imaging technique. As it has an advantage in terms of compactness, it is suitable for the experiment in limited areas of observation, such as visualizing cultured cells for an extended period in an incubator.

1.2 Miniaturized Microscopy

Miniaturized microscopy refers to the development of compact and portable imaging systems that enable high-resolution visualization of biological samples in a smaller form factor compared to conventional microscopy setups. These miniaturized devices offer several advantages, such as improved accessibility, point-of-care diagnostics, and *in vivo* imaging in hard-to-reach areas [7]–[12]. Various approaches have been explored to achieve miniaturization, including using microelectromechanical systems (MEMS) technology, fiber optics, and integrated optics. MEMS-based microscopes utilize tiny scanning mirrors or microlenses to capture and manipulate light, enabling high-resolution imaging in a compact design [13]–[15]. On the other hand, fiber optic probes utilize optical fibers to deliver and collect light from the sample, allowing for minimally invasive imaging [16]–[18]. Integration of optics combines multiple optical components, such as lenses, waveguides, and detectors, onto a single chip, reducing the size and complexity of the microscope. These miniaturized microscopy techniques have found applications in various fields, including biomedical research, and clinical diagnostics, enabling portable and point-of-care imaging solutions.

This approach has emerged as a powerful tool for cell observation [19], [20] and provides several advantages, including increased portability, reduced sample preparation requirements, and real-time monitoring capabilities [21]. These compact devices can provide detailed information about cellular dynamics non-invasively by integrating advanced optics, miniaturized light sources, and sensitive detectors. One example is enabling real-time cultured cell observation within the incubator, as shown in Figure 1. Therefore, this technique was considered to be used for this research for the purpose of time-lapse cell observation, more than others.

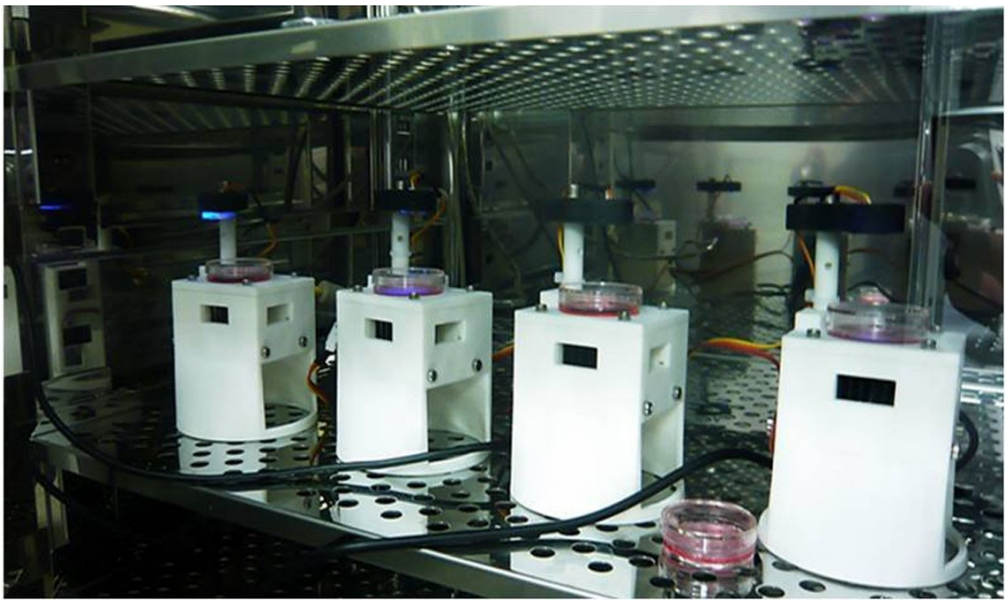

Figure 1 Lensfree video microscopes inside the standard incubator [21].

1.2.1 Lensless Microscopy

Lensless microscopy is an emerging technology that enables image acquisition without the use of lenses [10]. Instead of traditional optics, it utilizes image sensors, such as charge-couple devices (CCDs) or complementary metal-oxide semiconductors (CMOS) sensor arrays, combined with multiple measurements to obtain image information sufficiently. Lensless microscopy provides a wider field of view and can be miniaturized for various applications, including implantable and wearable devices, photography, and microscopy [22]–[24]. Integrating the lensless system with the advances in computational algorithms to reconstruct the images expands the possibilities to apply them to biological studies [25]. These applications include diagnostic tests and the real-time observation of cells, along with others, in addition to different imaging techniques, such as shadow imaging, holographic imaging, time-resolved imaging, and fluorescence imaging [26]–[36].

1.3 Fluorescence Microscopy

Fluorescence microscopy is an imaging technique that images fluorescent objects of interest contrasted to a black (or very dark) background. Fundamentals of excitation and emission of light by fluorescent molecules allow us to envision different cellular, subcellular, or molecular components [2].

1.3.1 Principle of Fluorescence Microscope

The main components of the fluorescence microscope consist of a powerful light source, a set of filter elements, objective lenses, and a detector. These components work together to enable the visualization of fluorescent samples. Figure 2 shows a schematic of the working principle of the fluorescence microscope. The role of each component is listed here:

- **Light Source:** A fluorescence microscope requires a powerful light source to excite the fluorescent samples. Typical light sources include mercury or xenon arc lamps, LEDs (light-emitting diodes), or lasers emitted light directly toward the sample.
- **Filter Elements:** A fluorescence microscope employs a set of filter elements (filter cube), including (i) An excitation filter to filter out unwanted wavelengths from the light source and to selectively transmit the excitation wavelength of the fluorescent sample. (ii) A dichroic mirror (beam splitter) to reflect light at the desired excitation wavelength toward fluorescent samples and transmit the emission wavelength from fluorescent samples towards a detector. This filter is set at 45 degrees between excitation and emission filters. (iii) An emission filter to filter out the excitation wavelength and transmit only the emission wavelength of the fluorescent samples.

- **Objective Lenses:** The objective lenses condense the light into a narrow beam on the sample and help to focus the emitted light from the fluorescent samples towards the detector.
- **Detector:** A detector is employed to capture and record the image of fluorescent samples. Typically, photomultiplier tubes (PMTs), avalanche photodiodes (APDs), charge-couple devices (CCDs), or complementary metal-oxide semiconductors (CMOS) are used as optical detectors[37].

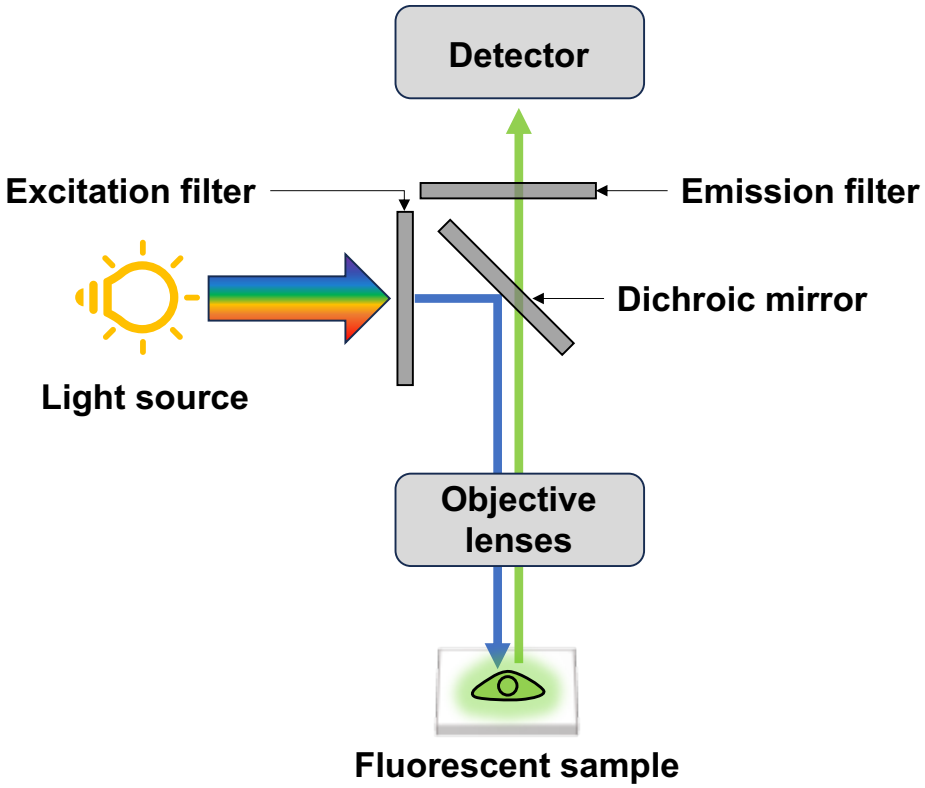

Figure 2 Schematic of the working principle of the fluorescence microscope.

Fluorescent samples are labeled with fluorescent molecules, also called fluorescent dyes, fluorophores, or fluorochromes, where molecules absorb light at a specific wavelength. The electrons are excited from the lower (ground state) to the higher energy level (excited state). Then,

the absorbed electrons lose their energy through processes called internal conversion and vibrational relaxation back to the ground state and release energy in the form of emitted light at longer wavelengths than the absorbed energy, resulting in a color shift [38]. A simple electronic state diagram of the fluorescence process is shown in Figure 3. The fluorescent samples are commonly stained using specific antibodies and chemical reagents or genetically labeled with fluorescent proteins (FPs) [39]. This phenomenon of luminescence plays a crucial role in fluorescence microscopy, enabling the precise labeling and detection of cellular structures and molecules in various scientific applications.

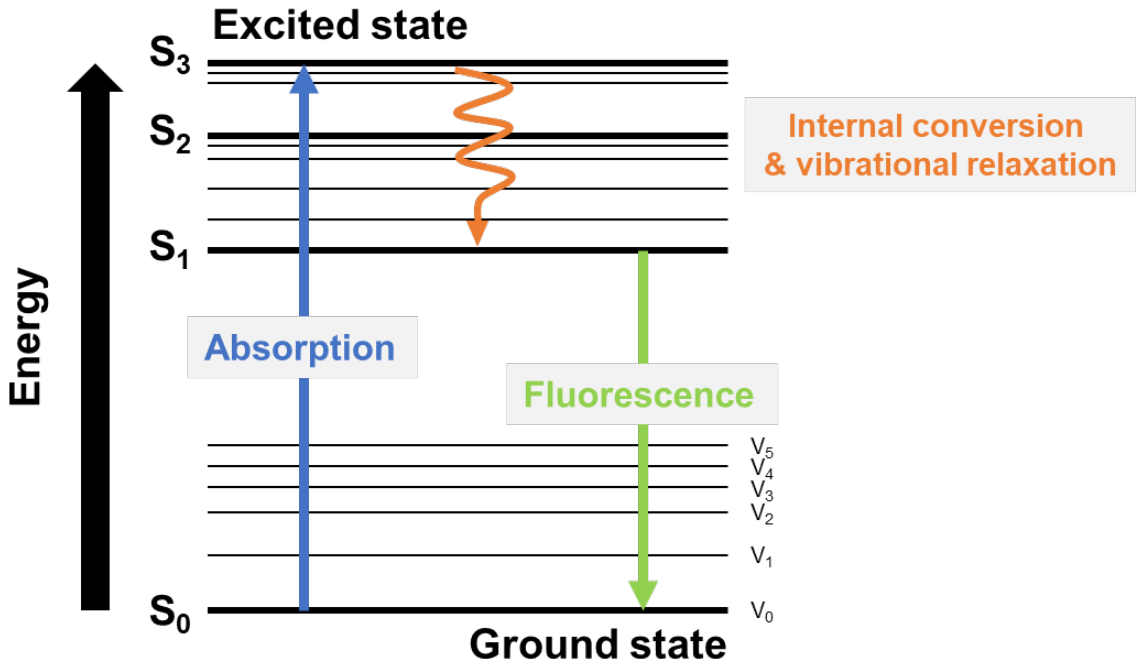

Figure 3 Simple electronic state diagram of the fluorescence process (Jablonski diagram).

Fluorescence microscopy offers advantages, including high sensitivity and specificity, which make it a powerful visualization tool in the field of biology for investigating various biological processes, biomedical science, as well as materials science.

1.2.2 Autofluorescence

Autofluorescence in fluorescence imaging refers to the inherent fluorescence emitted by biological samples or imaging components without the addition of exogenous fluorophores. It occurs from endogenous fluorophores, such as collagen, elastin, NADH, FAD, and lipofuscin, naturally occurring in biological tissues [40], [41]. Autofluorescence can provide valuable information about tissue composition and metabolic processes [42], but it can also interfere with the detection of specific fluorophores, leading to reduced sensitivity and specificity [43], [44]. To address the limitations of autofluorescence, various techniques have been employed, such as spectral unmixing methods [45], [46], specific emission filters to filter out autofluorescent wavelengths [47], treatment with chemicals (Figure 4) [46], [48]–[50], and the selection of fluorophores with distinct emission spectra. Advanced imaging modalities such as time-resolved fluorescence microscopy (FLIM) and multiphoton microscopy can further enhance contrast and specificity by exploiting differences in fluorescence lifetimes and excitation processes [51]–[54]. The precision and sensitivity of fluorescence imaging can be improved by understanding and careful control of autofluorescence.

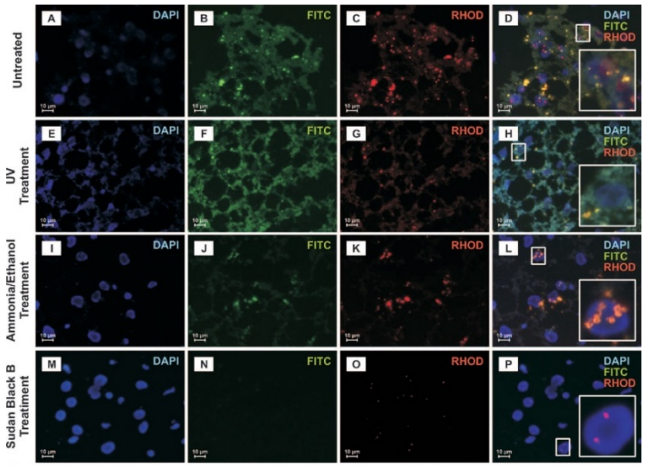

Figure 4 Histochemical treatments for controlling tissue autofluorescence [50].

1.4 Research Purpose

This research aims to implement a lensless microscopy platform combined with a hybrid emission filter for fluorescence imaging, which is the most commonly used technique for visualizing living cells. Therefore, the hybrid emission filter is proposed to improve imaging efficiency and utilize the advantages of interference and absorption filters with a fiber optic plate (FOP) for dual-color fluorescent detection, while excitation light is greatly rejected. The proposed hybrid filter mounted with a CMOS image sensor is used to detect red and green fluorescence simultaneously.

By taking advantage of the lensless features, this research proposes a time-lapse system for live-cell imaging that can be placed inside the incubator to monitor the living cells for extended periods. Live-cell imaging requires careful handling of cells in the appropriate conditions, as the heat generated by the imaging device can cause cell death. Therefore, a power control system for the imaging device is necessary.

1.5 Thesis Overview

This thesis is divided into five chapters. The entire substance of this thesis is briefly explained in this section.

Chapter 1: *Introduction*

This chapter presents a brief research background, including the significance of microscopy technology in biological research. This thesis focuses on miniaturized microscopy by implementing lensless microscopy with a fluorescence imaging technique.

The fundamental principle of fluorescence microscopy is provided in this chapter. Then, the research purpose is described and provides an overview of this thesis.

Chapter 2: *Lensless Imaging System for Fluorescence Imaging*

This chapter provides the fundamental concepts, followed by the advantages and limitations of lensless imaging systems. This chapter also provides the applications of lensless imaging systems that can be used for biological process studies and reviews the issues in lensless imaging systems used for fluorescence imaging. In addition, the basis of emission filters used in fluorescence microscopy includes interference and absorption filter. The shortcoming of using each filter is also stated. Then, an introduction to a principal structure of a hybrid emission filter is described in this chapter, which is the solution to compensate for the shortcoming of each filter.

Chapter 3: *Hybrid Filter for Lensless Dual-color Fluorescence Imaging*

This chapter focuses on a hybrid filter for lensless dual-color fluorescence imaging. This chapter describes the criteria for hybrid filter configuration. The results of the filter evaluation were discussed to determine the proposed hybrid filter structure. Then, filter preparation and device assembly processes are illustrated. Then, the device evaluation and experimental results are shown here to confirm that the proposed device is able to use for dual-color fluorescence imaging.

Chapter 4: *Time-lapse Live-cell Imaging System for Lensless Device*

The problem statement and purpose of using the proposed lensless imaging device for time-lapse cell observation are introduced in this chapter. The time-lapse system overview is demonstrated to solve the problem of using a lensless imaging device for live-cell

observation. Then, device evaluation results are shown, including temperature measurement and time-lapse bright-field imaging.

Chapter 5: *Conclusion and Future Prospects*

Lastly, the conclusion of all the experimental results is done. This chapter also provides the future prospects for advancing the development of the lensless imaging device.

Chapter 2

Lensless Imaging System for Fluorescence Imaging

2.1 Lensless Imaging System

Lensless imaging is an imaging technique that eliminates the need for lenses, offering various advantages over traditional lens-based microscopes. Lens-based microscopes are excellent in achieving high performance but often require a large field of view and high spatial resolution. However, recent advancements in image sensors and computers have gained popularity due to their ability to downsize instruments, create highly portable devices, and provide a wide field of view.

Although lensless imaging system has seen significant progress in bright-field observation, there has been limited research on fluorescence observation. It can be attributed to two factors: the lack of filters capable of achieving high rejection of excitation light in a lensless configuration and the challenge of achieving high spatial resolution in fluorescence imaging. To address these limitations, K. Sasagawa *et al.* [3] proposed a high-performance filter specifically designed for lensless devices, enabling the observation of cells expressing fluorescent proteins. However, the challenge of multicolor observation using multiple labels in fluorescence imaging remains a significant obstacle that needs to be overcome.

2.1.1 Advantages of Lensless Imaging System

The advantages of lensless imaging systems provide a wide range of applications, including flexibility, cost-efficiency, and imaging improvement capabilities. Here, some detailed advantages of a lensless imaging system are listed below:

- **Compactness:** Lensless imaging systems eliminate the need for bulky lenses, making them more compact and lightweight than conventional imaging systems. This advantage is particularly beneficial for portable or field applications with crucial size and weight constraints. In addition, due to its compactness, lensless imaging systems have the potential for integration into small-scale devices and microsystems. This advantage opens up possibilities for applications in areas such as biomedical imaging, endoscopy, and wearable technology[22], [23], [55].

- **Cost-effectiveness:** Fewer components are typically required in lensless systems and have simpler optical setups compared to lens-based systems. This simplicity can lead to cost-effectiveness in terms of manufacturing, maintenance, and potential scalability for mass production [56], [57].

- **Wide field of view:** It often provides a wide field of view in a lensless system, allowing for capturing larger areas or samples in a single image. This advantage is beneficial for applications such as cellular imaging, where a broader perspective is desired [29], [30], [58].

- **Scalable resolution:** High-resolution imaging can be achieved by implementing computational algorithms and image reconstruction techniques. This scalability in

resolution allows for the capture of fine details and facilitates image analysis in various fields, including biology, materials science, and remote sensing [59].

2.1.2 Limitations of Lensless Imaging System

In this section, some of the limitations of lensless imaging systems are noted. However, the extension of these limitations can vary depending on the specific implementation, design, and techniques.

- **Image quality:** The limitation of lensless imaging systems is achieving high image quality as conventional lens-based systems. This limitation happens due to the absence of a physical lens that can precisely focus light onto the image sensor. As a result, lensless imaging systems may suffer from reduced spatial resolution and lower image contrast, leading to a loss of fine details and potentially impacting image analysis and evaluation accuracy [60], [61].
- **Light collection:** Generally, imaging systems rely on the interaction of light with a detector to capture images. However, due to the absence of lenses, these systems often have limitations in light collection efficiency. Without lenses to convey light onto the sensor, lensless imaging systems may struggle to gather light appropriately. This limitation can result in decreased sensitivity and increased noise in captured images [58], [62]–[65].
- **Computational complexity:** A lensless system utilizes a computational algorithm for image reconstruction and enhancement. Computational complexity, particularly in cases where large amounts of data need to be processed in real-time or high-speed imaging applications. The computational complexity can result in longer processing

times, making it challenging to achieve real-time imaging or perform high-throughput analysis. Additionally, the need for complex algorithms and extensive computational resources can limit the scalability and practicality of lensless imaging systems in some applications [66]–[68].

- **Poor performance in fluorescence imaging:** In bright-field observation, the incident light scatters when interacting with the observed object, resulting in holographic images generated when light with high coherence is used. These holographic images contain valuable optical phase information, allowing for the reconstruction of high-resolution images through computational methods [69]. However, in fluorescence observation, the emitted light from individual points of interest lacks phase correlation. Consequently, it is impossible to reconstruct the image using image processing techniques as in bright-field observation. Additionally, there is a problem with the poor performance of the emission filter to eliminate the excitation light effectively [3].

2.2 CMOS Image Sensor

The sensor is a key component of the lensless imaging system, working as a fundamental physical structure. It plays a vital role in converting light into an electrical signal for storage, analysis, or visualization purposes. Based on their structure, image sensors can be categorized into two main types: charge-coupled devices (CCD) and complementary metal-oxide-semiconductor (CMOS) sensors. Compared to the first notable CCDs, CMOS sensors have introduced several advancements that offer significant advantages. One notable advantage is the capability to integrate sensing, analog, and digital processing at the pixel level. This integration brings benefits such as reduced power consumption, lower cost, and the ability to integrate multiple functionalities

on a single chip. These features make CMOS sensors highly attractive for various applications, as they offer enhanced performance, cost-effectiveness, and increased integration possibilities [70], [71]. Thus, a CMOS sensor is considered to use as an imaging device for this research.

2.2.1 Color of CMOS Image Sensor

Visible light sensors can be categorized into two main types: monochrome and color sensors. Monochrome sensors are designed to capture all incoming light at each pixel, regardless of color. It means that every pixel is sensitive to the entire spectrum of visible wavelengths. On the other hand, color sensors employ an additional filter layer known as a "color filter array" (CFA), which is positioned between the microlenses and photodiodes. Among the various CFAs available, the Bayer pattern is widely used, featuring alternating red, green, and blue filters arranged in columns and rows [72].

Each color pixel in the sensor responds to a specific wavelength, segregating the incoming light into different colors. For instance, if red or blue light strikes a green pixel, it is reflected and not recorded. The working principle of a color CMOS image sensor is depicted in Figure 5. However, in fluorescence observation applications, the performance of color filters often needs to improve in effectively reducing the excitation light.

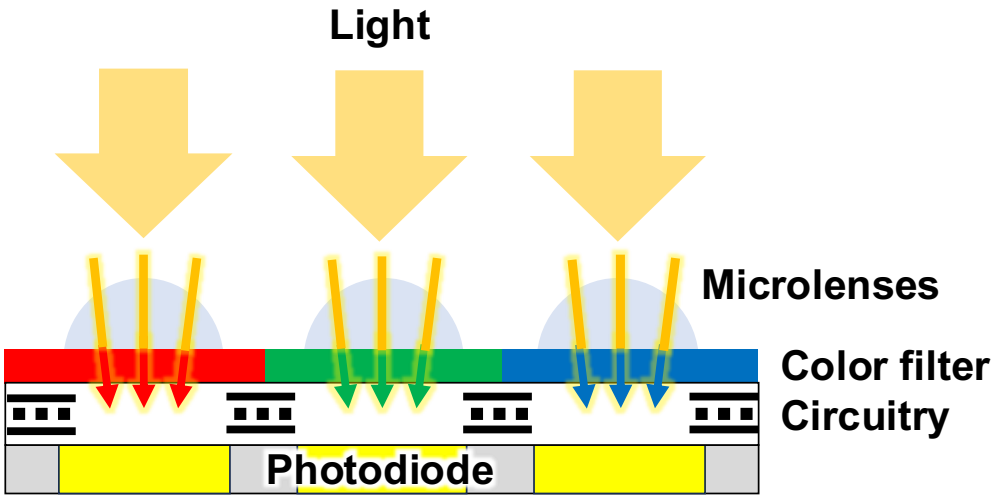

Figure 5 Illustration of the working principle of a color sensor.

2.3 Emission Filter for Lensless Imaging System

An emission filter is an optical component used to selectively transmit light emitted within specific wavelengths range while efficiently cutting off or attenuating unwanted wavelengths. Its primary function is eliminating unwanted signals, including excitation light and background noise, to transmit the desired fluorescence emission [30], [73].

Typically, fluorescence microscopy employs two types of emission filters: an interference filter and an absorption filter. Interference filters are based on the refractive indices of dielectric materials, enabling them to selectively reflect unwanted wavelengths and transmit desired wavelengths. Instead, absorption filters employ pigments or dyes to selectively absorb and transmit specific wavelengths of light [3], [73], [74]

In a conventional fluorescence microscope, the filter cubes typically consist of interference filters and beam splitter, enabling precise fluorescence detection. However, it is impossible to utilize them for a lensless imaging system for fluorescent signal detection. The fluorescence

intensity of the target is typically weak compared to the excitation light, often by orders of magnitude weaker than the excitation light [75]. As a result, it is difficult to reject the excitation light and precisely capture specific emission wavelengths. The emission filter is placed between the sample and the sensor in the lensless imaging system. Thus, an appropriate emission filter configuration is required for the lensless imaging system to achieve optimal performance and detect fluorescent signals precisely.

2.3.1 Interference Filter

Interference filters are based on a component of the refractive indices of two dielectric materials layers to transmit desired wavelengths while reflecting unwanted wavelengths selectively. These alternating layers of high and low refractive index media are precisely controlled in terms of their thickness. At the boundaries between materials with different refractive indices, Fresnel reflection occurs so that some are reflected and the rest is transmitted. The transmitted component is also partially reflected back at the boundary between the next layer and the next layer. These interactions determine the wavelengths to be reflected or transmitted. Figure 6 shows a schematic of the reflection and transmission by interference filters. The interference filter offers a steep transition of transmittance characteristics between rejected and transmitted wavelengths, as shown in Figure 7. In addition, almost no autofluorescence is emitted from the interference filter since incident light is reflected in the rejection band. Since the wavelength is determined by the refractive index and film thickness, there is a high degree of design freedom. Wavelength selectivity can also be increased by increasing the number of layers.

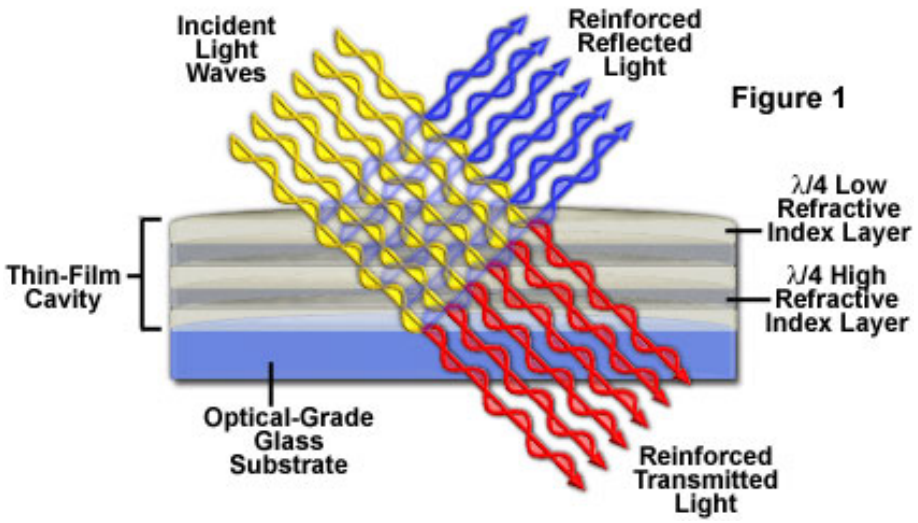

Figure 6 Reflection and transmission by interference filters.
[https://www.olympus-lifescience.com/en/microscope-resource/primer/java/filters/interference/]

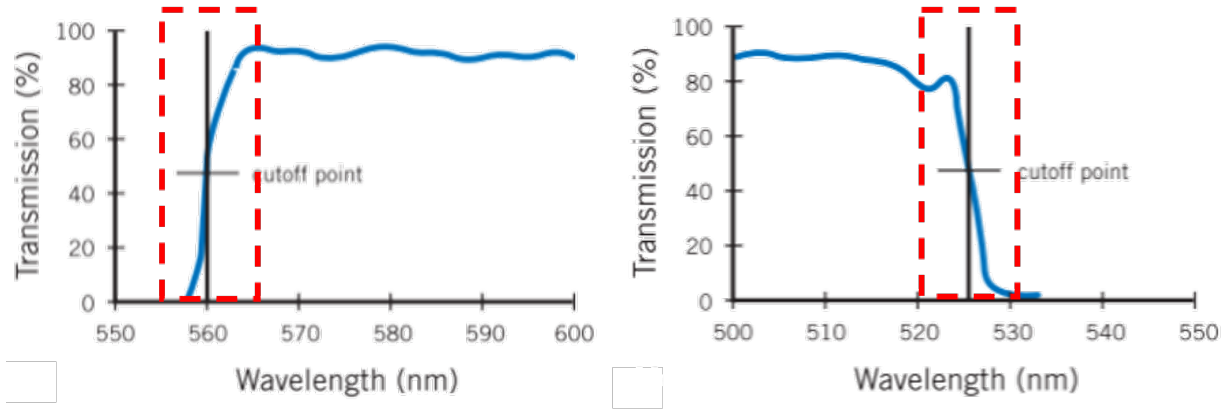

Figure 7 Transmittance characteristics of interference filter [74].

However, the interference filter's spectral characteristic is angle-dependent because the light path length in each layer depends on the incident angle, and the design of the filter is usually optimized to be used at 0 degrees angle of incidence (called normal incidence). As the angle of incident light increases, the spectral characteristic shifts towards shorter wavelengths, as shown in Figure 8. This phenomenon is referred to as “Blue-shifted” [76].

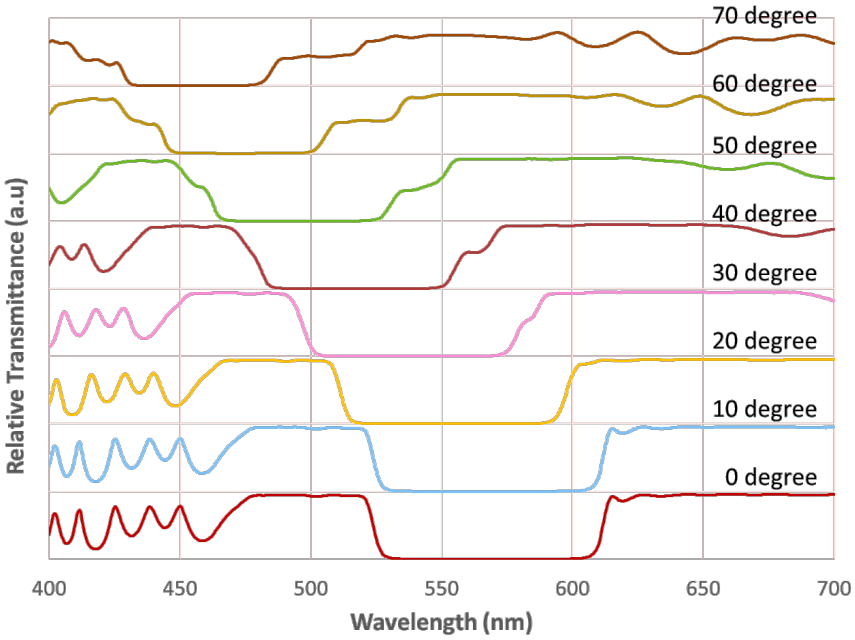

Figure 8 Spectral characteristics of the interference filter shift towards shorter wavelengths.

The excitation light is scattered by the object in different directions when the excitation light illuminates it. In a lens-based microscope, the optical system allows scattered light to enter the emission filter in a normal direction. However, in the lensless imaging setup, the observation target is directly placed on the filter. Although the scattered light is relatively small compared to the entire incident light, it cannot be ignored, especially when observing fluorescent or bioluminescent targets. It causes a significant reduction in fluorescence observation performance. A schematic diagram of the problems with interference filters in a lensless system is shown in Figure 9. Even if the excitation light is incident perpendicularly, light scattering occurs depending on the object to be observed, causing a component to be transmitted through the filter.

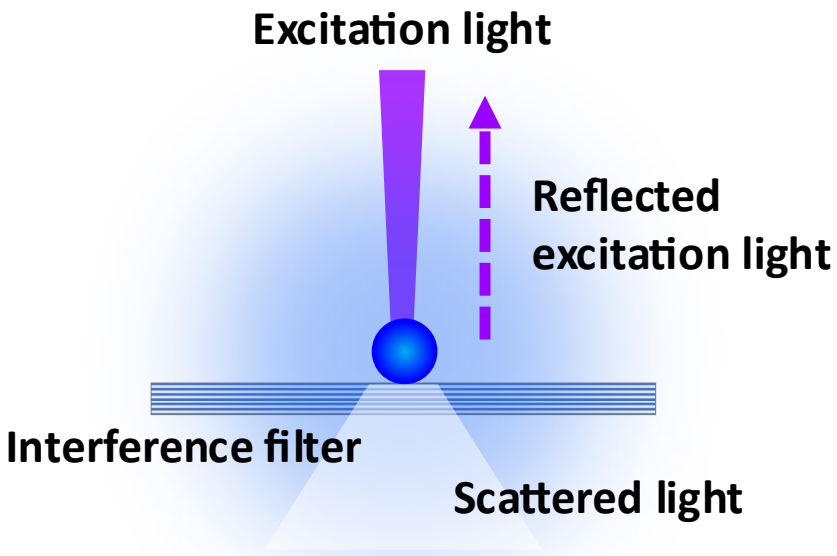

Figure 9 Schematic diagram of the problems with interference filters in a lensless system.

2.3.2 Absorption Filter

Absorption filters include pigment or dyes selectively absorbing undesired wavelengths of light [3]. The absorption filter offers the advantages of inexpensiveness, stability under normal conditions, and angle independence; the filter effectively reduces scattered light from the observation target and minimizes reflections. However, it has slope transition of transmittance characteristics between rejected and transmitted wavelengths and often low peak transmittance, as shown in Figure 10.

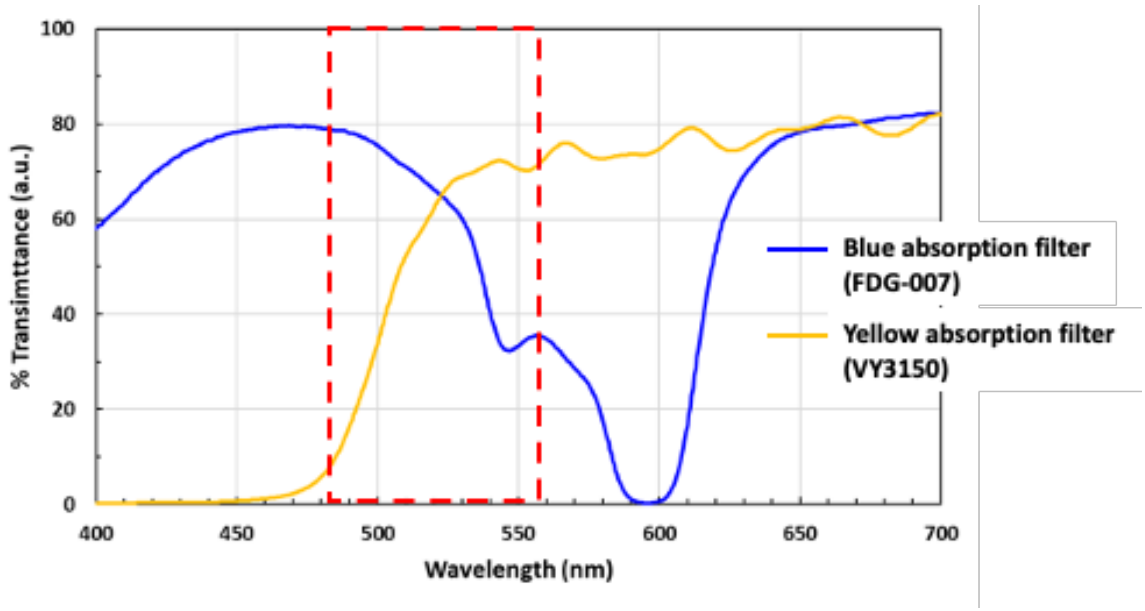

Figure 10 Transmittance characteristics of absorption filter.

In addition, the spectral performance depends on the filter's physical thickness. The blocking capability is increased by increasing the thickness but also decreases the peak transmittance within the desired wavelength range. Thus, an optimum thickness must be determined. Transmittance (T) refers to the proportion of incident light that successfully passes through a substance and passes through the other side. It is defined as

$$T = \frac{I}{I_o} = \exp(-\alpha L)$$

where I = transmitted light and I_o = incident light, %T is merely $\frac{I}{I_o} \times 100$

α is an absorption coefficient,

and L is the effective light path length (referred to as filter thickness) [3]

Even with this theory, designing a lensless imaging device with good performance is difficult. The absorption of excitation light indeed increases with thickness. However, it is

necessary to consider what happens to the absorbed energy afterward. Part of it is often converted back into light as autofluorescence. Unfortunately, this often coincides with the wavelength of the fluorescence being observed.

Additionally, the absorption filter may exhibit autofluorescence, which can be as strong as or even stronger than the emitted fluorescence signal, making it challenging to detect the target signal accurately. In a lens-based microscopy system, the issue can be avoided by creating a physical separation between the image sensor surface and the location in which the image is formed. However, in a lensless imaging system, the observation target is placed in close proximity to the filter, making it challenging to distinguish between the fluorescence of the target and the autofluorescence of the filter.

2.3.3 Hybrid Emission Filter

A crucial aspect of the fluorescence imaging technique relies on fluorescence labeling. It is important to consider the sensitivity of the imaging device because the luminescence intensity is typically weaker than the excitation light. Conventionally, lens-based fluorescence microscopy implements an emission filter consisting of interference and absorption filters to eliminate unwanted background light and allow only desired wavelengths to reach the detector. However, in a lensless fluorescence imaging system, the utilization of an interference filter is compromised due to the angle dependence of its spectral characteristics. Since any lens elements are not used to convey the light in the lensless imaging system, the observation target scatters the excitation light, causing it to be incident on the filter from different angles. The transmittance spectrum shifts with the angle of incidence and allows the scattered component to pass through the filter due to the angle-dependent spectral characteristics of the interference filter. The significant difference in

intensity between the scattered light and the target fluorescence signals negatively impacts the quality of fluorescence observation and performance. Even though the interference filter can reject normal incident light entirely, its efficiency is compromised in a lensless setup due to the angle dependence of spectral characteristics, and it impacts the results of fluorescence observation. An alternative solution is using an absorption filter, which exhibits angle-independent transmission characteristics. However, the emission of autofluorescence from this filter remains a concern, which indicates that the current filter options need to be improved for lensless fluorescence imaging systems.

A hybrid emission filter is demonstrated by combining the advantages and compensating for the disadvantages of interference and absorption filters to attain high performance. Figure 11 illustrates the schematic of the principal structure of a hybrid emission filter employing a fiber optic plate (FOP). The arrangement of the interference filter and absorption filter is important. If the excitation light enters the absorption filter first, it is converted to autofluorescence. Therefore, it is necessary to first reflect most of the power of the incident light by the interference filter.

For the fabrication of a thin absorption filter, it is practical to utilize a resin with a high concentration of dye or pigment. However, the use of a soft resin substrate is unsuitable for achieving high performance for the interference filter because it exhibits limited heat resistance. Consequently, a hybrid filter configuration is formed by sandwiching the interference filter and the absorption filter between two sides of a high-resolution FOP.

The FOP, consisting of a bundle of micro-optical fibers, enables the direct propagation of light from the input to the output surface, coupled with the inclusion of an absorber glass to capture any light leakage from the fiber bundle. The use of the FOP as the substrate for the hybrid filter

ensures the preservation of spatial resolution, while the need to consider focal length in the design is unnecessary.

The interference filter is placed on the uppermost side of the FOP to efficiently attenuate the excitation light intensity at a normal angle of incidence to an extremely low level. On the other hand, the absorption filter is placed on the lower side, to absorb the remaining excitation light that passes through the interference filter and any scattered excitation light. Consequently, the absorption filter effectively reduces autofluorescence because the intensity of excitation light is powerless. Additionally, the complexity of the hybrid emission filter can be enhanced by incorporating additional layers of interference and absorption filters, depending on the specific observation target and application requirements.

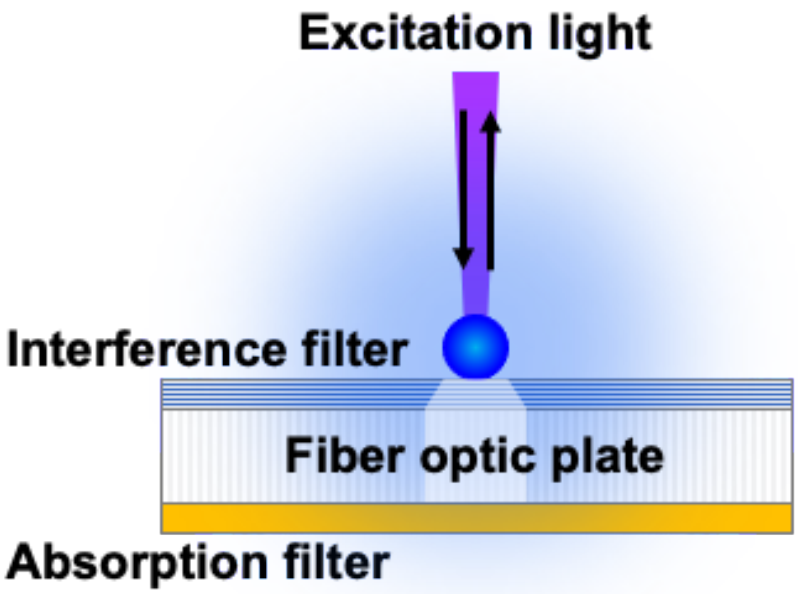

Figure 11 Schematic of the principal structure of a hybrid emission filter.

Figure 12 compared the observation results of a fluorescent sample when an interference filter, an absorption filter, and a hybrid filter were mounted on the lensless device. The edges of the pattern appear brighter when only the interference filter is used. This suggests that the oblique incidence component transmitted through the interference filter is generated by light scattering. In the case of the absorption filter, the angle of incidence problem is not an issue, and a pattern similar to that observed with the fluorescence microscope can be seen. However, the contrast is low because the autofluorescence exhibited itself. In contrast, the hybrid filter has improved the contrast of the image.

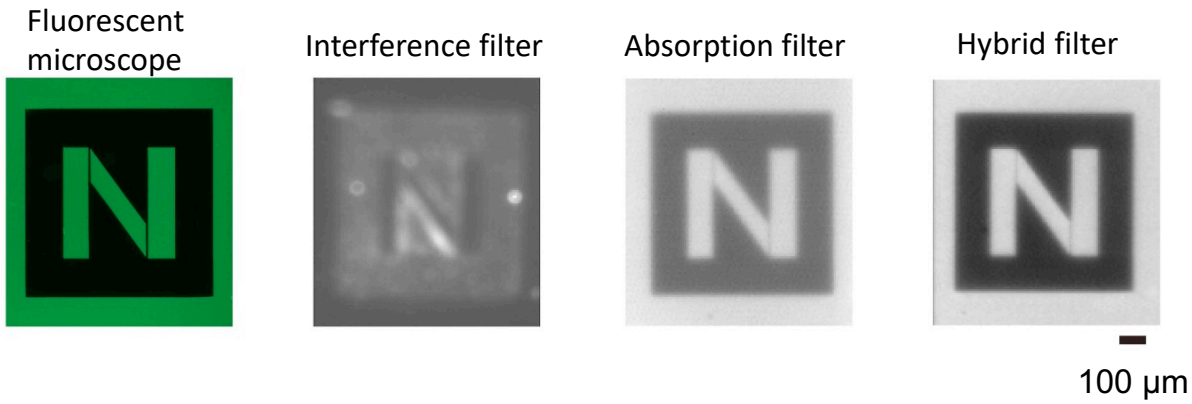

Figure 12 Example of fluorescence observation using a device equipped with an interference filter, an absorption filter, and a hybrid filter [3].

Figure 13 shows an example of fluorescent beads image observed using a lensless imaging device with an absorption filter only and a hybrid filter. It shows that the hybrid filter significantly improved the contrast. In the hybrid filter, the excitation light is reflected by the interference filter on the surface. Thus, the object can be excited efficiently with the same intensity of excitation light.

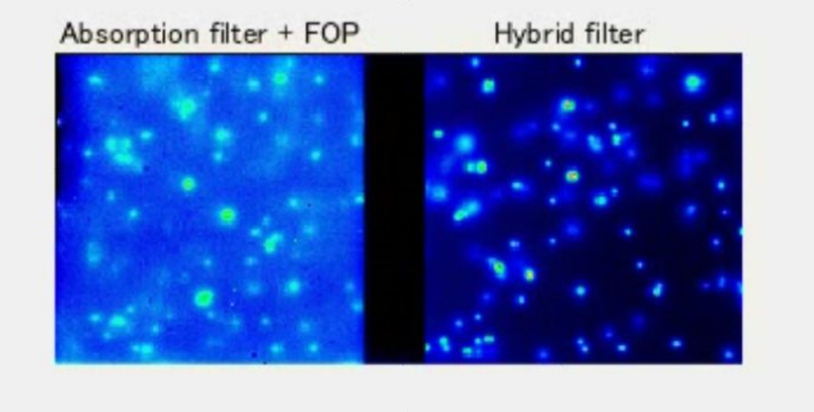

Figure 13 Fluorescent beads by a lensless device with absorption and hybrid filters on each half of the pixel array [3].

As mentioned earlier, the advantages of lensless imaging devices are their compactness and wide field of view. Figure 14 shows a schematic of an example of a lensless device structure with a hybrid filter using a commercially available large image sensor. Typically, the image sensor is sealed in a package with a glass lid, but by utilizing the FOP, the height of the imaging surface can be raised above the package frame. In this device example, the hybrid filter with bandpass filter characteristic improves the performance of green fluorescence observation. The image area is large enough to observe an entire mouse brain slice at once, as shown in Figure 15, and the spatial resolution is large enough to detect individual cells.

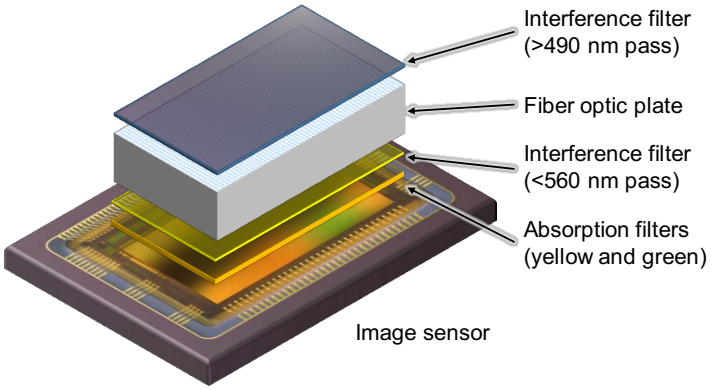

Figure 14 Example structure of a device with a hybrid filter on a packaged image sensor [30].

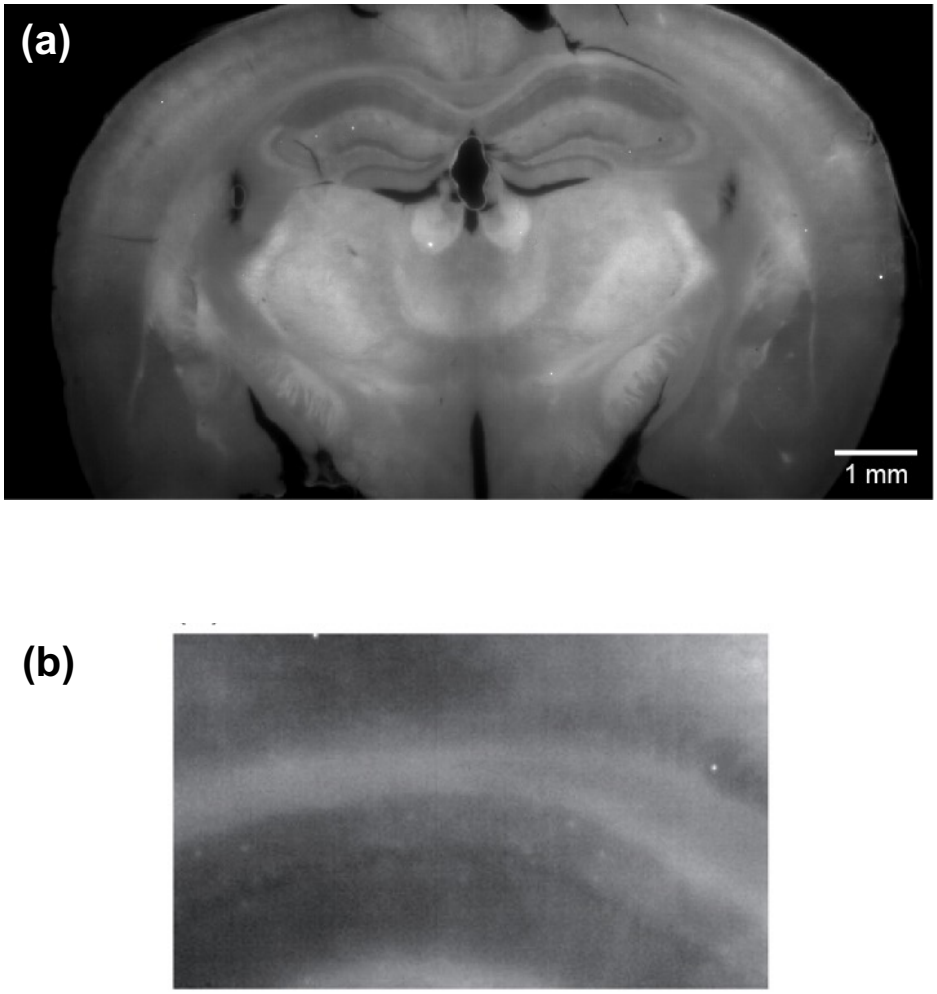

Figure 15 Brain slices of GFP-expressing mice imaged by a large image sensor. The slice thickness is 100um. (a) Overall view, (b) magnified view of the hippocampus [30].

2.3.4 Application of Lensless Fluorescence Imaging System for Biological Process Study

Lensless microscopy has been increasingly used in microbiological processes and biomedical studies, providing a cost-effective and high-throughput imaging tool. This section provides some key applications for lensless imaging systems that have been found in various studies of biological processes.

A. F. Coskun *et al.* (2010) presented a compressive sampling algorithm for on-chip fluorescence imaging devices, which enables the utilization of micro-scale spatial resolution for sparse objects across an ultra-large field of view through digital reconstruction and decoding techniques. Figure 16 shows a schematic diagram of the lens-free on-chip fluorescent imaging platform. This approach effectively reduces fluorescence spot artifacts and enables fluorescence observation with wide imaging areas and high spatial resolution. However, it should be noted that the compressive sampling method may not be suitable for images with substantial information content due to theoretical limitations. Additionally, the use of a large prism for excitation light reduction can increase the size and weight of the device, compromising its portability [34].

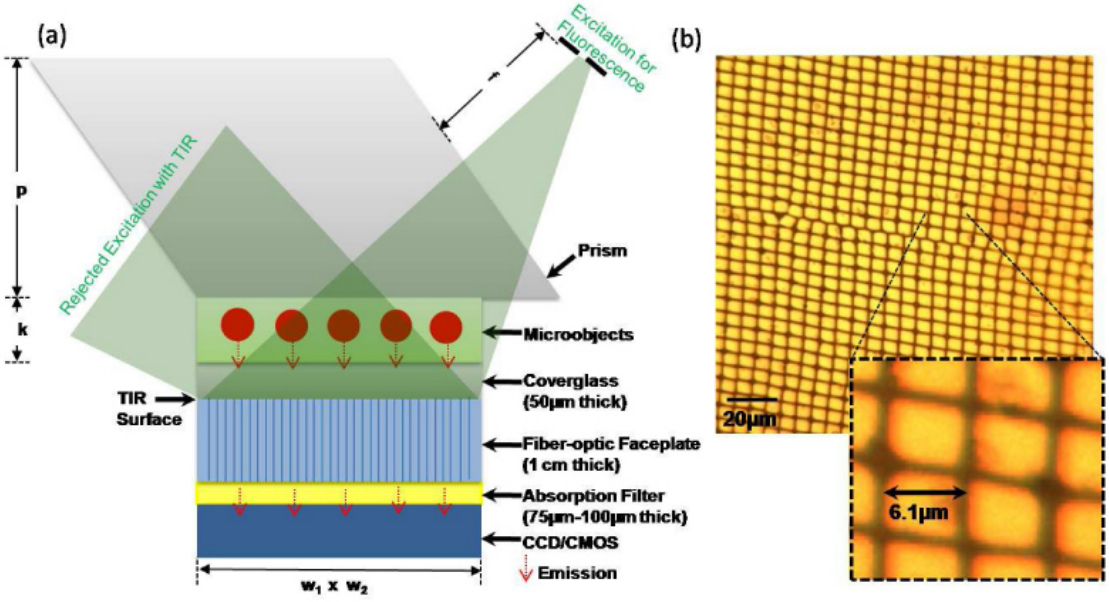

Figure 16 Schematic diagram of the lensfree on-chip fluorescent imaging platform [34].

S. Pang *et al.* (2012) introduced an initial approach to wide-field Talbot-grid-based fluorescence microscopy in their study. They successfully labeled human breast cancer cells (SK-BR-3) using quantum dots and achieved green fluorescence protein expression in the nucleus of

human embryonic kidney 293 cells (HEK) [33]. Furthermore, applying the microscopic slide-imaging system to Talbot-grid-based fluorescence microscopy demonstrated the potential for imaging two additional protozoan parasites, namely *Giardia* and *Cryptosporidium* [31]. In another innovative application, C. Han *et al.* (2013) combined Talbot fluorescence microscopy with a time-lapse fluorescence microscopy system, integrating a microfluidic perfusion subsystem. This integration enabled direct cell culture imaging within the incubator, introducing a compact and simplified imaging method for cell culture in incubators. Figure 17 shows the concept of their Talbot Fluorescence ePetri system [32]. In this study, the absorption filter has been replaced with an interference filter because there is a limitation in its performance, as described later in section 2.3.2. The decision to switch to an interference filter was made due to the perceived inadequate performance of the absorption filter. However, in order to take advantage of the high performance of the interference filter, an optical system incorporating a relay lens is employed, resulting in an increase in the overall size of the device.

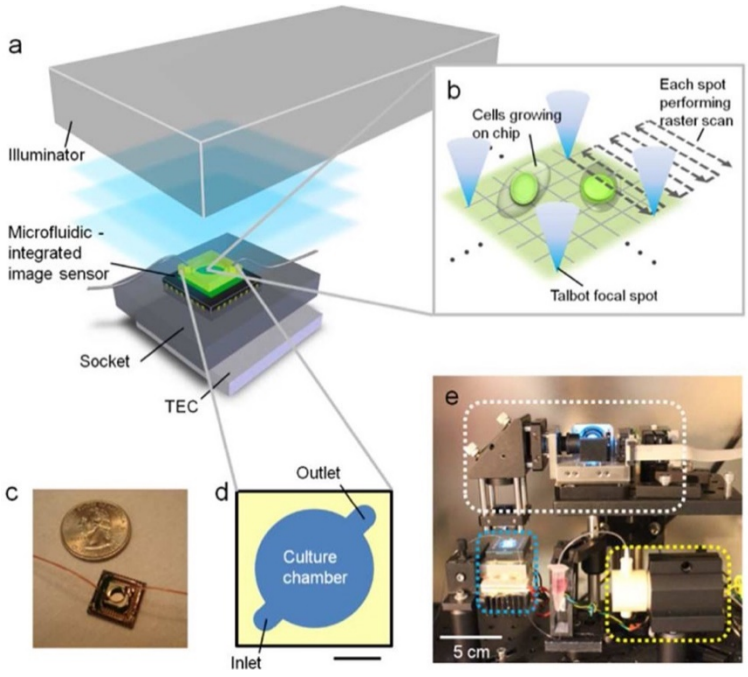

Figure 17 The concept of Talbot Fluorescence ePetri system [32].

Recently, K. Chen *et al.* (2023) enabled label-free imaging based on digital holographic microscopy and analysis of cells, providing valuable insights into cell morphology, dynamics, and behavior [77], [78]. Label-free imaging offers less damage to cells and real-time observation, and cost-effectiveness. However, it lacks specificity and sensitivity compared to labeled fluorescence imaging, which provides high specificity, contrast enhancement, and versatility but introduces autofluorescence and photobleaching. It must consider factors such as the level of specificity and sensitivity required, the complexity of sample analysis, and the potential for multiplexing when deciding which imaging approach to utilize in the studies. In cell biology, developmental biology, and tissue engineering, lensless imaging systems assist in studying cell growth, migration, division, and interactions [79], [80]. Additionally, these systems facilitate high-throughput screening of large cell populations, allowing for rapid imaging and analysis of cells, playing a crucial role in screening drug candidates, identifying rare cell events, and characterizing cellular responses to various stimuli [79], [81], [82].

Lensless imaging systems also offer a cost-effective and portable approach to microorganism identification and classification [83]. S. Jiang *et al.* demonstrated the application of an integrated ptychographic sensor for lensless cytometric analysis of microbial cultures. It enables rapid microbial analysis, including detecting bacteria and monitoring microbial growth in environmental, clinical, and food safety applications [84]–[87]. Ptychography is an imaging technique that utilizes scanning and computational reconstruction to achieve high-resolution imaging and aberration correction. It offers a significant advantage in achieving high-resolution imaging even with a poor objective lens. This is a key distinguishing feature of ptychography compared to traditional imaging techniques. In conventional microscopy, the resolution of the captured image is mostly determined by the objective lens quality. However, in ptychography, the

resolution is determined by the overlapping diffraction patterns captured during the scanning process rather than relying on the lens quality. On the other hand, lensless imaging refers to a broader class of techniques that capture images without lenses and rely on computational algorithms for image reconstruction. Both approaches have unique strengths and applications but have similar purposes of developing high-performance imaging with poor optics helped by computational methods. Moreover, lensless imaging systems show promise in point-of-care diagnostics. They can be integrated into portable devices, enabling the detection and quantification of biomarkers, which provides for rapid and low-cost diagnostic testing, particularly in resource-limited settings [37], [68], [88]–[90].

Lensless imaging systems are extensively utilized in neuroscience research, providing non-invasive and high-throughput imaging and analysis of neuronal activity, neuronal networks, and neural dynamics. Enabling imaging of neurons facilitates a deeper understanding of neural processes and interactions [91]–[94]. Additionally, lensless imaging systems can be used for 3D imaging and reconstruction of tissue samples, eliminating the need for physical sectioning. It allows for visualizing tissue and specific cell markers [24], [95], [96].

J. K. Adams *et al*. (2017) demonstrated notable ultraminiature lensless FlatScope, a three-dimensional (3D) fluorescence imaging method for miniature size microscopy using a 3D volume reconstruction algorithm with mask and spacer layer installed above the imaging sensor (Figure 18). In this device, diffraction elements interfered with the light on the image sensor surface to capture images, and a hybrid filter structure is used as the corresponding emission filter. The technique successfully introduced significant residing microscopy with all components, including mask, spacer, and filter layer under 300 μm. However, the performance of this method was compromised by the autofluorescence of the gel filter, resulting in 64% dynamic range reduction,

but it was considered to solve this limitation using a thin-film absorption filter that potentially conjunct an omnidirectional reflector [96].

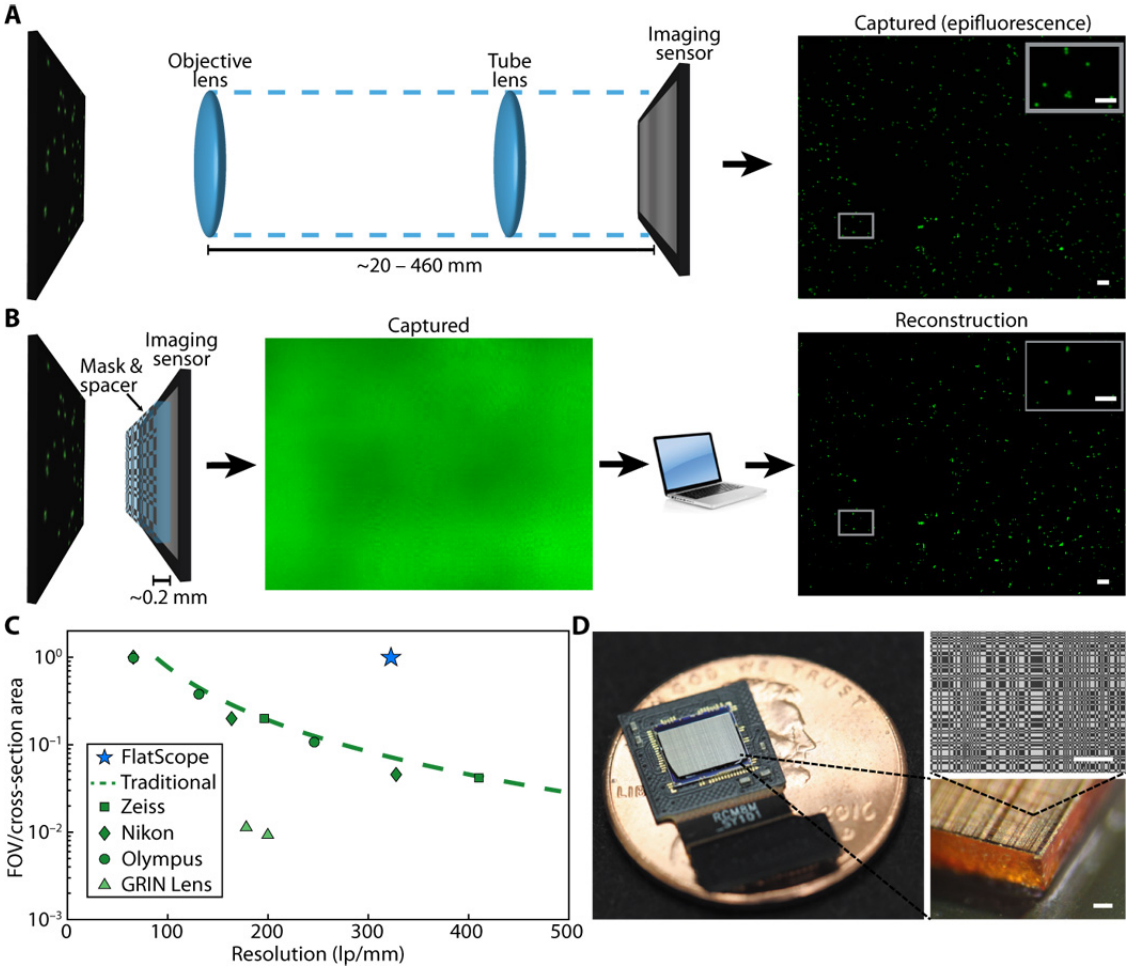

Figure 18 FlatScope concept versus traditional microscope [96].

N. Antipa *et al.* (2018) demonstrated significant advancements in the field of computational imaging by presenting a compact and easily constructed camera designed for single-shot three-dimensional (3D) imaging [95]. By utilizing a simple optical system with a diffuser placed in front of the sensor, they have successfully achieved single-shot 3D imaging capabilities. This groundbreaking approach allows for encoding precise 3D point source locations within caustic patterns, thereby enabling accurate and efficient 3D imaging.

In the related study, G. Kuo *et al*. (2020) introduced a random micro-lens diffuser, comprising numerous small lenslets randomly distributed on the mask surface (Figure 19). In this research, the combination of an absorption and an interference-based color filter was also utilized and well-suited for removing excitation light at the high angles of incidence potentially present in this system. This device uses a random microlens structure as a scattering element instead of the diffraction element of J. K. Adams *et al.* [96]. The hybrid filter structure was also used as the emission filter. This novel technique offers improved performance in low-light conditions, making it suitable for monitoring *in vivo* fluorescence signals and tracking 3D models of biological organisms. The random micro-lens diffuser presents promising applications in the field of biological imaging, enhancing the visualization and analysis of complex biological structures and processes [97].

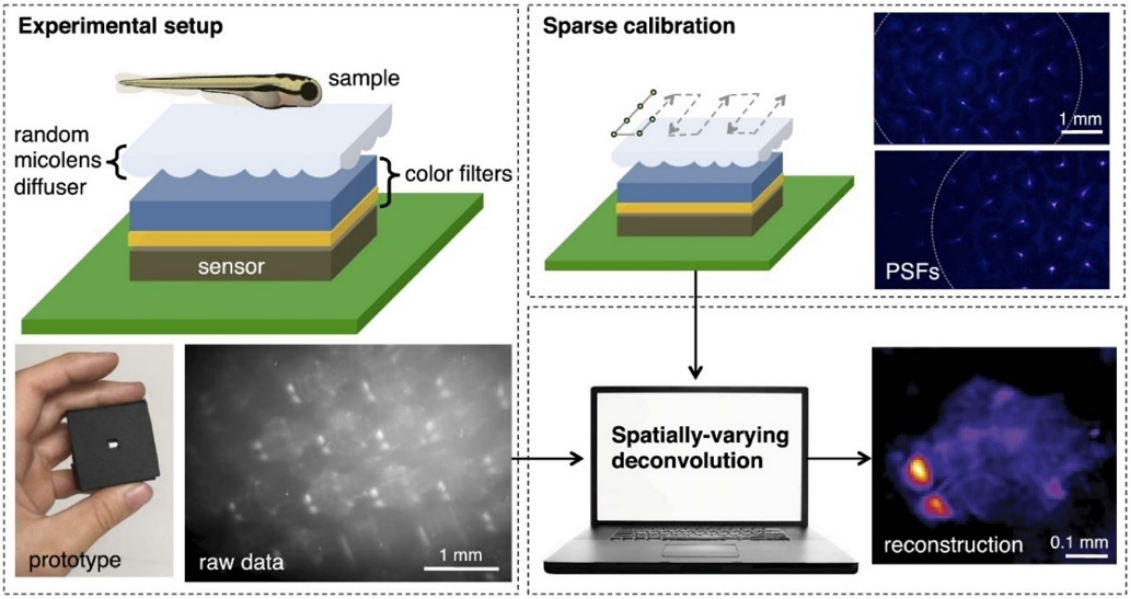

Figure 19 Schematic of light-weight and portable on-chip microscope [97].

K.Yanny *et al.* (2020) demonstrated a substitution of an optimized multifocal phase mask to change conventional 2D miniscope to 3D microscopy (Figure 20). The result of the change is size reduction, and providing a variety of focal lengths enables a uniform resolution across a wide depth range. By solving the sparsity-constrained inverse algorithm, 3D imaging resolution is recovered. It is ideal for various applications where space is limited. It includes imaging the neural activity within freely moving animals to study their volumetric behavior and conducting 3D motion analysis of dynamic samples in controlled environments in incubators and lab-on-a-chip devices [98]

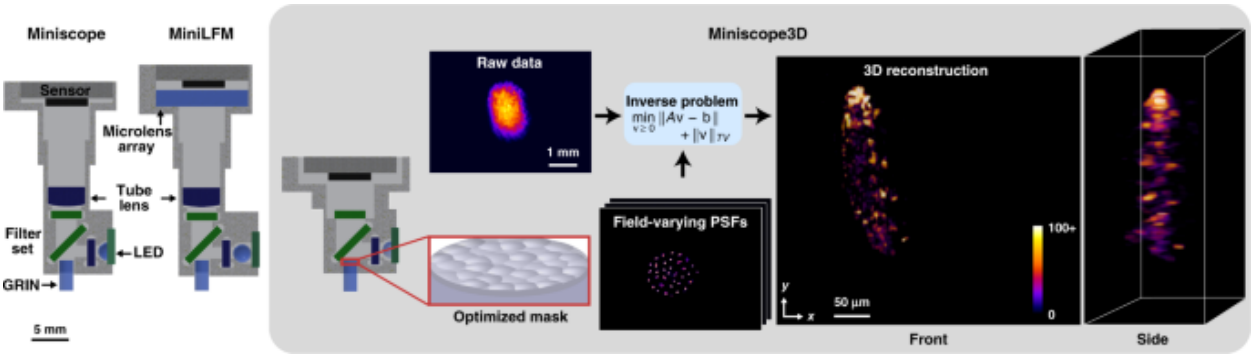

Figure 20 Miniscope 3D fluorescence microscopy system overview [98].

The detailed result above shows that the wide-ranging applications of lensless imaging systems highlight their versatility and potential for advancing our understanding of various biological processes.

2.4 Summary & Discussion

This chapter presents an overview of lensless imaging systems that utilize simple optical components. In contrast to conventional lens optics that rely on an infinity focal spot, these systems employ filters at different angles of incidence. Hybrid filters have emerged as a powerful method for achieving high excitation rejection performance even under such conditions. Although this method was initially proposed for lensless fluorescence imaging, hybrid filters have also demonstrated effectiveness in quasi-lensless configurations, such as thin imaging devices utilizing scattering and diffractive optics. These developments have gained significant attention and are now widely employed in practical applications.

However, the applicable wavelengths are monochromatic. For applications such as cell observation, multiple staining with two or more colors and labeling with fluorescent proteins are widely used. Developing a hybrid filter that can handle multiple colors is essential in such applications. When considering multicolor hybrid filters, there are few problems with interference filters due to the high degree of design freedom offered by their stacked structure. Also, multicolor bandpass filters are now commercially available.

On the other hand, there is an extent to consider for the absorption filter part. Two options to resolve the problems are utilizing absorption filters with two absorption bands for the entire filter or applying a filter with one absorption band to each pixel. The former option may suffer from low wavelength selectivity and decreased overall performance because the transmittance at wavelengths shorter than the absorption peak tends to be lower than that at longer wavelengths. The latter option presents difficulties in applying a filter to each pixel, as it requires high absorption performance to remove excitation light effectively. Coating individual pixels becomes problematic,

unlike color filters for general color image sensors requiring a low absorption rate. Very high absorption performance is necessary to remove excitation light for such a fluorescence imaging application.

As a consequence, the thickness of the absorbing layer must be thicker, making it difficult to coat the filter to each tiny pixel individually. Additionally, crosstalk between pixels causes another problem. A solution to this issue will be proposed in the next chapter.

Chapter 3

Hybrid Filter for Lensless Dual-color Fluorescence Imaging

3.1 Overview

3.1.1 Issues in Lensless Dual-color Fluorescence Imaging Device

The hybrid emission filter has been developed and used in many studies until these days. Previously, a lens-free imaging device proposed for Förster resonance energy transfer (FRET) imaging was demonstrated by implementing a hybrid filter and CMOS image sensor. FRET describes the physical phenomenon whereby the nonradiative energy is transferred between two fluorophores, consisting of a donor and an acceptor fluorophore. The lens-free dual-color fluorescence imaging device was successfully developed to simultaneously detect two different colors of donor and acceptor fluorophores. The lens-free dual-color fluorescence imaging device was specifically designed for single-color excitation, as shown in Figure 21 [62].

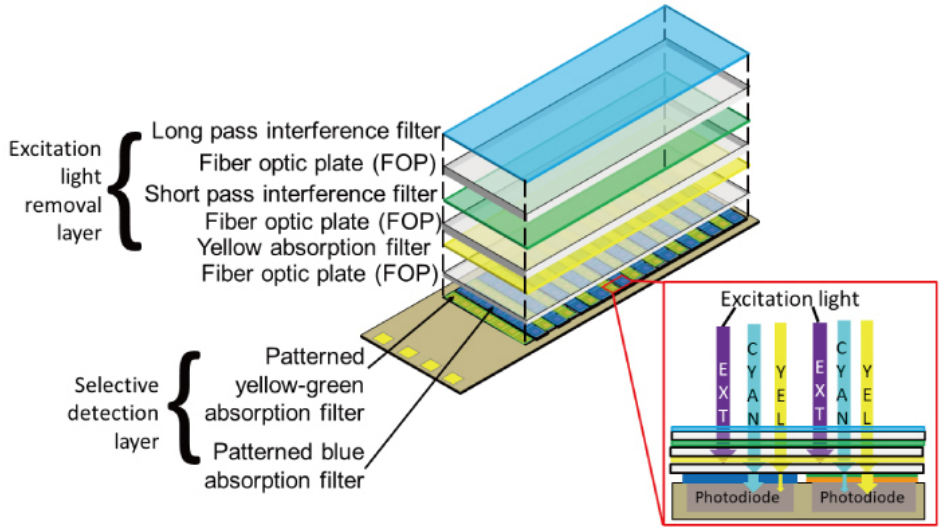

Figure 21 Illustration of the hybrid filter structure for FRET imaging [62].

In a selective detection layer, the line arrangement pattern of yellow-green and blue absorption filters was coated directly on the image sensor's pixel array (Figure 21). The limitation of detection capability was present due to the relatively weak fluorescence emission intensity of cyan and yellow fluorescent proteins. Since the image sensor realized the color by applying the color filter array method, if the wavelength selectivity of the filter is low, the performance to reject the unwanted light is also low. Moreover, adjacent pixels present a challenge due to optical and electrical crosstalk, where unwanted excitation light can pass through the filter and impact neighboring pixels. Additionally, the output values can be changed because the strong excitation light can leak into the neighboring pixels when the excitation wavelength overlaps with the emission wavelength of the adjacent pixels. Thus, it is necessary to control the angle of incidence or use a thick absorption filter as a physical barrier between the pixels to minimize optical crosstalk. In this work, the hybrid filter was created and successfully solved this problem and achieved high sensitivity performance of fluorescent detection by applying an excitation light removal layer on the selective detection layer. Another solution was introducing the black pixel to function as offset pixels to improve the point of effect due to temperature changes. However, the sensitivity spectrum characteristics of this device remained insufficient.

Alternatively, a multi-band filter can be utilized to realize multicolor fluorescence imaging. This method is created by applying a bandpass filter designed to remove unwanted wavelength ranges and allow only desired wavelengths to pass through them. Unlike the method mentioned above, the multi-band filter is covered uniformly on the image sensor's pixel array, avoiding electrical crosstalk between adjacent pixels. Therefore, it is reasonable to employ this method to design a hybrid filter for a lensless dual-color fluorescence observation approach. The hybrid filter can be formed by combining interference and absorption filters. The interference filters can be

customized for a specific passband, while the absorption filters with different spectral characteristics can be overlaid to create multi-band features.

3.1.2 Criteria for Hybrid Filter Configuration

This research aims to develop a lensless imaging device that utilizes a hybrid emission filter to visualize dual-color fluorescence observation excited by a dual-color excitation light to observe green and red fluorescence components, which are the most commonly used fluorescent targets. To accomplish this, a combination of interference and absorption filters is utilized to fabricate a hybrid filter. It is crucial to place the interference filter on top because it emits lower autofluorescence compared to the absorption filter, which can lead to a decrease in imaging performance even though it is easier to form the absorption filter on the top layer, as described in chapter 2.3.4.

A fiber optic plate (FOP) was utilized to create a bandpass characteristic by depositing a longpass interference filter on one side and a notch interference filter on the other side. The arrangement of these interference filters was carefully determined to optimize the performance of excitation light rejection. However, it was observed that the incident light scatters within the FOP, causing changes in the spectral characteristics of the interference filter, which depends on the angle of incidence. Consequently, the performance of excitation light rejection for the interference filter located on the bottom side of the FOP reduces, particularly for highly angled excitation light can pass through it.

In this study, two fluorescent proteins, green fluorescent protein (eGFP) and mCherry fluorescence, were considered as the fluorescent target. The green fluorescent protein exhibits a peak excitation spectrum of approximately 510 nm, while the red fluorescent protein has a peak

excitation spectrum of approximately 625 nm, as shown in Figure 22 and Figure 23, respectively. A central wavelength of 434 nm was selected for green fluorescent protein excitation to effectively excite both fluorescent targets, while a central wavelength of 594 nm was selected for red fluorescent protein excitation. The hybrid filter was proposed to reject the excitation light from reaching the detector and enable dual-color fluorescence observation accurately.

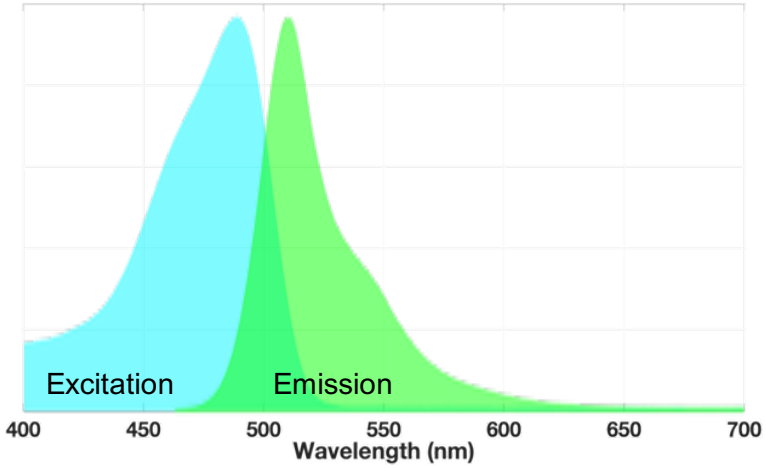

Figure 22 Emission and excitation spectra of green fluorescent protein (eGFP).

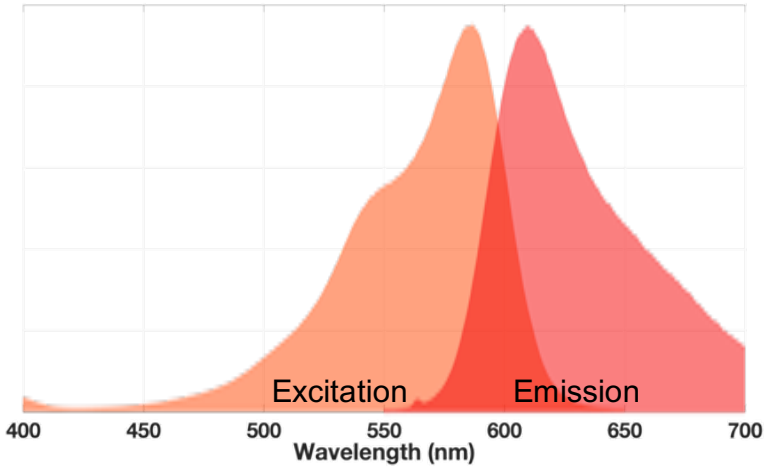

Figure 23 Emission and excitation spectra of red fluorescent protein (mCherry).

3.2 Filter Evaluation

3.2.1 Transmittance Spectrum Characteristics

In this study, the bandpass interference filter was specifically designed to effectively reject excitation light at approximately 450 nm for green fluorescence and 594 nm for red fluorescence excitation. The transmittance spectra of the longpass and notch interference filters are shown in Figure 24. The longpass interference filter cut off the wavelengths shorter than 505 nm, and the notch interference filter cut off the wavelengths between 530-630 nm. However, the presence of excitation light scattering within the FOP limits the performance of excitation light rejection for the interference filters. The arrangement of these interference filters needs to be carefully determined. To indicate that, the bandpass interference filter deposited on the FOP was placed in front of the excitation light source to roughly evaluate the performance of excitation light rejection of each filter.

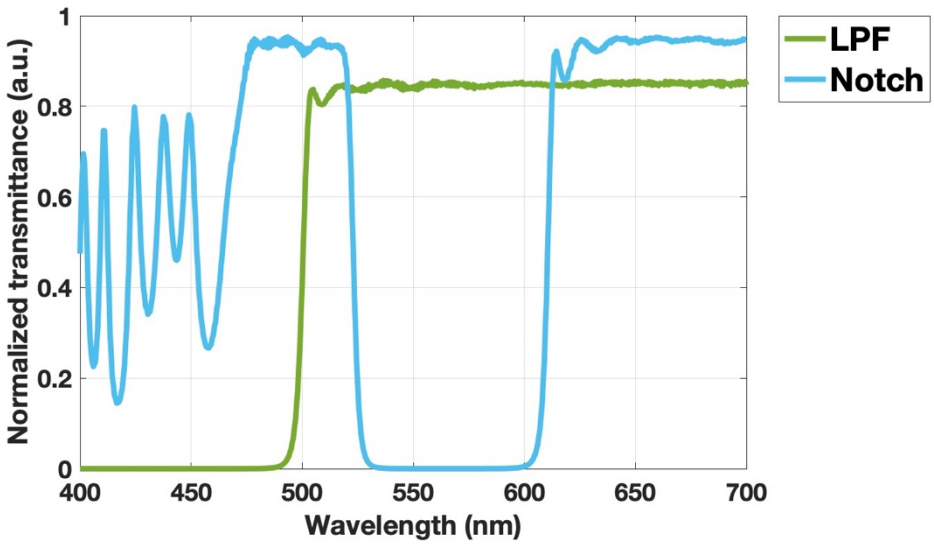

Figure 24 Transmittance spectra of the notch and longpass interference filters (LPF).

Figure 25 shows the results of the excitation light scattering in the FOP when irradiated with a 594 nm light source, as observed with the interference filters. The notch interference filter exhibited high performance of excitation light rejection when facing the light source, as shown in Figure 25(a). However, in the opposite direction, some scattered components in the FOP passed through the notch interference filter, resulting in a brighter beam shape, as shown in Figure 25(b). The same observations were observed with blue light, indicating that using the FOP as a substrate for the interference filter compromised the performance of the filter on the bottom side.

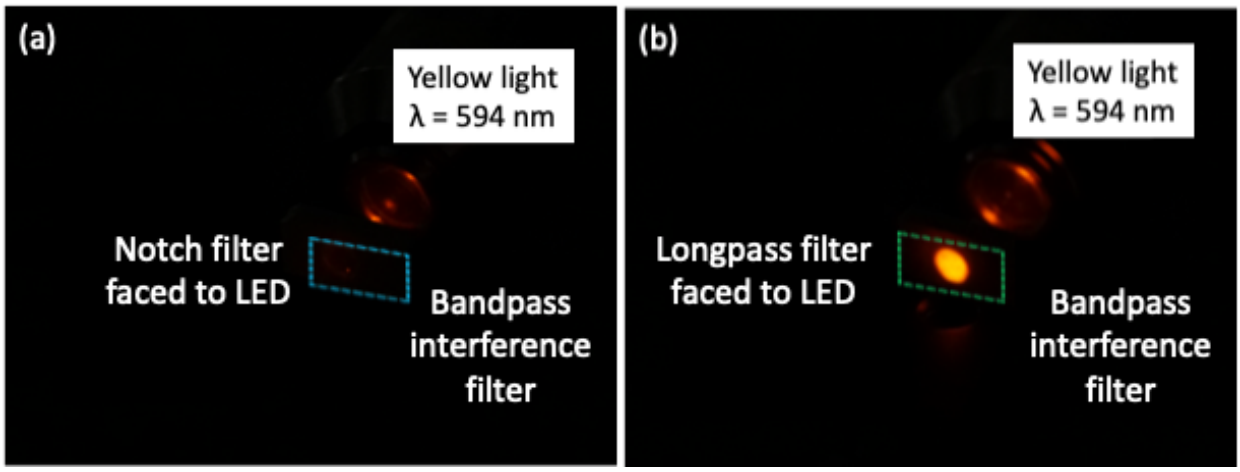

Figure 25 Comparison of excitation light rejection performance of the bandpass interference filter deposited on the FOP.
(a) Notch interference filter and (b) Longpass interference filter facing to the light source. The wavelength of excitation light (LED) was 594 nm.

In order to achieve the desired dual-band characteristic, the absorption filter was also used in the hybrid filter configuration to absorb the scattered components while allowing specific wavelengths of light to pass through it. Typically, it is challenging for an absorption filter to form a bandpass characteristic with high wavelength selectivity because it has a gradual transition of transmittance characteristics. Although the excitation light absorption performance can be increased by increasing the physical thickness, autofluorescence occurs. Therefore, it is almost

impossible to increase the excitation light absorption performance while the transmission of fluorescence emission increases. It is crucial to determine the thickness of the absorption filter.

This study used a yellow dye (Valifast Yellow 1108, Orient Chemical, Japan) to absorb the light in the blue wavelength range. This dye has a longpass transmittance characteristic and exhibits low autofluorescence. Additionally, a dye with a sharp absorption peak (FDG-007, Yamada Chemical Co., Ltd., Japan) was used to absorb the light in the yellow wavelength range. To form the dual-bandpass characteristic, these absorption filters are overlaid and placed on the bottom side of the FOP. Figure 26 shows the transmittance spectra of the yellow and blue absorption filters. The blue filter has a high absorption characteristic at approximately 594 nm. However, since the high absorption bandwidth was narrow, it was necessary to shorten the wavelength of the excitation light. The arrangement of these absorption filters was yellow and blue from top to bottom, respectively, because the yellow (VY1108) filter exhibits lower autofluorescence than the blue filter (FDG-007).

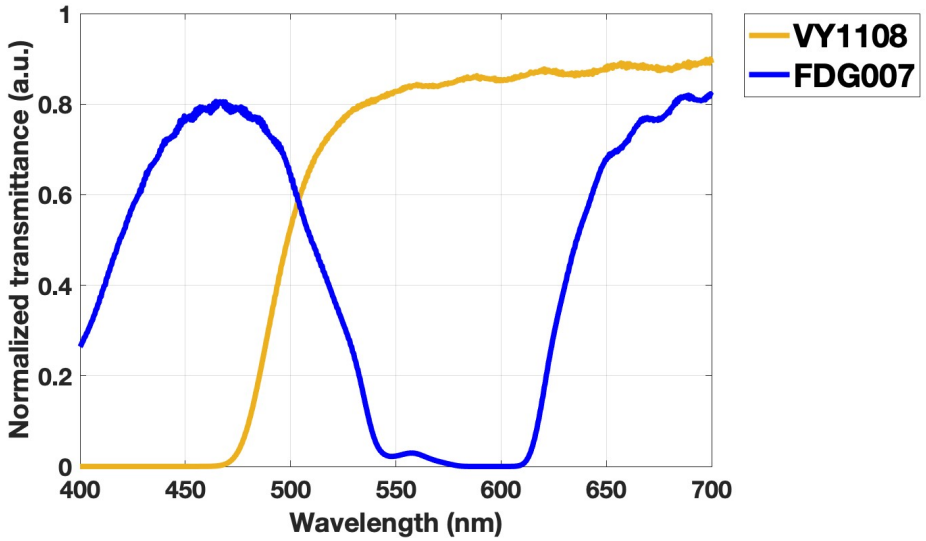

Figure 26 Transmission spectra of the yellow and blue absorption filters.
VY1108: Yellow absorption filter and FDG007: Blue absorption filter

3.2.2 Autofluorescence Evaluation

Besides the consideration of scattered components from the interference filter, it is also important to consider the presence of autofluorescence originating from the FOP layer itself. In the case of this study, Figure 27 shows the autofluorescence exhibited by the FOP equipped with interference filters when irradiated with a 440 nm laser. A yellow filter was employed to observe the autofluorescence and remove the excitation light component. The FOP was deposited directly on the surface with both notch interference and longpass interference filters.

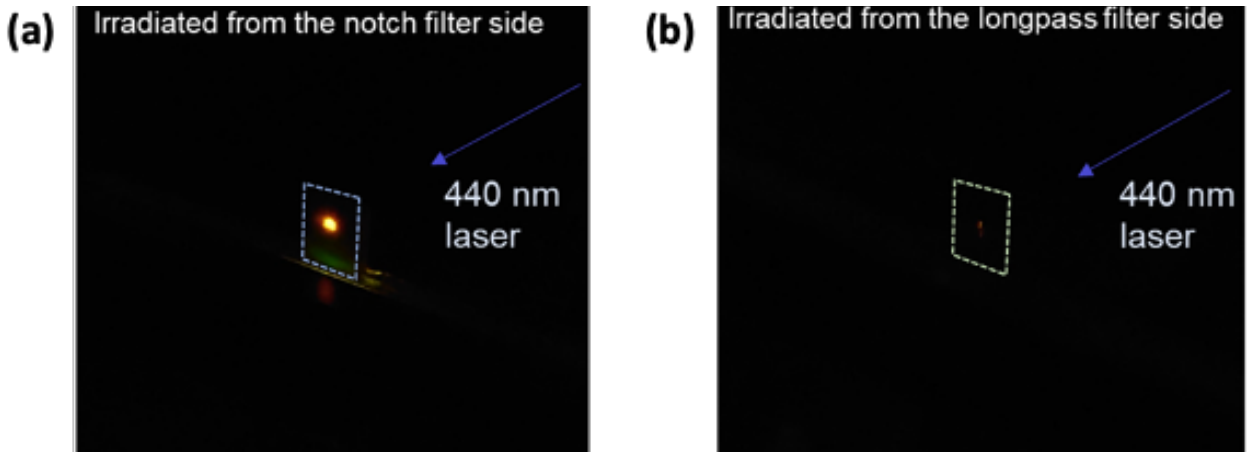

Figure 27 Example of autofluorescence observation from an FOP with the interference filters.

To evaluate that, blue light from a laser light source (440 nm) was irradiated from the notch interference filter side, as shown in Figure 27(a), and in the opposite direction, from the longpass interference filter side, as shown in Figure 27(b). However, despite the use of these interference filters, it was found that the strong excitation light component could not be completely eliminated during the irradiation. As a result, when the blue excitation light passed through the notch interference filter side, it caused an increase in the autofluorescence emitted by the FOP. This

indicates that the autofluorescence signal observed in the FOP is influenced by the presence and characteristics of the interference filters.

As stated earlier, in this study, these absorption filters were determined to arrange the blue filter after the yellow filter from the excitation light side because the yellow filter (VY1108) exhibits lower autofluorescence compared to the blue filter (FDG-007). To eliminate the autofluorescence exhibited by the yellow filter in the wavelength range of 550-610 nm, a blue absorption filter was placed after the yellow filter to effectively remove the autofluorescence.

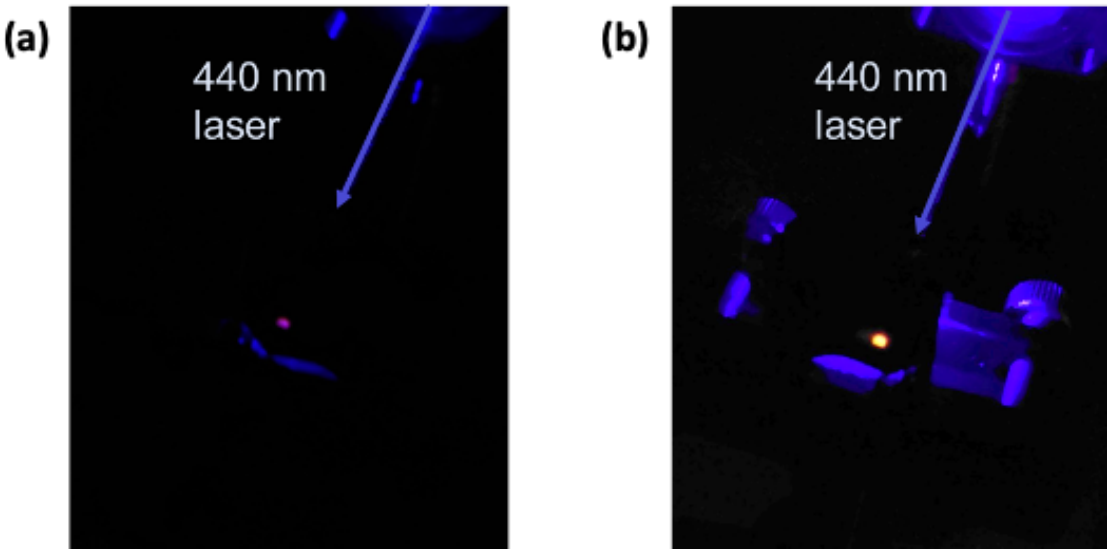

Figure 28 Autofluorescence observation results when the blue and yellow filters were stacked.

Figure 28 shows a comparison of autofluorescence observed when the absorption filters are arranged in different orders. Figure 28(a) shows the autofluorescence exhibited when the filter is arranged from yellow to blue absorption filters. In the opposite direction, Figure 28(a) shows the autofluorescence exhibited when the filter is arranged from blue to yellow absorption filters. It indicates that the blue absorption filter exhibits stronger autofluorescence compared to the yellow absorption filter, resulting in a brighter spot on the filter. Thus, the order of the absorption filters

was yellow and blue, attaching to the FOP on the notch interference filter side, respectively. This arrangement was determined to prevent strong autofluorescence emitted by the blue absorption filter from interfering with the imaging process.

The presence of autofluorescence can be a challenge in accurately detecting target fluorescence signals and be a significant factor to consider when using such imaging techniques. Therefore, it is essential to understand and manage the autofluorescence when using the FOP with interference filters and autofluorescence characteristics in absorption filters to ensure imaging results accurately.

3.2.3 Effective Transmittance and Absorption Filter Thickness

Another significant factor related to autofluorescence is the absorption filter thickness, as mentioned in section 2.3.2. The absorption filter exhibits autofluorescence, interfering with the detection of the target signals. The optimal filter thickness should be determined. To address this limitation and achieve the high performance of the emission filter, it is necessary to determine the optimal thickness of the absorption filter to balance between high absorption performance and autofluorescence emission characteristics.

In the measurement, the absorption filters with different thicknesses was placed on the bandpass filter deposited on the FOP. For the effective transmittance measurement of the yellow absorption filter, the blue excitation light with a wavelength of 434 ± 8.5 nm was irradiated to the stacked emission filters. The relationship between the transmittance characteristics and the absorption filter thickness of the yellow absorption filter is shown in Figure 29. It indicates that this filter has an inflection point near 2.5 μm, but the addition of the notch and longpass interference filters deposited on the FOP shows a significant deviation at approximately 1.5 μm,

resulting in stronger autofluorescence compared to the yellow absorption filter. In particular, when the excitation light was irradiated on the notch interference filter side, as shown in Figure 27(a) in the previous section. The effective transmittance was reversed when the light was irradiated on the longpass interference filter side (Figure 27(b)).

Figure 30 shows the relationship between the transmittance characteristics and the absorption filter thickness of the blue absorption filter. The blue absorption filter was irradiated with the yellow excitation light at a wavelength of 594 ± 5 nm. According to the Lambert–Beer law, the transmittance decreases exponentially as the thickness increases up to a thickness of 5 µm. In addition, the addition of the interference filters deposited on the FOP exhibits a similar curve, and the intensity of autofluorescence is small in this wavelength band.

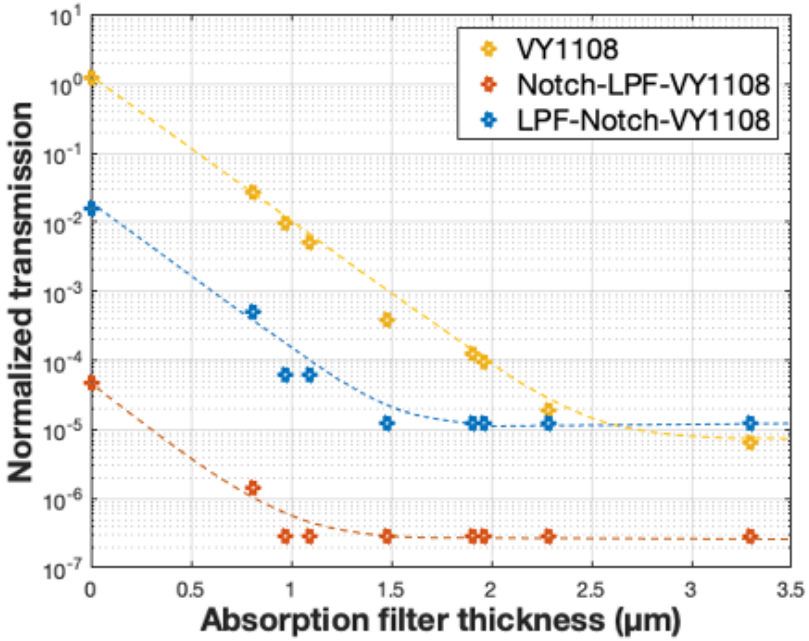

Figure 29 Relationship between transmittance characteristics and yellow absorption filter thickness.
Transmittance characteristics of the yellow absorption filter irradiated with the excitation light at a wavelength of 434 ± 8.5 nm.

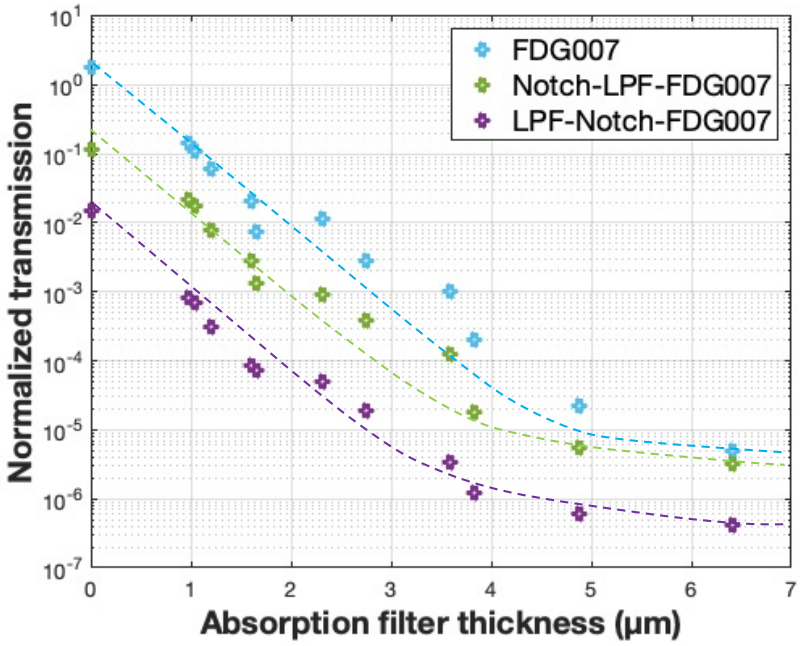

Figure 30 Relationship between transmittance characteristics
and blue absorption filter thickness.
Transmittance characteristics of the blue absorption filter
irradiated with the excitation light at a wavelength of 594 ± 5 nm.

In order to optimize the performance of the interference filters, the arrangement of the filter must be appropriately determined based on the performance of each filter. In this study, the autofluorescence generated by the FOP when irradiated with blue excitation light caused a limitation on the effective transmittance, as previously shown in Figure 27. To address this, a longpass interference filter was arranged on the top of the FOP, while a notch interference filter was arranged on the other side. This configuration was selected to reduce the impact of autofluorescence and enhance the optimal performance of the imaging system.

Based on the filter evaluation results, the filters were arranged as follows: longpass interference filter, notch interference filter, yellow absorption filter, and blue absorption filter. The thicknesses of the yellow and blue absorption filters were approximately 2 μm and 5 μm,

respectively. Figure 31 shows a plot of the transmission spectrum of each filter in a semi-logarithmic plot.

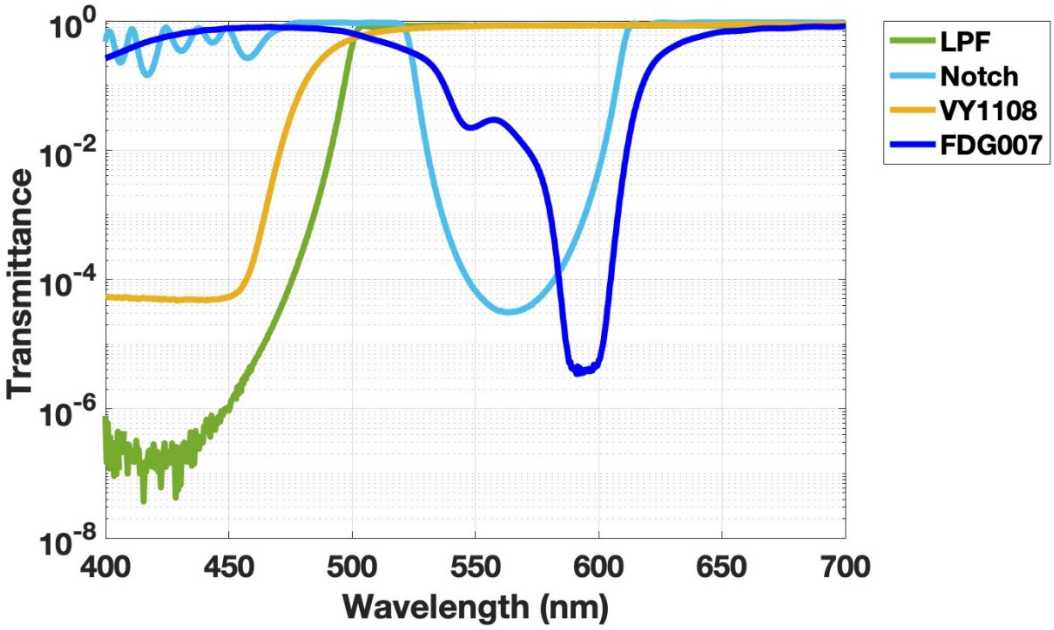

Figure 31 Transmission spectrum of each filter used in the proposed hybrid filter configuration (in semi-logarithmic plot).

3.3 Proposed Hybrid Filter Structure

In the structure of the proposed hybrid filter, the uppermost and bottom sides of the FOP (fiber optic plate) were equipped with longpass and notch interference filters, respectively. Additionally, yellow and blue absorption filters were attached to the bottom side, as shown in a schematic of the proposed hybrid filter structure in Figure 32. This hybrid filter, subsequent to fabrication, was mounted onto a commercially available color CMOS image sensor, which worked as the imaging device. The following sections will provide a detailed description of the hybrid filter preparation and device assembly process. Figure 33 shows a photograph of the proposed hybrid filter mounted onto an image sensor with the image sensor's package.

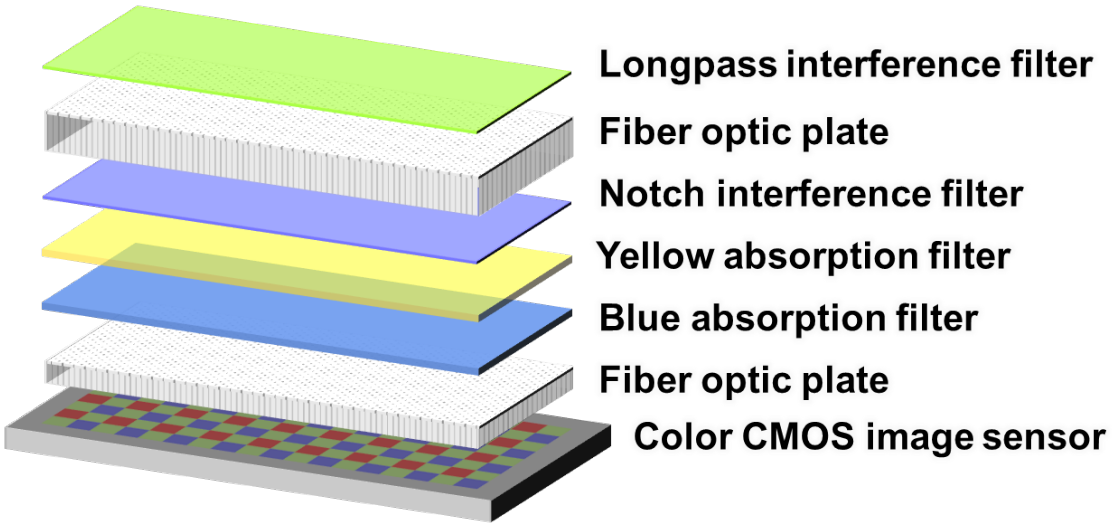

Figure 32 Schematic of the proposed hybrid filter structure and image sensor structure.

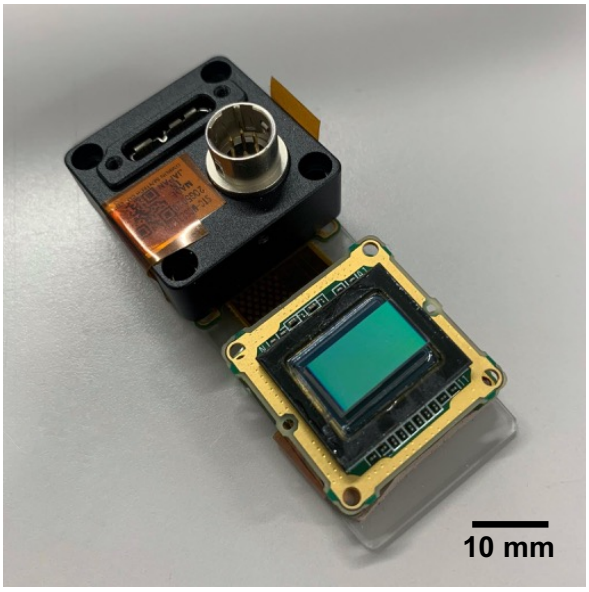

Figure 33 Photograph of a lensless imaging device with the proposed hybrid filter.

3.4 Filter Preparation and Device Assembly

3.4.1 Filter Preparation

1) An amorphous fluoropolymer CYTOP-M (AGV Chemical, Japan) was coated on a cover glass (24 mm × 24 mm) through spin coating, as shown in Figure 34(a). This film was prepared as a substrate, enabling the absorption filter to be easily peeled off from the cover glass.
2) Yellow dye powder (Valifast yellow 1108 (VY1108), Orient Chemical, Japan), cyclopentanone (Wako, Japan), and optical adhesive (NOA 63, Norland Products Inc., USA) were mixed at a ratio of 1:4:1. A surfactant (Megaface R-41, DIC Corporation, Japan) was added at approximately 1% by weight to obtain a yellow absorption solution.
3) The yellow absorption solution was spin-coated at a rotation speed of 1000 rpm on a cover glass coated with the amorphous fluoropolymer CYTOP-M. After spin coating, it was cured using ultraviolet light for 60 secs and then baked at 150°C for 45 mins to form a layer of yellow dye film, as shown in Figure 34(b).
4) The 3 μm core pitch FOP (J5734, Hamamatsu Photonics, Japan) was attached with a notch interference filter with a rejection wavelength of 530–610 nm and a longpass interference filter (cut-on wavelength of 505 nm) on both sides, which was fabricated by a thin-film deposition company (Tac Coat, Japan). The FOP with the notch interference filter surface was attached to the yellow absorption filter using epoxy resin (Z-1, Nissin resin, Japan) and left for 24 hours until solid and dry, as shown in Figure 34(c). Then, the FOP was removed from the cover glass by cutting the edges of the cured epoxy and yellow dye film, as shown in Figure 34(d). This process was performed to obtain a yellow absorption filter on the FOP.

5) Blue dye powder (FDG-007, Yamada Chemical Co., Ltd., Japan), cyclopentanone, and epoxy resin were mixed at a ratio of 1:10:10, and the surfactant was added at approximately 1% by weight to form a blue absorption solution.
6) The blue absorption solution was spin-coated at a rotation speed of 1000 rpm on a cover glass coated with the amorphous fluoropolymer CYTOP-M and left to solidify and dry overnight, as shown in Figure 35(a).
7) The FOP with the yellow absorption filter surface was attached to the blue absorption filter using epoxy resin and left for 24 hours to solidify and dry, and it was then removed from the cover glass, as shown in Figure 35(b) and (c). This process was performed to obtain a hybrid filter (Figure 35(d)).

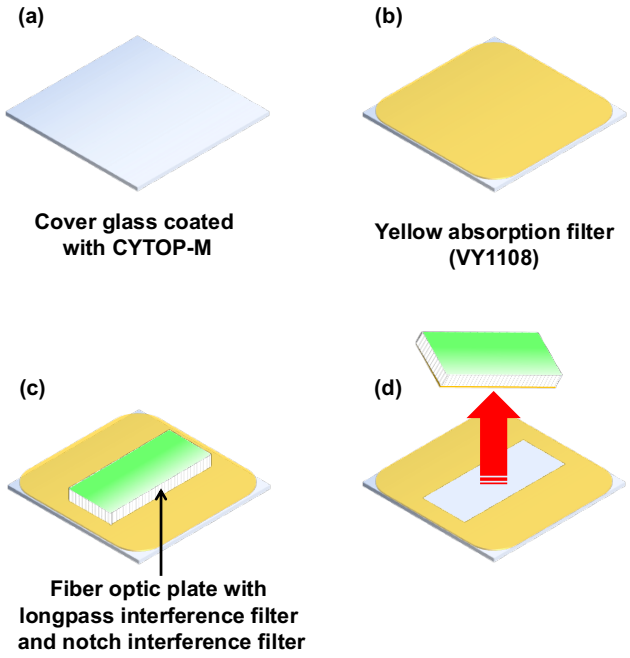

Figure 34 Schematic diagram of the yellow absorption filter preparation processes. (a) Cover glass coated with a CYTOP-M layer. (b) Cover glass covered with CYTOP-M was coated with yellow absorption solution. (c) FOP with a notch interference filter surface attached to the yellow absorption filter. (d) Yellow absorption filter was removed from the cover glass and glued with the FOP.

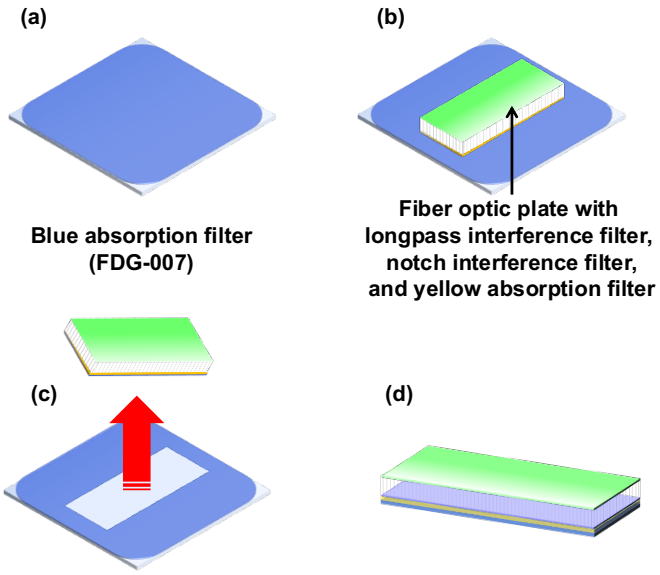

Figure 35 Schematic diagram of the proposed hybrid filter preparation processes. (a) Cover glass covered with CYTOP-M coated with blue absorption solution. (b) FOP with a yellow absorption filter surface attached to the blue absorption filter. (c) Blue absorption filter removed from the cover glass and glued with the FOP. (d) The completed hybrid filter.

In a lensless system, the blue dye (FDG-007) has been used as an absorption filter to remove the excitation light for red fluorescence in the dual-color fluorescence observation. This dye has a sharp absorption peak at 590 nm shows relatively high transmittance in the green wavelength band. Thus, it was considered to fabricate the blue absorption filter with high concentration.

To fabricate a high concentration of the blue absorption filter, an NOA63 was first used as a base material. However, it could not increase the concentration because it was crystallized easily, which affects uneven the dye film surface. Therefore, the absorption rate will be insufficient even if the film thickness is the same as before. In addition, the spatial resolution will be reduced if the film thickness is increased to compensate for this in the lensless system.

The epoxy resin was used as a base material for the blue absorption filter fabrication, which has a fluorescence intensity higher than NOA63, but it has high mechanical strength and a strong resin matrix. Therefore, it was determined that the epoxy resin is expected to form a stronger matrix than NOA63.

3.4.2 Device Assembly

The glass lid originally from the commercially available CMOS image sensor (IMX249, Sony, Japan) was detached from the package. The details are provided in Appendix A. This image sensor has 1936×1216 effective pixels and a 5.86 μm ×5.86 μm pixel size. The glass lid that covered the surface of the sensor package was removed, and a 1.2 mm-thick FOP was added before mounting the hybrid filter. Subsequently, the fabricated hybrid filter was mounted onto the color CMOS image sensor using an epoxy resin. Figure 36 shows a schematic of the device assembly process for the lensless dual-color fluorescence imaging device with a hybrid filter.

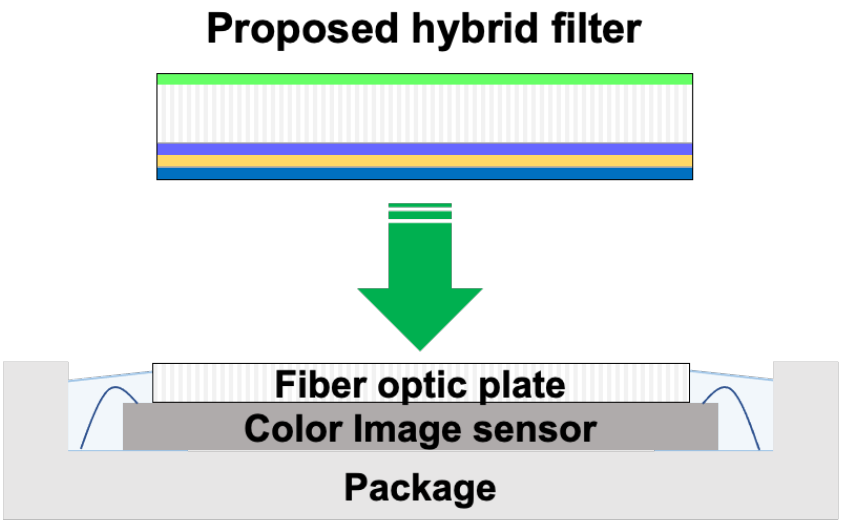

Figure 36 Schematic of the device assembly process for the lensless dual-color fluorescence imaging device with hybrid filter.

3.5 Device Evaluation

3.5.1 Sensitivity Spectrum Characteristics

In fluorescence observation, a high sensitivity performance of an imaging device is essential since it allows for detecting weak fluorescence signals, making it possible for fluorescent samples with low fluorescence intensity. It also helps distinguish fluorescence signals from background noise and improves the signal-to-noise ratio. Moreover, a highly sensitive device enables the detection of a wide range of fluorophores, facilitating multiplexing and the simultaneous imaging of multiple targets. In this work, the hybrid filter consisted of stacked longpass and notch interference filters and yellow and blue absorption filters mounted on an image sensor to achieve a sensitivity of dual-band for green and red fluorescence components.

In the evaluation, a spectrometer (micro-HR, Horiba Jobin Yvon) with a white light source (HPLS30-04, Thorlabs, USA) was used to measure the sensitivity spectrum. The curves of the emission spectra of green (eGFP) and red (mPlum) fluorescent proteins and the sensitivity spectrum of the proposed device were compared in Figure 37. The device was insensitive to the blue and yellow excitation light wavelength bands. The FOP was sandwiched between the interference filters in the proposed method. Since light is scattered in the FOP, the influence of multiple reflections between the interference filters was negligible. The proposed device exhibited green and red wavelengths sensitivity at the expected transmittance wavelengths of approximately 510 and 650 nm, respectively.

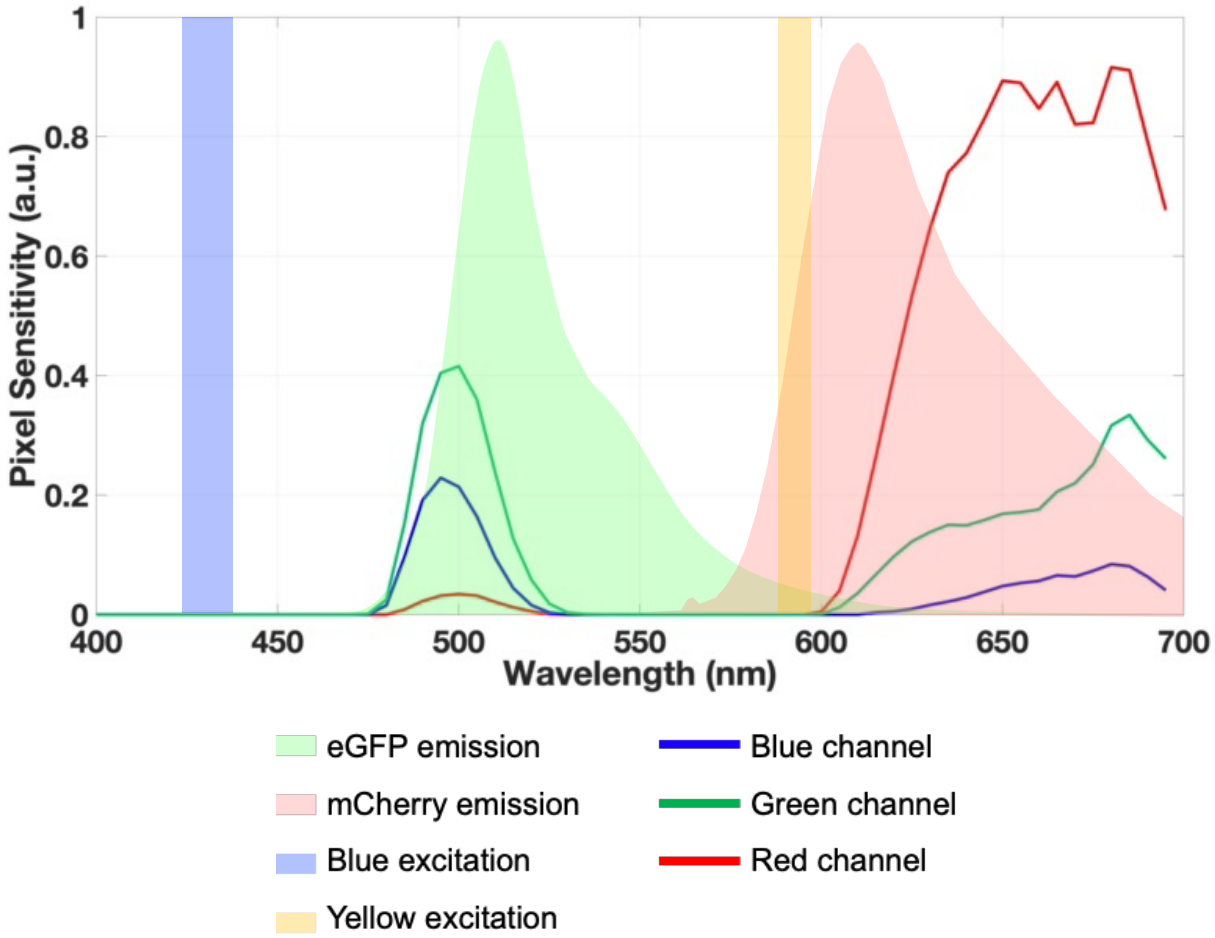

Figure 37 Sensitivity spectrum of the imaging device with a hybrid filter.

As previously mentioned, a commercially available color image sensor with a color filter was utilized in this study. Although the red pixels had high color selectivity, the blue and green pixels exhibited partial sensitivity to red in addition to the wavelength band of green fluorescence. Consequently, even when the signals of each pixel were isolated, the resulting image contained signals other than green or red. Thus, image processing to obtain a clear color-separated image was required.

3.5.2 Dual-color Fluorescent Microbeads Imaging Experiment

In order to ensure that the proposed lensless imaging device with a hybrid filter can be used for the dual-color fluorescence observation, the fluorescence imaging experiment in fluorescent microbeads was conducted. The proposed imaging device was placed onto the stage of a fluorescence microscope (BX51WI, Olympus, Japan) and placed under an objective lens (Mplan N5×/0.10NA, Olympus, Japan). The microscope was used to capture reference images, and a mercury lamp (U-RFL-T, Olympus, Japan) was utilized as the light source. Excitation filters were applied to limit the central excitation wavelength for the blue (MF434-17, Thorlabs, Japan) and yellow (86-737, Edmund Optics, USA) excitation lights at 434 nm and 594 nm, respectively. Throughout the experiment, the microscope's filter cubes were switched to irradiate the blue and yellow excitation lights, and the proposed imaging device was irradiated with blue or yellow excitation light at a normal incident angle corresponding to the excitation wavelength of the fluorescent targets. A schematic and photograph of the dual-color fluorescence imaging experimental setup are shown in Figure 38 and Figure 39, respectively.

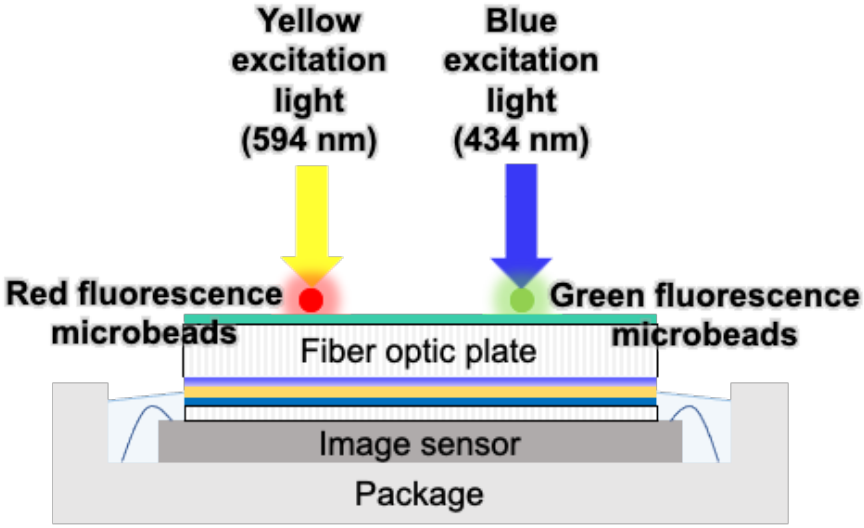

Figure 38 Schematic of the dual-color fluorescence imaging experimental setup.

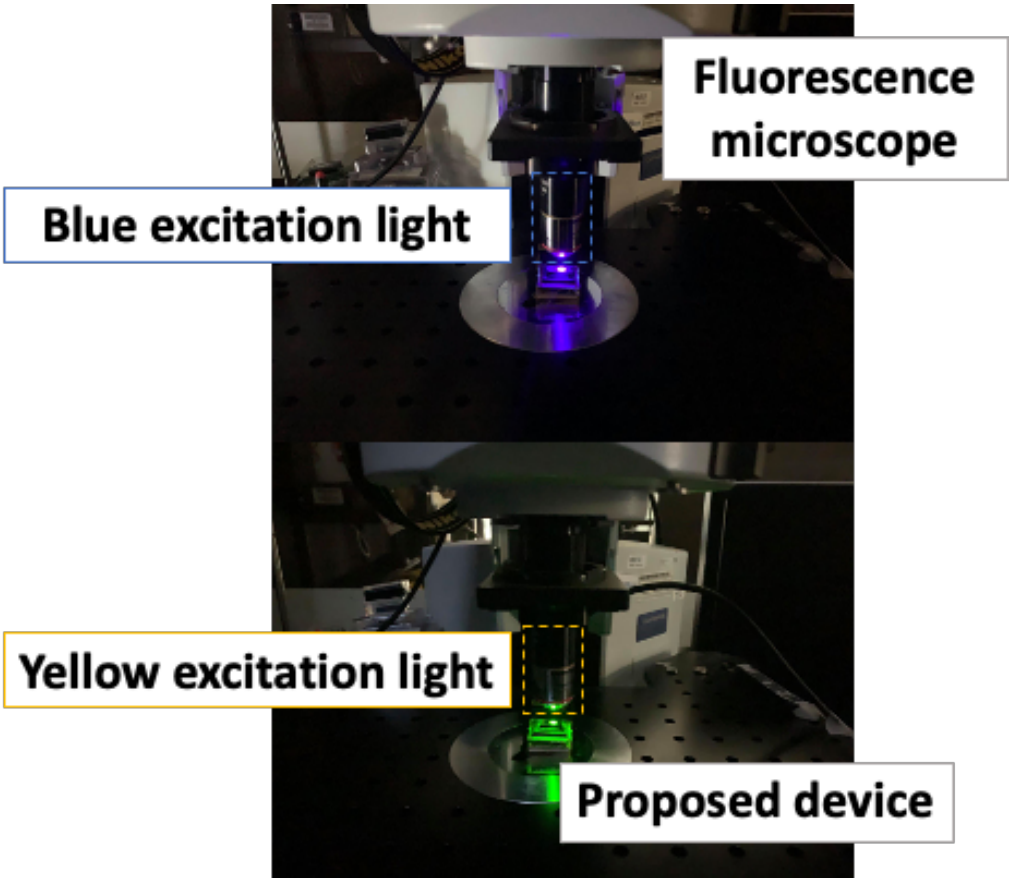

Figure 39 Photograph of the dual-color fluorescence imaging experimental setup. Experimental setup when irradiated with (top) blue and (bottom) yellow excitation lights.

In this experiment, yellow–green fluorescence microbeads (F8844, Thermo Fisher Scientific, USA) and crimson fluorescence microbeads (F8839, Thermo Fisher Scientific, USA) were used to contribute a fluorescence light. The excitation and emission spectra of the yellow–green and red (crimson) fluorescence microbeads were 505/515 nm and 625/645 nm, respectively. Both types of fluorescence microbeads were the same, with a diameter of 15 μm. The blue (434 nm) and yellow (594 nm) excitation lights were irradiated to excite the yellow–green and crimson fluorescence microbeads. The imaging area was 11.2 mm × 6.8 mm obtained from the imaging device. The images captured using the proposed device are shown in Figure 40.

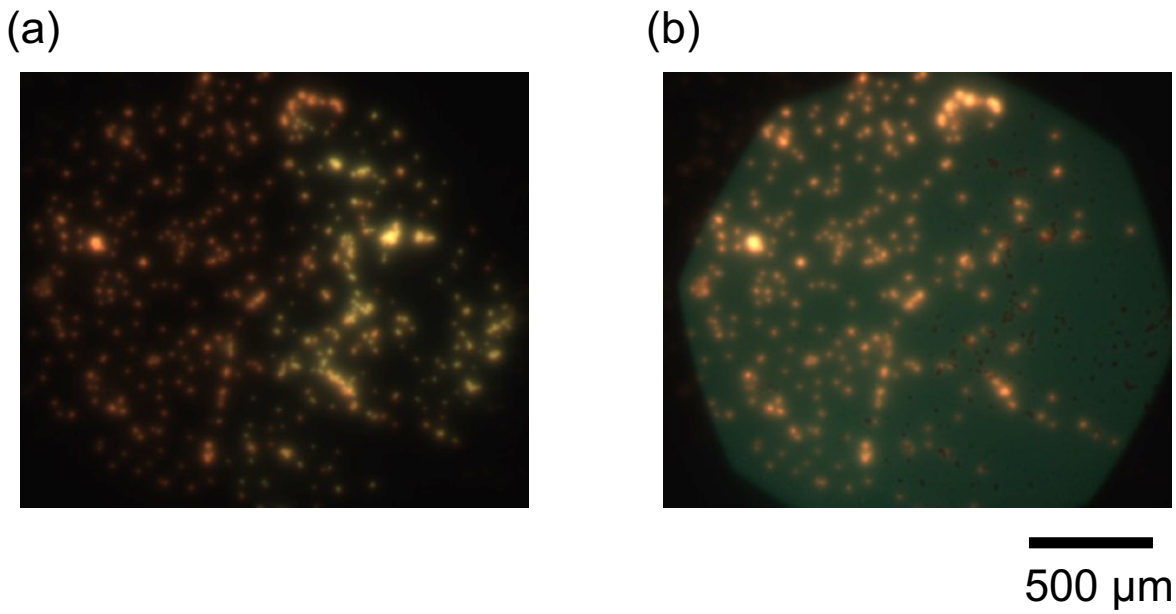

Figure 40 Images of yellow–green and crimson fluorescence microbeads captured by the proposed device.

During the observation, the yellow–green and red fluorescence microbeads were spread on a cover glass, and the beads were placed on the imaging device. The yellow–green and crimson fluorescent microbeads images excited blue and yellow excitation light were captured separately by the proposed device. The background of the captured images was almost black and strongly contrasted with both the yellow–green and red fluorescence microbeads. The results indicated that the proposed hybrid filter can reject both blue and yellow light excitation.

3.6 Image Processing for Color Separation of Fluorescent Target

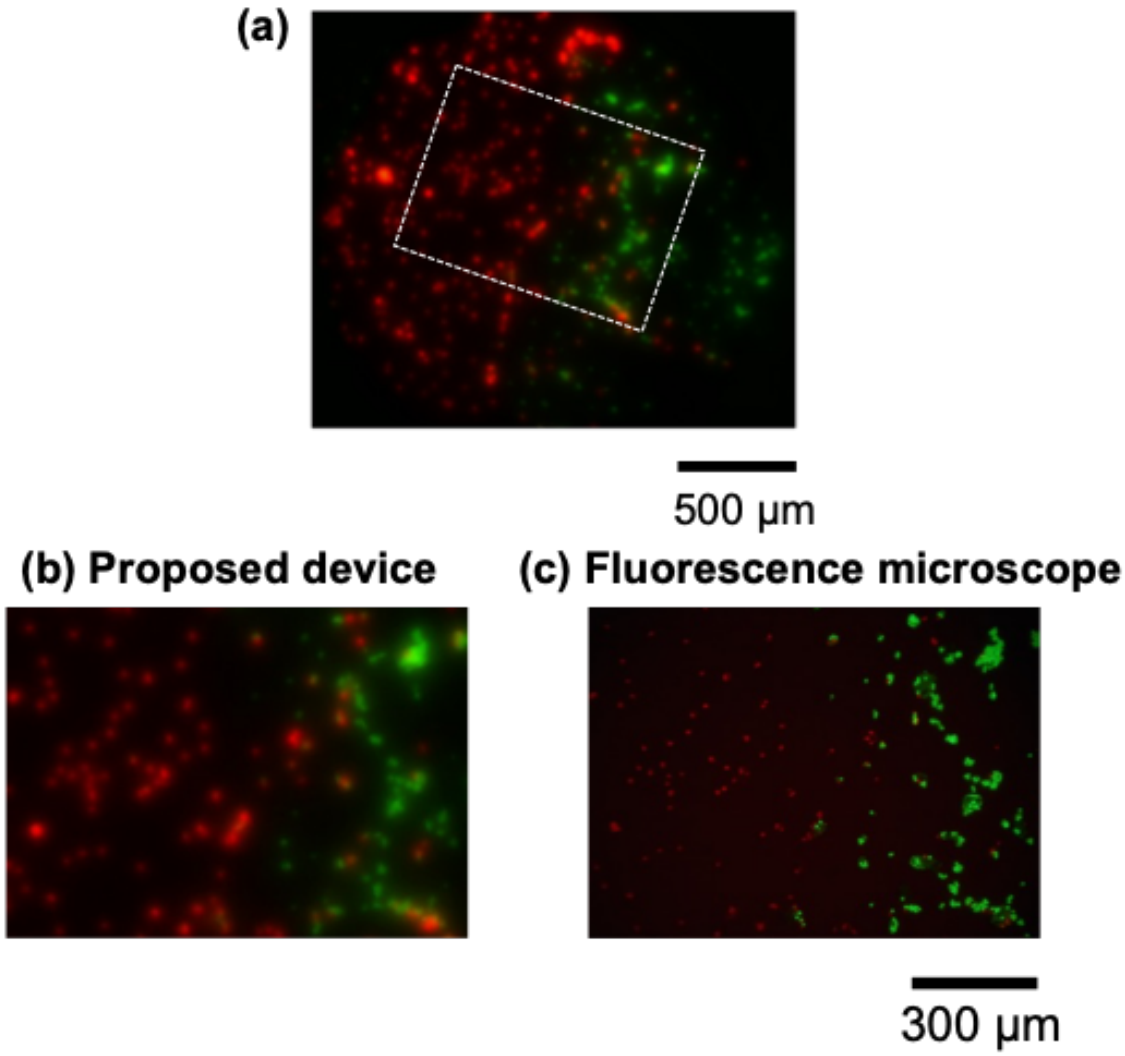

Figure 41 Processed images of fluorescent microbeads captured by the proposed device. Enlarged view of the part surrounded by the white dashed line captured from the (b) proposed device and (c) fluorescence microscope.

Figure 41 shows the images obtained by the post-image processing compared with that obtained by fluorescence microscope. The captured image from the lensless imaging device with the proposed hybrid filter indicates that this device filter exhibited a difference in sensitivity for fluorescence from the green and red beads but could not distinguish them separately. However, simple image processing was sufficient because an image of only red fluorescent beads could be

obtained by yellow excitation. Therefore, image processing was employed to separate the two fluorescence components. The process involved subtracting the yellow-excited red pixel image from the green pixel image of the blue-excited image, effectively removing the red beads image. The red pixel image was multiplied by a coefficient that canceled the red bead image. The results of the composite image of the red and yellow-green fluorescence microbeads are shown in Figure 41. Figure 41(a) shows the image obtained through image processing after the experiment. Enlarged images of the selected region outlined by the white dashed line in Figure 41(a) was captured using the proposed device (Figure 41(b)) compared with a fluorescence microscope (Figure 41(c)). Although the spatial resolution of the proposed device was low, the green and red beads were clearly observed.

3.7 Discussion

3.7.1 Transmittance Characteristics and Hybrid Filter Configuration

The configuration of the proposed hybrid filter was determined based on the transmittance characteristics of each filter, considering the matter of scattered light when light passes through the FOP, which can compromise the performance of the interference filter. The longpass interference filter was arranged on top of the FOP, while the notch interference filter was arranged on the opposite side to achieve the optimum excitation rejection performance. This arrangement demonstrated superior characteristics compared to the reverse structure. The yellow absorption filter (VY1108) and blue absorption filter (FDG-007) were arranged below the FOP to absorb the excitation light.

In terms of green fluorescence detection, in this study, the blue excitation light was effectively rejected by six orders of magnitude, as shown in Figure 29, while the transmission of the green wavelength band was confined using a bandpass filter. The wavelength selectivity of the yellow absorption filter was improved by changing the yellow dye type from VY3150 to VY1108. The absorption filter fabricated from the VY1108 dye exhibited higher wavelength selectivity compared to the VY3150 dye used in the previous study, enabling efficient transmission of green fluorescence. The imaging results with fluorescent microbeads confirmed the device's ability to detect green fluorescence. Table 1 provides a comprehensive comparison of the device characteristics and performance between the current study and the previous report.

In the case of red fluorescence detection, the yellow excitation light was significantly reduced by five orders of magnitude or more, as shown in Figure 30. Within this wavelength range, both the FOP and FDG-007 exhibited low autofluorescence, allowing for a higher rate of excitation light reduction by the absorption filter layer. However, it was observed that the excitation light removal performance of the notch interference filter was not as effective as that of the longpass interference filter in the blue wavelength band. Furthermore, in the hybrid filter configuration, the excitation light passes through the FOP before reaching the notch interference filter. To prevent warpage caused by filter formation, each filter had to be deposited on both sides of the FOP, which function as a stable substrate. However, a challenge remains as the scattering caused by the FOP limits the utilization of the filter performance. Nevertheless, it is possible to improve the filter characteristics by arranging the notch and longpass interference filters on one side without any issues. Table 1 provides a comprehensive comparison of the device characteristics and performance between the current study and the previous report.

	K. Sasagawa *et al.* [3]	K. Sasagawa *et al.* [30]	W. S. Hee *et al.* [62]	This study
Target fluorescence	Green	Green	Cyan and yellow (FRET)	Green and red
Excitation wavelength (nm)	450	448	434	434 and 594
Excitation light transmittance	10^{-8}	-	10^{-5}	10^{-6}
Transmission band of hybrid filter (nm)	>510	510-570	470-560	495-515 and >625
Imaging area (mm^2)	0.9×2.0	11.26×5.98	0.9×2.0	11.2×6.8

Table 1 Comparison of the device characteristics and performance from this study with from our previous reports.

3.7.2 Issues in Fluorescence Separation

The issue of the green channel appearing as red presents a challenge in this study. Although image processing techniques were employed to resolve this problem, artifacts remained near regions with intense red fluorescence due to the higher sensitivity of red compared to green. The filter configuration used in this study did not effectively eliminate the longer-wavelength side of the red wavelength band. However, this can be addressed by making specific areas transparent and adjusting the balance between green and red sensitivity. Furthermore, the sensitivity of green pixels was approximately 40% of that of red pixels around a wavelength of 700 nm, suggesting that accuracy could be improved by reducing sensitivity in this range. While a commercially

available color image sensor was utilized to capture green and red signals in this study, alternative methods that do not rely on filters can be explored to observe intermediate wavelengths [99].

3.7.3 Spatial Resolution

The spatial resolution in contact imaging devices, such as the one demonstrated in this study, decreases with increasing distance. This reduction is particularly noticeable in fluorescence observation, where the emitted fluorescence from the target exhibits isotropic characteristics. In comparison to a fluorescence microscope, the proposed method exhibited lower resolution, as shown in Figures 41(a) and (b). To improve the resolution, deconvolution and image restoration techniques based on sparse sampling can be employed. However, restoring densely sampled images remains challenging. Recent studies have explored the integration of image processing with simple optical systems using methods like incident angle limitation or phase masks, which are highly compatible with the proposed method [95]–[97], [100]–[102]. To overcome the spatial resolution limitations, interference filters can be applied by utilizing film formation or transfer on a thin glass substrate. Although the FOP layer needs to be removed because a distance can be left on the sensor, this method can be considered to resolve the current issue.

3.8 Summary

The objective of this study was to develop a lensless system capable of highly sensitive dual-color fluorescence observation. To achieve this, a dual-band hybrid filter was fabricated, which exhibited a high excitation light rejection performance in the blue and yellow wavelength bands while transmitting green and red fluorescence excited by these wavelengths. The filter configuration was integrated into a commercially available color image sensor. A hybrid filter

composed of longpass and notch interference filters was deposited on both sides of the FOP to realize bandpass characteristics. The yellow (VY1108) and blue (FDG-007) absorption filters were also used in the proposed hybrid filter configuration to absorb blue and yellow excitation light. Green and red fluorescent beads were successfully separated through image processing techniques. These results indicate the potential use of the proposed lensless imaging device for observing the activity of cultured cells, particularly due to its compact size and the ability to capture fine details. Further investigations and applications of this device have great potential for advancing fluorescence imaging in cellular studies.

Chapter 4

Time-lapse Cell Observation System for Lensless Imaging Device

4.1 Overview

Time-lapse cell imaging is a powerful technique that enables real-time observation and analysis of living cells over a specific period. This approach has reformed cell biology research by providing valuable insights into dynamic cellular processes, including cell division, migration, and intracellular signaling [103], [104]. Time-lapse imaging allows the study of cellular behavior and responses to external stimuli by capturing a series of sequential images, contributing to a better understanding of various biological processes.

This system relies on the use of specific microscopy techniques to capture high-resolution images of living cells over time. Various microscopy approaches can be employed, including brightfield microscopy, fluorescence microscopy, and confocal microscopy. Utilizing sensitive detectors, high-speed cameras, and advanced imaging software to acquire sequential images at specific intervals enables the capabilities of the visualization of cellular events.

4.2 Problem Statement and Purpose

Real-time imaging of cells requires precise control of environmental conditions to ensure the viability of cells. The factors such as temperature, pH, cell medium composition, growth conditions, and osmolarity play crucial roles in maintaining optimal conditions during image

acquisition. Mammalian cells are typically cultured in a defined medium supplemented with growth factors and buffered to maintain a constant pH. Most cell culture methods rely on a 5% CO_2 atmosphere to maintain physiological pH conditions. Another critical factor for mammalian cell viability is temperature, which is usually cultured at 37°C.

The purpose of this work is to implement a lensless microscopy platform integrated with a time-lapse imaging system for observing cultured cells. Conducting long-term cell observation experiments outside the incubator presents a challenge due to the factors of cell viability, as mentioned above. The proposed device will be placed within a CO_2 incubator, enabling the monitoring of cell behavior over several hours. Careful handling of cells under appropriate conditions for live-cell imaging is essential. However, the generation of heat by the imaging device can be detrimental to cell viability since mammalian calls typically respond to the temperature range of 33 to 40°C, and it has been recognized that temperatures between 40 and 47°C cause cell death in a predictable manner [105]–[108]. Therefore, the development of a power control system for the imaging device is crucial. This research aims to provide a solution for real-time microscopy within a CO_2 incubator, allowing for long-term observation of cultured cells and advancing our understanding of cellular dynamics.

4.3 System Overview

To solve the problem of the heat generated by the imaging device, a time-lapse imaging system was demonstrated, incorporating a power control system for the image sensor. This system allowed for selective power shutdown, reducing the device's temperature. In the prototype system, a relay board, designed in our laboratory, was used to control the power supply of the USB 3.0 camera (STC-MCS231U3V, Omron Sentech) through a power switch IC (RT9728AHGE,

Richtek). The relay board was inserted between the lensless imaging device and the computer, and it was connected to the imaging software (StViewer, Omron Sentech). To command the light source system and relay board, an embedded system Arduino board (UNO-R3, Arduino) was employed.

This study aimed to develop a lensless imaging device suitable for long-term observation of cultured cells. The imaging device would be placed inside an incubator and used overnight in practical experiments. To operate the imaging process, automation scripts were created to control the imaging software. These scripts, implemented with AutoIt, a freeware tool for automating Windows GUI, enabled the continuous operation of the imaging experiment. Additionally, the automation scripts communicated with an Arduino board to turn on/off the light source and power of the imaging device by disconnecting it from the computer. The block diagram and photograph of a prototype of the time-lapse cell imaging system are shown in Figures 42 and 43.

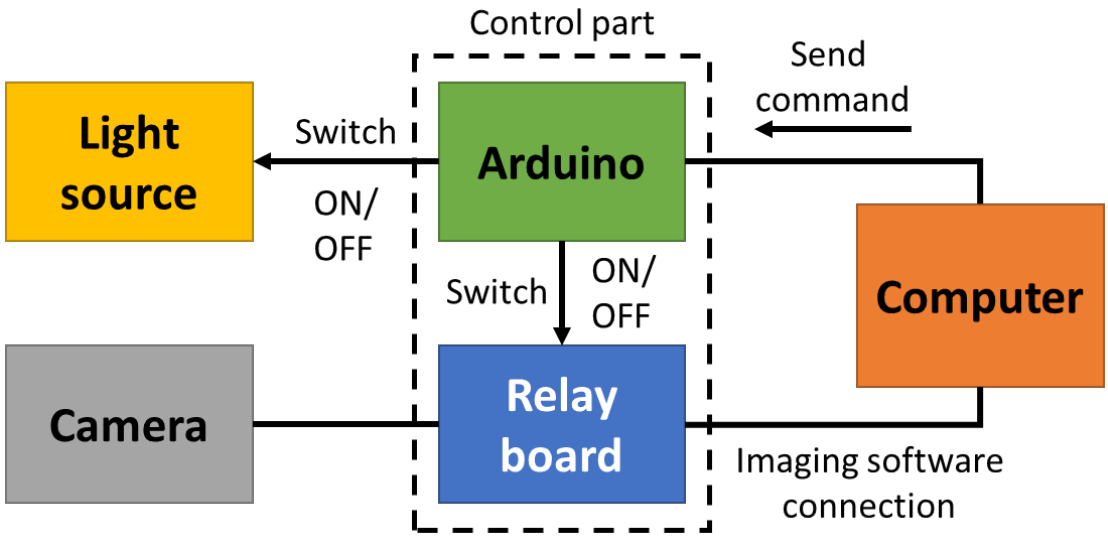

Figure 42 Block diagram of a prototype time-lapse cell imaging system.

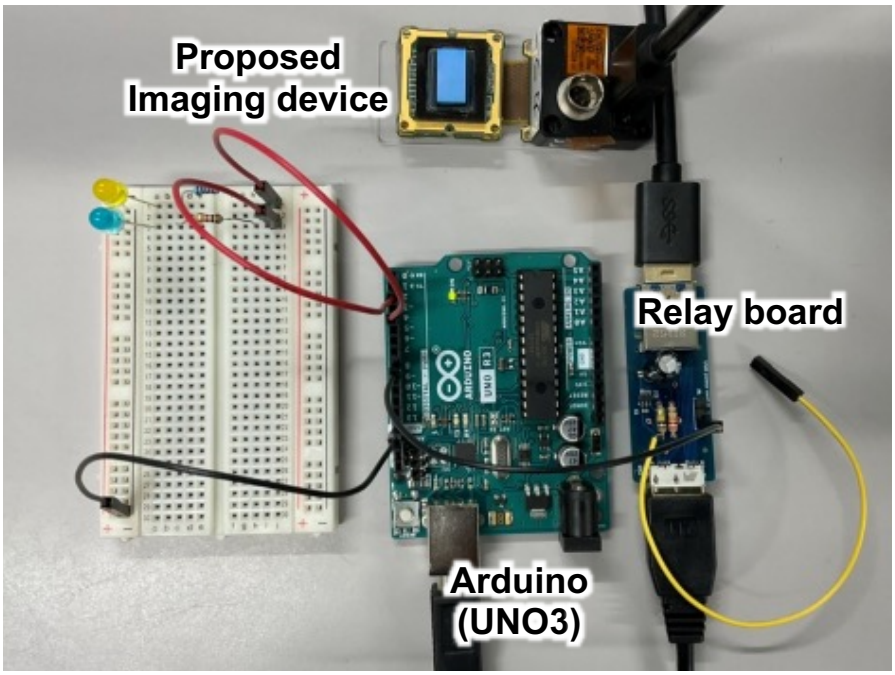

Figure 43 Photograph of the prototype time-lapse imaging system.

4.4 Device Evaluation

4.4.1 Device Temperature Measurement

The lensless imaging device proposed in this study is aimed to use for time-lapse imaging in living cells. The temperature of the imaging device is attempted to maintain the optimal environment for cell growth. The temperature is 33 to 40°C for most human and mammalian cells to maintain the cell lines, preferably at 37°C. The imaging device generates high heat once it is connected to the computer. The temperature of the imaging device can be maintained by controlling the operating time for the imaging device. The temperature of the imaging device was measured using a thermocouple thermometer (BAT7001H, Physitemp, USA) and temperature transducer (AD590, Analog Devices, USA). The AD590 is a 2-terminal integrated circuit temperature transducer that produces an output current proportional to absolute temperature. The

transducer received 7V from the DC power supply and directed an electric current through a 15kΩ resistor, generating a voltage across the resistor. The Arduino was used to read the voltage across the resistor and calculate the temperature at that specific moment. A schematic of the circuit connected with the AD590 transducer is shown in Figure 44. The constant current is 1 μA/K produced by AD590 and was calibrated to 298.2 μA output at 298.2 K (25°C). The temperature can be calculated by:

$$T = (I / (1\mu A / K)) - 273.2$$

where I is the current produced by the AD590, and T is the temperature in degree Celsius.

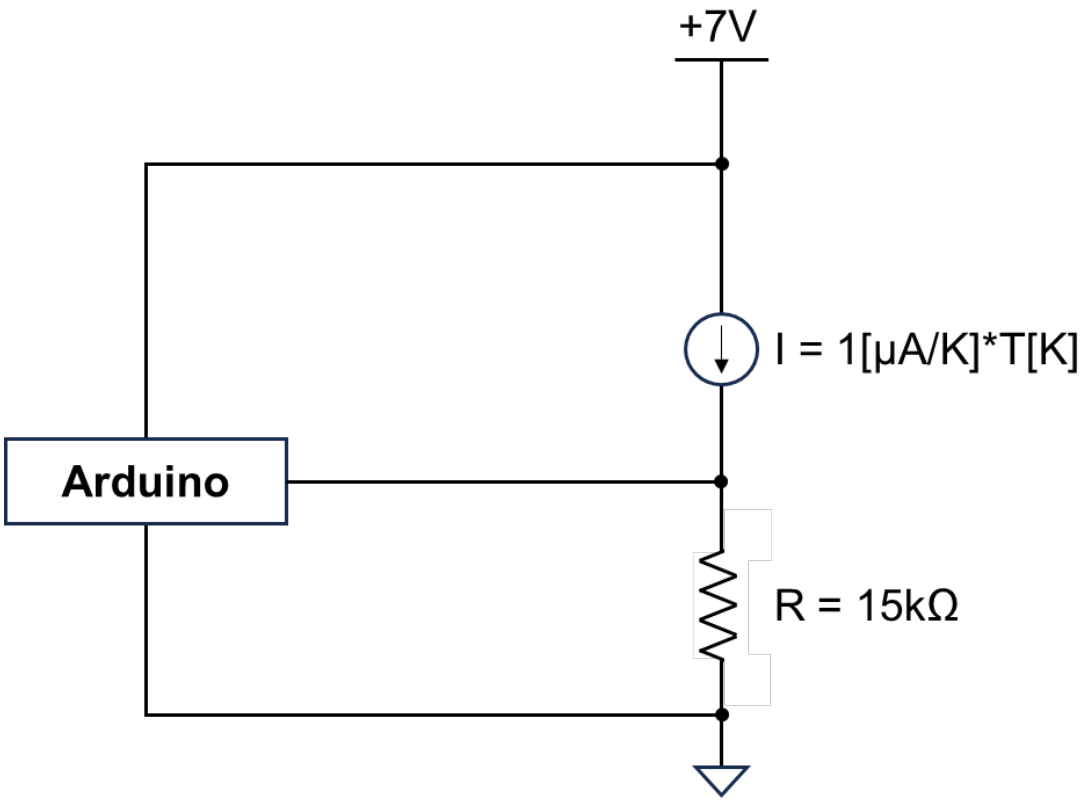

Figure 44 Schematic of the circuit connected with the AD590 transducer.

The graph plotted to indicate a relationship between time and temperature during the imaging process is shown in Figure 45. The result shows that the period for the imaging device to increase the temperature from 37 to 41°C is 30 seconds once the image sensor is operated. Reversely, the period for the image sensor to decrease the temperature from 41 to 37°C is 4 minutes while the camera was disconnected. Thus, it was considered that time-lapse imaging should be performed at 4-min intervals to maintain the optimal temperature for cell viability. The time for the imaging period of the imaging device is controlled by applying this measurement result with the power control part in the proposed time-lapse cell imaging system.

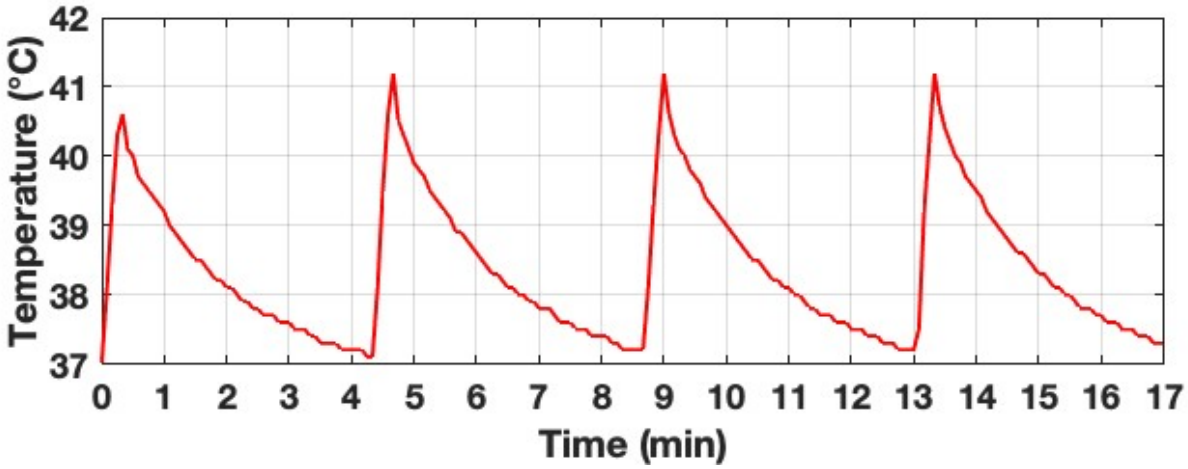

Figure 45 Relationship between time and temperature during the imaging process.

4.5 Time-lapse Cell Imaging Experiment

4.5.1 Cell Culture

HeLa cells were first cultured in mammalian cell culture medium, Dulbecco's Modified Eagle's Medium, high glucose with GlutaMAX™ supplement (DMEM, 10566-016; Thermo Fisher Scientific, USA) supplemented with 10% fetal bovine serum (FBS, SH30071.03; Thermo

Fisher Scientific, USA). The cells were introduced into the tissue culture dish, maintained in a 5% CO_2 humidified atmosphere at 37°C, and cultured for 3 days before the experiment. Next, the cells were harvested with trypsin (0.5% Trypsin-EDTA (10×), no phenol red, 15400054; Thermo Fisher Scientific, USA) and resuspended in DMEM. Finally, the cells were seeded onto a cover glass bottom chamber of 0.1-mm-thick used for a time-lapse cell imaging experiment and were rested in the incubator for 1 night for the cell growth at the bottom of the chamber. The photograph of the cell chamber is shown in Figure 46.

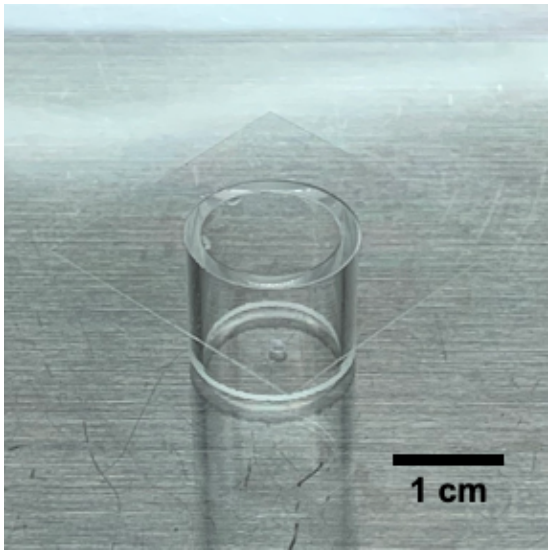

Figure 46 The cover class bottom chamber for cell imaging experiment.

4.5.2 Experimental Setup

In the experimental setup, red surface-mount LEDs with a center wavelength of 644 nm (TLRE1002A, Toshiba, Japan) were used as the light source for bright-field imaging. These LEDs were set at 9 cm above the imaging area of 11.2 mm × 6.8 mm. and positioned at the center of the image sensor's pixel array. The photograph of the time-lapse bright-field imaging experimental setup is shown in Figure 47.

Throughout the imaging process, HeLa cells were seeded onto a cover glass bottom chamber fabricated in our laboratory, and it was placed contacted with the imaging device's pixel array. The time-lapse imaging at 4-min intervals was performed inside the CO_2 incubator for 1 hour. The imaging process was controlled by the proposed prototype system. Thus, the light source and the power of the imaging device were switched on/off, and the images were captured automatically.

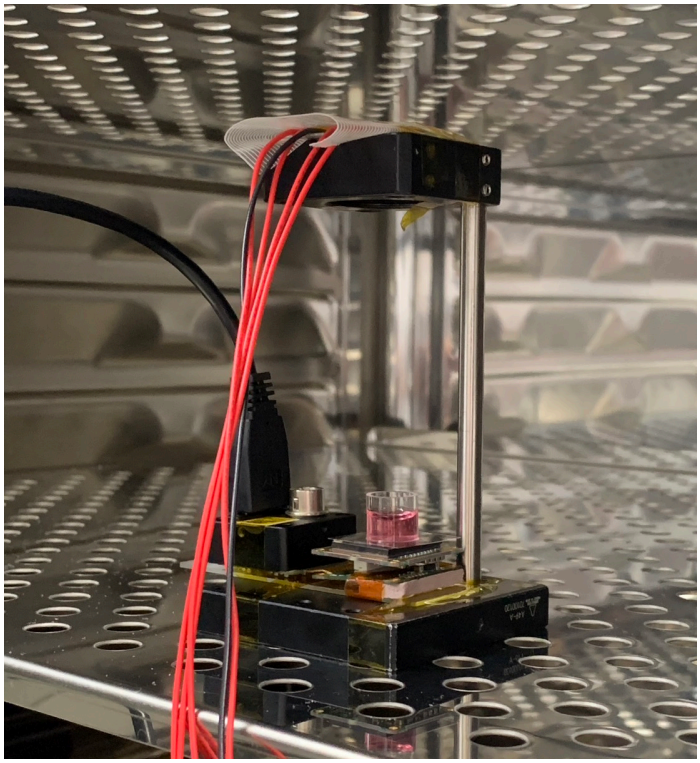

Figure 47 Photograph of time-lapse bright-field imaging experimental setup in the incubator.

4.5.3 Time-lapse Bright-field Imaging in Cultured Cells

The time-lapse bright-field imaging in cultured cells was conducted to ensure that the proposed prototype time-lapse system can be used with the lensless imaging device for cell observation. Figure 48 shows the image captured by the proposed lensless imaging device. The

cultured cells were seeded onto the cover glass bottom chamber with DMEM cell culture medium. The cell chamber was placed on the pixel array of the imaging device, which has a 5.86 µm × 5.86 µm pixel size. The average cell size is 15.7 µm in diameter. The result shows that the raw images of the cultured cells originally captured by the proposed device exhibit low contrast with the background, making it difficult to see the cells clearly. However, by simply adjusting the contrast and brightness, a clear image of the cultured cells can be easily obtained.

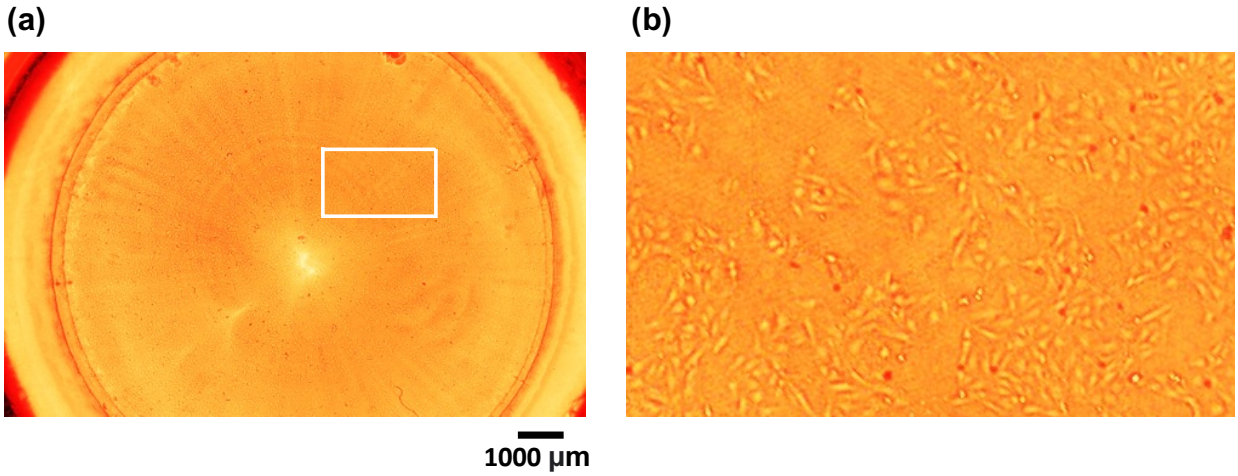

Figure 48 The bright-field image of cultured cells captured by the lensless imaging device.
(a) Raw image captured by the proposed device.
(b) Cropped image from (a) in the outlined area.

Figure 49 shows the processed imaging from time-lapse bright-field imaging. The images displayed on the right side are the cropped images from the image on the left side. The cropped area is outlined in the red rectangle line. The cell's shape and movement changes are outlined in white dashed circles. The clear images of cultured cells were obtained after adjusting the contrast and brightness. The time-lapse imaging results confirm that the cells could be grown during the experiment, represented by the movement of the cells, as shown in Movie 1 in Appendix D.

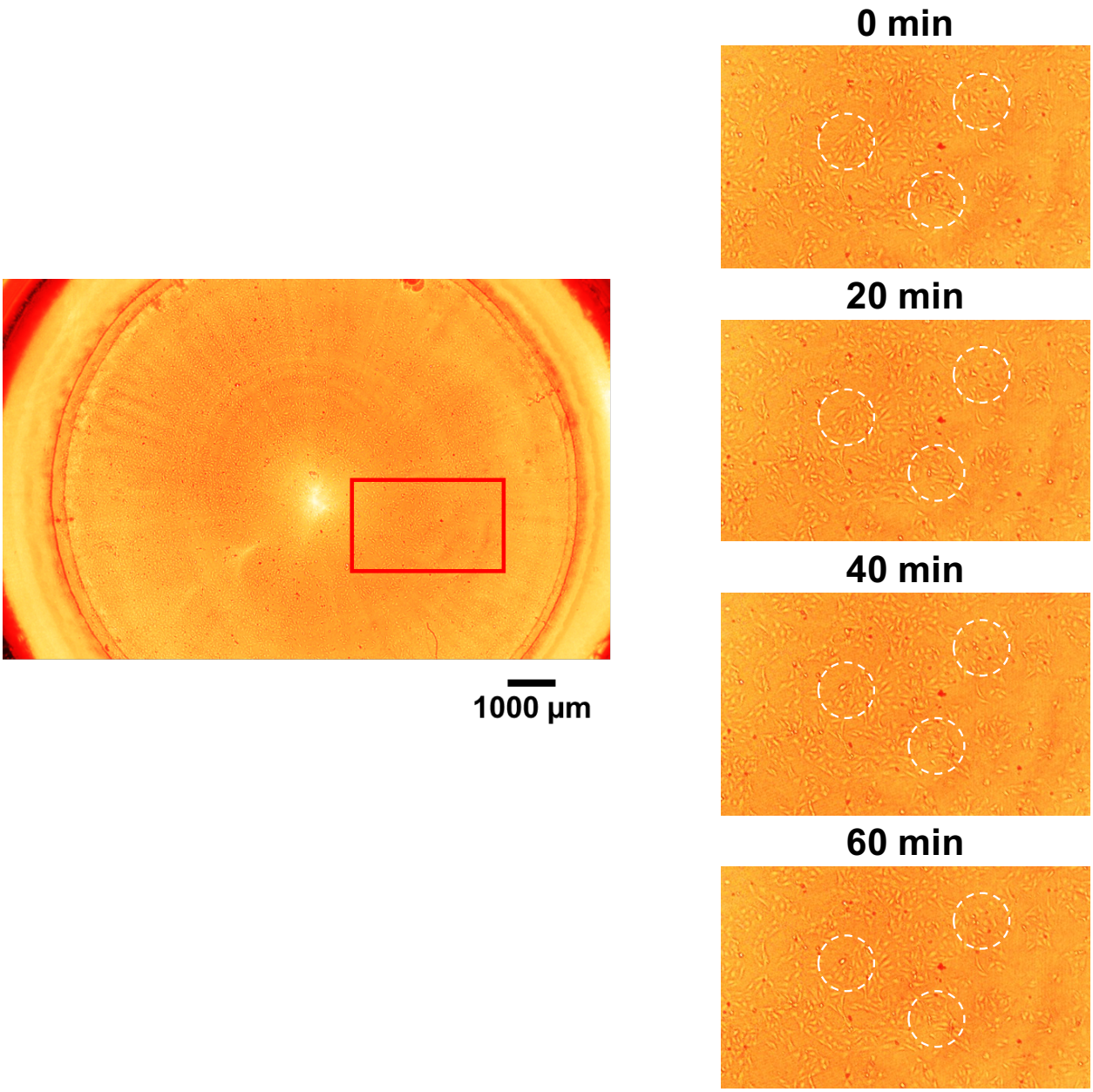

Figure 49 Processed time-lapse bright-field imaging images.

4.5 Summary & Discussion

A time-lapse system was demonstrated for the observation in living cells. This imaging technique allows for continuous monitoring and non-invasive observation of cell behaviors. This work proposes to utilize the advantage of a lensless imaging device in terms of its compactness to perform real-time cultured cell observation in the incubator over time. Employing the time-lapse imaging technique can give us a better understanding of dynamic cellular processes, which is fundamental to biological study.

In this work, the commercially available USB 3.0 camera was used as an imaging device. For the live-cell imaging purpose, the imaging device was considered to place in the incubator for long-term cell observation conducted for several hours under the condition of 5% CO_2 at 37°C to maintain cell viability. Thus, the temperature of the imaging device should be at 37°C to keep the cell in a healthy condition. Currently, general image sensors commonly feature integrated analog-to-digital converters (ADCs) for each row of pixel arrays, aiming to reduce noise and increase operational speed. However, this integration increases heat generation. Therefore, the camera was modified, removing its packaging for lensless imaging purposes, and equipped with thermally conductive materials to improve heat dissipation. However, this imaging device still generated temperatures exceeding 50°C during operation due to the power consumption of the image sensor even outside the incubator.

Moreover, the ambient temperature is high in the incubator, and the heat dissipation efficiency is low. This temperature issue was resolved by controlling the power of the imaging device, and the temperature decreased when it was disconnected from the computer. The evaluation of the imaging device's temperature and time-lapse imaging results indicate that it is sufficiently possible to perform imaging at a 4-min interval time for the time-lapse imaging while

keeping the optimal condition for cell growth. To improve the heat dissipation efficiency of the imaging device, a heat sink with a specific design might be required, but it is still challenging because of the maximum temperature generated at the center of the image sensor pixel array. Thus, adding any heat transfer material is difficult because the observation target must contact the image sensor's pixel array. Another method is to design a dedicated image sensor for specific applications. Unlike general image sensors, the pixels in this dedicated image sensor are designed to consume low power and generate minimal heat. Under conditions like those in this study, where high-speed operation is not required, integrating power-intensive circuits such as analog-to-digital converters (ADCs) within the chip becomes unnecessary. By placing these circuits outside the chip, the heat load on the cells can be effectively reduced.

Another important aspect of this work is light source intensity, which is related to the ability of object detail to be distinguished when compared to the background of images. The captured images of cultured cells present low contrast to the background, and there is the reflection of the light with the cover glass bottom chamber appears at the center of the images. However, these issues were resolved by simply adjusting the contrast and brightness of images.

In addition, a lensless imaging system based on the holographic microscopy technique can be applied to bright-field imaging since it is not necessary to place the observation target close to the image sensor, avoiding the issue of the heat generated from the imaging device. Additionally, the resolution can be improved because this technique relies on the phase information scattered by the observation target. However, the inability to observe fluorescence significantly limits its application. The recent advancement in fluorescence holography microscopes that use lenses has realized a possible solution [109]. It is expected that successfully incorporating these technologies

would allow for fluorescence observation with high spatial resolution while maintaining the advantages of lensless systems in terms of compactness.

In summary, the proposed prototype time-lapse system for cell observation using a lensless imaging device was able to address the limitation of heat generated by the imaging device, and it can be utilized for time-lapse bright-field imaging in cultured cells with a wide field of view, which suggests the capability to apply for further development for fluorescence imaging with the proposed hybrid filter.

Chapter 5

Conclusion and Future Prospects

5.1 Conclusion

Lensless microscopy has emerged as a promising alternative to conventional lens-based microscopy due to its compactness, versatility, and potential for high-resolution imaging. However, there remain certain obstacles to address, particularly in fluorescence observation and multicolor imaging, which require additional improvement for the emission filter to reach a high performance of excitation light rejection. Therefore, this research purposed to implement a lensless imaging device with a hybrid filter for dual-color fluorescence and time-lapse cell observation. The proposed lensless dual-color fluorescence imaging device employs the hybrid filter to selectively transmit the wavelengths of fluorescent targets and eliminate excitation light. The hybrid filter was assembled with an image sensor to visualize green and red fluorescence components. The blue and yellow excitation lights with the central wavelength of 434 and 594 nm functioned for the green and red fluorescence excitation with respect to emission spectra of green (eGFP) and red (mCherry) fluorescent proteins.

The hybrid filter utilized the fiber optic plate (FOP) to form a bandpass characteristic by depositing the interference filters on both sides. The interference filters, including longpass and notch interference filters, were employed to selectively eliminate the blue and yellow excitation wavelengths. The arrangement of the interference filters was attentively considered to avoid the issues of light scattering and autofluorescence exhibited within the FOP, as well as to achieve high performance of excitation light rejection. Thus, based on the evaluation results, the longpass

interference filter was determined to place on the top side of the FOP in the direction of the excitation light incident. The yellow (VY1108) and blue (FDG-007) absorption filters were introduced in the hybrid filter configuration to absorb the scattered components passed through the bandpass interference filter. In the case of the absorption filter, the optimal performance was considered based on the autofluorescence observation and the relationship between effective transmittance and the absorption filter's thicknesses results. Thus, the arrangement of the proposed hybrid filter was determined to be the longpass and notch interference filters, yellow and blue absorption filters, respectively. This filter's arrangement rejects the light in blue and yellow wavelength bands with an excitation rejection ratio of up to 10^{-6}. In addition, this arrangement of the interference filters shows lower autofluorescence than the reverse case. When equipped with the proposed hybrid filter with a lensless imaging device, it is sensitive to green and red wavelengths of approximately 510 and 650 nm. Green and red fluorescent components presented in images obtained using the proposed lensless imaging device were successfully separated, with the involvement of image processing.

Furthermore, the lensless imaging device implemented with the prototype time-lapse imaging system for cell observation can resolve the issues of heat generated by the imaging device. The proposed system can control the temperature of the imaging device to be at optimal conditions for cell growth. In addition, this proposed device has a wide field of view with an imaging area of 67 mm^2 and the capability to grasp the details of the cell culture images obtained from time-lapse bright-field imaging. This ensures that the proposed lensless imaging device is well-suited for studying biological processes.

5.2 Future Prospects

Lensless microscopy holds excellent potential in microscopy technology by enabling the development of comprehensive and portable imaging systems. Further advancements in this research area can lead to significant breakthroughs in various scientific and biomedical applications. The first potential is implementing the hybrid filter with a lensless microscopy platform for fluorescence imaging in cultured cells. Even though the time-lapse bright-field imaging results suggest that the proposed device can be used for live-cell observation, some details of the cellular processes cannot be obtained only from bright-field images. Thus, the fluorescence imaging technique could enhance a better understanding of the biological processes study.

To conduct time-lapse dual-color fluorescence imaging, the main object that has to consider is the excitation light source. In the experimental setup, blue and yellow excitation lights are used, switching during the experiment to excite fluorescence targets, and it has to collimate the light when irradiated to the samples. In addition, the intensity of the light source is crucial. Thus, a complex setup for the excitation light source is required.

The second potential is applying the proposed time-lapse system with a wireless system. Since the imaging device should be placed in the CO_2 incubator during the observation, the peripheral wires of the electrical components that connect with the components outside the incubator might be an obstacle in the experiment if the incubator door cannot close properly because the incubator door openings are crucial factors in maintaining a stable environment for cell cultures.

Lastly, further development of the hybrid filter with a lensless microscopy platform could hold significant potential for other biological studies, such as developing into implantable

neuroscience devices. Its applicability extends to other fields, such as material science, chemistry, and medical research.

References

[1] B. Alberts, A. Johnson, J. Lewis, M. Raff, K. Roberts, and P. Walter *Molecular Biology of the Cell*, 6th ed, Garland Science, 2017.

[2] J. W. Lichtman, and J. A. Conchello, "Fluorescence microscopy," *Nature Methods*, vol. 2, no. 12, pp. 910–919, 2005.

[3] K. Sasagawa, A. Kimura, M. Haruta, T. Noda, T. Tokuda, and J. Ohta, "Highly sensitive lens-free fluorescence imaging device enabled by a complementary combination of interference and absorption filters*," Biomedical Optics Express*, vol. 9, no. 9, pp. 4329-4344, 2018.

[4] J. Joshi, M. Rubart, and W. Zhu, "Optogenetics: Background, Methodological Advances and Potential Applications for Cardiovascular Research and Medicine," *Frontiers in Bioengineering and Biotechnology*, vol. 7, 466, 2020.

[5] P. W. Hawkes, and J.C.H. Spence, *Science of Microscopy*, Springer, vol. 1, pp.130-131, 2007.

[6] P. Michel, A. Antony, C. Trefois, A. Stojanovic, A. S. Baumuratov, and K. Kozak, "Light microscopy applications in systems biology: opportunities and challenges," *Cell Communication and Signaling*, vol. 11, no. 1, 24, 2013.

[7] P. N. Hedde, "miniSPIM—A Miniaturized Light-Sheet Microscope," *ACS Sensors*, vol. 6, no. 7, pp. 2654–2663, 2021.

[8] M. L. Rynes, D. A. Surinach, S. Linn, M. Laroque, V. Rajendran, J. Dominguez, O. Hadjistamoulou, Z. S. Navabi, L. Ghanbari, G. W. Johnson, and M. Nazari, "Miniaturized

head-mounted microscope for whole-cortex mesoscale imaging in freely behaving mice," *Nature Methods*, vol. 18, no. 4, pp. 417–425, 2021.

[9] J. Senarathna, K. Murari, R. Etienne-Cummings, and N. V Thakor, "A Miniaturized Platform for Laser Speckle Contrast Imaging," *IEEE Transaction on Biomedical Circuits and Systems*, vol. 6, no. 5, pp. 437–445, 2012.

[10] K. K. Ghosh, L. D. Burns, E. D. Cocker, A. Nimmerjahn, Y. Ziv, A. E. Gamal, and M. J. Schnitzer, "Miniaturized integration of a fluorescence microscope," *Nature Methods*, vol. 8, no. 10, pp. 871–878, 2011.

[11] D. Aharoni, B. S. Khakh, A. J. Silva, and P. Golshani, "All the light that we can see: a new era in miniaturized microscopy," *Nature Methods*, vol. 16, no. 1, pp. 11–13, 2019.

[12] J. H. Park, J. Platisa, J. V Verhagen, S. H. Gautam, A. Osman, D. Kim, V. A. Pieribone, and E. Culurciello, "Head-mountable high speed camera for optical neural recording," *Journal of Neuroscience Methods*, vol. 201, no. 2, pp. 290–295, 2011.

[13] F. C. Tabak, E. C. M. Disseldorp, G. H. Wortel, A. J. Katan, M. B. S. Hesselberth, T. H. Oosterkamp, J. W. M. Frenken, and W. M. van Spengen, "MEMS-based fast scanning probe microscopes," *Ultramicroscopy*, vol. 110, no. 6, pp. 599–604, 2010.

[14] P. Reinig, H. G. Dallmann, M. Schwarzenberg, J. Ziebarth, J. Knobbe, J. Junek, R. Herbst, J. Rathert, R. Gerlach, U. Blache, and S. Tretbar "MEMS-based confocal laser scanning fluorescence microscopy for tumor demarcation in oncological surgery," in *Advanced Biomedical and Clinical Diagnostic and Surgical Guidance Systems XX*, vol. 11949, pp. 32-40, 2022.

[15] C. Yin, A. K. Glaser, S. Y. Leigh, Y. Chen, L. Wei, P. C. S. Pillai, M. C. Rosenberg, S. Abeytunge, G. Peterson, C. Glazowski, and N. Sanai, "Miniature in vivo MEMS-based line-scanned dual-axis confocal microscope for point-of-care pathology," *Biomedical Optics Express*, vol. 7, no. 2, pp. 251-263, 2016.

[16] E. Rustami, K. Sasagawa, K. Sugie, Y. Ohta, M. Haruta, T. Noda, T. Tokuda, and J. Ohta, "Needle-Type Imager Sensor With Band-Pass Composite Emission Filter and Parallel Fiber-Coupled Laser Excitation," *IEEE Transactions on Circuits and Systems I: Regular Papers*, vol. 67, no. 4, pp. 1082–1091, 2020.

[17] I. N. Papadopoulos, S. Farahi, C. Moser, and D. Psaltis, "High-resolution, lensless endoscope based on digital scanning through a multimode optical fiber," *Biomedical Optics Express*, vol. 4, no. 2, pp. 260–270, 2013.

[18] L. V. Doronina-Amitonova, I. V. Fedotov, O. I. Ivashkina, M. A. Zots, A. B. Fedotov, K. V. Anokhin, and A. M. Zheltikov, "Implantable fiber-optic interface for parallel multisite longterm optical dynamic brain interrogation in freely moving mice," *Scientific Reports*, vol. 3, no. 1, 3265, 2013.

[19] X. Cui, M. Lee, X. Heng, W. Zhong, P. W. Sternberg, D. Psaltis, and C. Yang, "Lensless high-resolution on-chip optofluidic microscopes for Caenorhabditis elegans and cell imaging," *Proceedings of the National Academy of Sciences*, vol. 105, no. 31, pp. 10670-10675, 2008.

[20] S. Lindström, and H. Andersson-Svahn, "Miniaturization of biological assays — Overview on microwell devices for single-cell analyses," *Biochimica et Biophysica Acta (BBA) - General Subjects*, vol. 1810, no. 3, pp. 308–316, 2011.

[21] S. V. Kesavan, F. Momey, O. Cioni, B. David-Watine, N. Dubrulle, S. Shorte, E. Sulpice, D. Freida, B. Chalmond, J. M. Dinten, "High-throughput monitoring of major cell functions by means of lensfree video microscopy," *Scientific Reports*, vol. 4, no. 1, 5942, 2014.

[22] K. Sasagawa, M. Haruta, Y. Ohta, H. Takehara, and J. Ohta, "Miniaturized CMOS imaging device for implantable applications," in *2020 International Symposium on VLSI Design, Automation and Test (VLSI-DAT)*, p. 1, 2020.

[23] A. Ozcan, and E. McLeod, "Lensless Imaging and Sensing," *Annual Review of Biomedical Engineering*, vol. 18, no. 1, pp. 77–102, 2016.

[24] V. Boominathan, J. K. Adams, J. T. Robinson, and A. Veeraraghavan, "PhlatCam: Designed Phase-Mask Based Thin Lensless Camera," *IEEE Transactions on Pattern Analysis and Machine Intelligence*, vol. 42, no. 7, pp. 1618–1629, 2020.

[25] A. Ozcan, "Mobile phones democratize and cultivate next-generation imaging, diagnostics and measurement tools," *Lab on a Chip*, vol. 14, no. 17, pp. 3187–3194, 2014.

[26] D. Lange, C. W. Storment, C. A. Conley, and G. T. A. Kovacs, "A microfluidic shadow imaging system for the study of the nematode Caenorhabditis elegans in space," *Sensors and Actuators B: Chemical*, vol. 107, no. 2, pp. 904–914, 2005.

[27] S. Seo, T. W. Su, D. K. Tseng, A. Erlinger, and A. Ozcan, "Lensfree holographic imaging for on-chip cytometry and diagnostics," *Lab on a Chip*, vol. 9, no. 6, pp. 777–787, 2009.

[28] Z. Göröcs, and A. Ozcan, "On-Chip Biomedical Imaging," *IEEE Reviews in Biomedical Engineering*, vol. 6, pp. 29–46, 2013.

[29] A. F. Coskun, T. W. Su, and A. Ozcan, “Wide field-of-view lens-free fluorescent imaging on a chip,” *Lab Chip*, vol. 10, no. 7, pp. 824–827, 2010.

[30] K. Sasagawa, Y. Ohta, M. Kawahara, M. Haruta, T. Tokuda, and J. Ohta, “Wide field-of-view lensless fluorescence imaging device with hybrid bandpass emission filter,” *AIP Advances*, vol. 9, no. 3, p. 035108, 2019.

[31] S. Pang, C. Han, J. Erath, A. Rodriguez, and C. Yang, “Wide field-of-view Talbot grid-based microscopy for multicolor fluorescence imaging,” *Optics Express*, vol. 21, no. 12, pp. 14555-14565, 2013.

[32] C. Han, S. Pang, D. V Bower, P. Yiu, and C. Yang, “Wide field-of-view on-chip Talbot fluorescence microscopy for longitudinal cell culture monitoring from within the incubator,” *Analytical Chemistry*, vol. 85, no. 4, pp. 2356–2360, 2013.

[33] S. Pang, C. Han, M. Kato, P. W. Sternberg, and C. Yang, “Wide and scalable field-of-view Talbot-grid-based fluorescence microscopy,” *Optics Letters*, vol. 37, no. 23, pp. 5018–5020, 2012.

[34] A. F. Coskun, I. Sencan, T. W. Su, and A. Ozcan, “Lensless wide-field fluorescent imaging on a chip using compressive decoding of sparse objects,” *Optics Express*, vol. 18, no. 10, pp. 10510-10523, 2010.

[35] A. Velten, T. Willwacher, O. Gupta, A. Veeraraghavan, M. G. Bawendi, and R. Raskar, “Recovering three-dimensional shape around a corner using ultrafast time-of-flight imaging,” *Nature Communications*, vol. 3, no. 1, 745, 2012.

[36] R. Horaud, M. Hansard, G. Evangelidis, and C. Ménier, “An overview of depth cameras and range scanners based on time-of-flight technologies,” *Machine Vision and Applications*, vol. 27, no. 7, pp. 1005–1020, 2016.

[37] U. A. Gurkan, S. Moon, H. Geckil, F. Xu, S. Wang, T. J. Lu, and U. Demirci, “Miniaturized lensless imaging systems for cell and microorganism visualization in point-of-care testing,” *Biotechnology Journal*, vol. 6, no. 2. pp. 138–149, 2011.

[38] H. H. Jaffe, and A. L. Miller, “The fates of electronic excitation energy,” *Journal of chemical education*, vol. 43, no. 9, pp. 469–473, 1966.

[39] T. Suzuki, T. Matsuzaki, H. Hagiwara, T. Aoki, and K. Takata, “Recent advances in fluorescent labeling techniques for fluorescence microscopy,” *Acta Histochemica et Cytochemica*, vol. 40, no. 5. pp. 131–139, 2007.

[40] Y. Wu, and J. Y. Qu, “Autofluorescence spectroscopy of epithelial tissues,” *Journal of Biomedical Optics*, vol. 11, no. 5, 054023, 2006.

[41] M. Monici, “Cell and tissue autofluorescence research and diagnostic applications,” *Biotechnology Annual Review*, vol. 11, pp. 227–256, 2005.

[42] D. Gorpas, J. Phipps, J. Bec, D. Ma, S. Dochow, D. Yankelevich, J. Sorger, J. Popp, A. Bewley, R. Gandour-Edwards, L. Marcu, and D. G. Farwell, “Autofluorescence lifetime augmented reality as a means for real-time robotic surgery guidance in human patients,” *Scientific Reports*, vol. 9, no. 1, 1187, 2019.

[43] N. M. Cordina, N. Sayyadi, L. M. Parker, A. Everest-Dass, L. J. Brown, and N. H. Packer, "Reduced background autofluorescence for cell imaging using nanodiamonds and lanthanide chelates," *Scientific Reports*, vol. 8, no. 1, 4521, 2018.

[44] Y. Inoue, K. Izawa, S. Kiryu, A. Tojo, and K. Ohtomo, "Diet and abdominal autofluorescence detected by in vivo fluorescence imaging of living mice," *Molecular Imaging*, vol. 7, no. 1, pp. 21–27, 2008.

[45] V. Sadashivaiah, M. Tippani, S. C. Page, S. H. Kwon, S. V. Bach, R. A. Bharadwaj, T. M. Hyde, J. E. Kleinman, A. E. Jaffe, and K. R. Maynard, "SUFI: an automated approach to 82 spectral unmixing of fluorescent multiplex images captured in mouse and post-mortem human brain tissues," *BMC Neuroscience*, vol. 24, no. 1, 6, 2023.

[46] M. Neumann, and D. Gabel, "Simple Method for Reduction of Autofluorescence in Fluorescence Microscopy," *Journal of Histochemistry and Cytochemistry*, vol. 50, no. 3, pp. 437-439, 2002.

[47] N. Billinton, and A. W. Knight, "Seeing the Wood through the Trees: A Review of Techniques for Distinguishing Green Fluorescent Protein from Endogenous Autofluorescence," *Analytical Biochemistry*, vol. 291, no. 2, pp. 175–197, 2001.

[48] S. A. Schnell, W. A. Staines, and M. W. Wessendorf, "Reduction of Lipofuscin-like Autofluorescence in Fluorescently Labeled Tissue," *Analytical Biochemistry*, vol. 47, no. 6, pp. 719-730, 1999.

[49] B. Clancy, and L. J. Cauller, "Reduction of background autofluorescence in brain sections following immersion in sodium borohydride," *Journal of Neuroscience Methods*, vol. 83, no. 2, pp. 97–102, 1998.

[50] V. C. Oliveira, R. C. V Carrara, D. L. C. Simões, F. P. Saggioro, C. G. Carlotti, D. T. Covas Jr, and L. Neder, "Sudan Black B treatment reduces autofluorescence and improves resolution of in situ hybridization specific fluorescent signals of brain sections," *Histology Histopathology*, vol. 25, no. 8, pp. 1017-1024, 2010.

[51] U. Alexiev, P. Volz, A. Boreham, and R. Brodwolf, "Time-resolved fluorescence microscopy (FLIM) as an analytical tool in skin nanomedicine," *European Journal of Pharmaceutics and Biopharmaceutics*, vol. 116, pp. 111–124, 2017.

[52] R. Zhang, R. Chouket, M. A. Plamont, Z. Kelemen, A. Espagne, A. G. Tebo, A. Gautier, L. Gissot, J. D. Faure, L. Jullien, and V. Croquette, "Macroscale fluorescence imaging against autofluorescence under ambient light," *Light: Science Applications*, vol. 7, no. 1, 97, 2018.

[53] W. R. Zipfel, R. M. Williams, and W. W. Webb, "Nonlinear magic: multiphoton microscopy in the biosciences," *Nature Biotechnology*, vol. 21, no. 11, pp. 1369–1377, 2003.

[54] K. König, "Multiphoton microscopy in life sciences," *Journal of Microscopy*, vol. 200, no. 2, pp. 83–104, 2000.

[55] A. Greenbaum, N. Akbari, A. Feizi, W. Luo, and A. Ozcan, "Field-Portable Pixel Super-Resolution Colour Microscope," *PLoS One*, vol. 8, no. 9, e76475, 2013.

[56] D. Tseng, O. Mudanyali, C. Oztoprak, S. O. Isikman, I. Sencan, O. Yaglidere, and A. Ozcan, "Lens-free microscopy on a cellphone," *Lab on a Chip*, vol. 10, no. 14, pp. 1787–1792, 2010.

[57] S. O. Isikman, W. Bishara, S. Mavandadi, F. W. Yu, S. Feng, R. Lau, and A. Ozcan, "Lens-free optical tomographic microscope with a large imaging volume on a chip," *Proceedings of the National Academy of Sciences*, vol. 108, no. 18, pp. 7296–7301, 2011.

[58] M. I. Azmer, K. Sasagawa, E. Rustami, K. Sugie, Y. Ohta, M. Haruta, H. Takehara, H. Tashiro, and J. Ohta, "Miniaturized LED light source with an excitation filter for fluorescent imaging," *Japanese Journal of Applied Physics*, vol. 60, no. SB, SBBG07, 2021.

[59] W. Bishara, H. Zhu, and A. Ozcan, "Holographic opto-fluidic microscopy," *Optics Express*, vol. 18, no. 26, pp. 27499–27510, 2010.

[60] V. Boominathan, J. T. Robinson, L. Waller, and A. Veeraraghavan, "Recent advances in lensless imaging," *Optica*, vol. 9, no. 1, pp. 1-16, 2022.

[61] J. K. Adams, D. Yan, J. Wu, V. Boominathan, S. Gao, A. V Rodriguez, S. Kim, J. Carns, R. Richards-Kortu, C. Kemere, A. Veeraraghavan, and J. T. Robinson, "In vivo lensless microscopy via a phase mask generating diffraction patterns with high-contrast contours," *Nature Biomedical Engineering*., vol. 6, no. 5, pp. 617–628, 2022.

[62] W. S. Hee, K. Sasagawa, A. Kameyama, A. Kimura, M. Haruta, T. Tokuda, and J. Ohta, "Lens-free Dual-color Fluorescent CMOS Image Sensor for Forster Resonance Energy Transfer Imaging," *Sensors and Materials*, vol. 31, no. 8, pp. 2579-2594, 2019.

[63] K. Sasagawa, E. Rustami, Y. Ohta, M. Haruta, H. Takehara, H. Tashiro, and J. Ohta, "Image sensor with hybrid emission filter for in vivo fluorescent imaging," *Electronics and Communications in Japan*, vol. 141, no. 3, pp. 71-76, 2021.

[64] Y. Wu, and A. Ozcan, “Lensless digital holographic microscopy and its applications in biomedicine and environmental monitoring,” *Methods*, vol. 136, pp. 4–16, 2018.

[65] E. Rustami, Erus, K. Sasagawa, K. Sugie, Y. Ohta, H. Takehara, M. Haruta, H. Tashiro, and J. Ohta, “Thin and Scalable Hybrid Emission Filter via Plasma Etching for Low-Invasive Fluorescence Detection,” *Sensors*, vol. 23, no. 7, 3695, 2023.

[66] Y. Rivenson, Z. Göröcs, H. Günaydin, Y. Zhang, H. Wang, and A. Ozcan, “Deep learning microscopy,” *Optica*, vol. 4, no. 11, pp. 1437–1443, 2017.

[67] M. T. McCann, K. H. Jin, and M. Unser, “Convolutional Neural Networks for Inverse Problems in Imaging: A Review,” *IEEE Signal Process Mag*, vol. 34, no. 6, pp. 85–95, 2017.

[68] Y. Bian, T. Xing, K. Jiao, Q. Kong, J. Wang, X. Yang, S. Yang, Y. Jiang, R. Shen, H. Shen, and C. Kuang, “Computational Portable Microscopes for Point-of-Care-Test and TeleDiagnosis,” *Cells*, vol. 11, no. 22, 3670, 2022.

[69] A. Greenbaum, W. Luo, T. W. Su, Z. Göröcs, L. Xue, S. O. Isikman, A. F. Coskun, O. Mudanyali, and A. Ozcan, “Imaging without lenses: Achievements and remaining challenges of wide-field on-chip microscopy,” *Nature Methods*, vol. 9, no. 9, pp. 889–895, 2012.

[70] J. Ohta, Smart CMOS image sensors and applications. 2017.

[71] A. El Gamal, and H. Eltoukhy, “CMOS image sensors,” *IEEE Circuits and Devices Magazine*, vol. 21, no. 3, pp. 6–20, 2005.

[72] B. E. Bayer, and N. Y. Rochester, “A sensing array for color imaging includes individual,” 1976

[73] Y. Dattner, and O. Yadid-Pecht, “Low light cmos contact imager with an integrated polyacrylic emission filter for fluorescence detection,” *Sensors*, vol. 10, no. 5, pp. 5014–5027, 2010.

[74] B. Ramjiawan, M. Jackson, and H. Mantsch, “Fluorescence Imaging,” *Encyclopedia of Analytical Chemistry*, 2000.

[75] L. Wei, W. Yan, and D. Ho, “Recent advances in fluorescence lifetime analytical microsystems: Contact optics and CMOS time-resolved electronics,” *Sensors (Switzerland)*, vol. 17, no. 12. 2800, 2017.

[76] T. Treepetchkul, N. Kulmala, K. Sasagawa, H. Takehara, M. Haruta, H. Tashiro, and J. Ohta., “Dual-color lensless fluorescence imaging by using a notch interference filter and absorption filters,” in *Biophotonics Congress 2021, Optica Publishing Group*, 2021, DM3A.6.

[77] K. Chen, D. Chen, H. Guan, F. Chen, and X. Chen, “Label-free cell imaging based on multi-wavelength lensless digital holography,” in *Label-free Biomedical Imaging and Sensing (LBIS) 2023*, SPIE, 2023, 123910T

[78] Y. Chen, Z. Zhou, S. Zhu, Z. Ni, and N. Xiang, “Label-free microfluidics for single-cell analysis,” *Microchemical Journal*, vol. 177, 107284, 2022.

[79] T. W. Su, S. Seo, A. Erlinger, and A. Ozcan, “High-throughput lensfree imaging and characterization of a heterogeneous cell solution on a chip,” *Biotechnol Bioeng*, vol. 102, no. 3, pp. 856–868, 2009.

[80] A. Greenbaum, Y. Zhang, A. Feizi, P. L. Chung, W. Luo, S. R. Kandukuri, and A. Ozcan, “Wide-field computational imaging of pathology slides using lens-free on-chip microscopy,” *Science Translational Medicine*, vol. 6, no. 267, p. 267ra175 2014.

[81] Y. Huang, S. Jiang, R. Wang, P. Song, J. Zhang, G. Zheng, X. Ji, and Y. Zhang, “Ptychography-based high-throughput lensless on-chip microscopy via incremental proximal algorithms,” *Optics Express*, vol. 29, no. 23, pp. 37892–37906, 2021.

[82] O. Mudanyali, A. Erlinger, S. Seo, T. W. Su, D. Tseng, and A. Ozcan, “Lensless On-chip Imaging of Cells Provides a New Tool for High-throughput Cell-Biology and Medical Diagnostics,” *Journal of Visualized Experiments*, no. 34, e1650, 2009.

[83] O. Mudanyali, D. Tseng, C. Oh, S. O. Isikman, I. Sencan, W. Bishara, C. Oztoprak, S. Seo, B. Khademhosseini, and A. Ozcan, “Compact, light-weight and cost-effective microscope based on lensless incoherent holography for telemedicine applications,” *Lab on a Chip*, vol. 10, no. 11, pp. 1417–1428, 2010.

[84] S. Jiang, C. Guo, Z. Bian, R. Wang, J. Zhu, P. Song, P. Hu, D. Hu, Z. Zhang, K. Hoshino, “Ptychographic sensor for large-scale lensless microbial monitoring with high spatiotemporal resolution,” *Biosensors and Bioelectronics*, vol. 196, 113699, 2022.

[85] B. Behera, G. K. Anil Vishnu, S. Chatterjee, V. S. N. Sitaramgupta V, N. Sreekumar, A. Nagabhushan, N. Rajendran, B. H. Prathik, and H. J. Pandya, “Emerging technologies for antibiotic susceptibility testing,” *Biosensors and Bioelectronics*, vol. 142, 111552, 2019.

[86] J. Clausell-Tormos, D. Lieber, J.-C. Baret, A. El-Harrak, O. J. Miller, L. Frenz, J. Blouwolff, K. J. Humphry, S. Köster, H. Duan, and C. Holtze, "Droplet-Based Microfluidic Platforms 92 for the Encapsulation and Screening of Mammalian Cells and Multicellular Organisms," *Chemistry & Biology*, vol. 15, no. 5, pp. 427–437, 2008.

[87] A. M. Maiden and J. M. Rodenburg, "An improved ptychographical phase retrieval algorithm for diffractive imaging," *Ultramicroscopy*, vol. 109, no. 10, pp. 1256–1262, 2009

[88] J. Kun, M. Smieja, B. Xiong, L. Soleymani, and Q. Fang, "The Use of Motion Analysis as Particle Biomarkers in Lensless Optofluidic Projection Imaging for Point of Care Urine Analysis," *Scientific Reports*, vol. 9, no. 1, 17255, 2019.

[89] Y.-C. Chang, X. Ge, L.-J. Wang, S. S. Lee, M. H. Paulsen, Q. M. Khan, Z. M. Khalid, J. A. Bhalli, U. Waheed, C. D. Simpson, and D. Du "An ultra low-cost smartphone device for insitu monitoring of acute organophosphorus poisoning for agricultural workers," *Sensors Actuators B: Chemical*, vol. 275, pp. 300–305, 2018.

[90] M. J. Lopera, and C. Trujillo, "Portable cellphone-based digital lensless holographic microscope," in *Laser Science*, 2021, JTh5A.14.

[91] J. Adams, V. Boominathan, S. Gao, A. Rodriguez, D. Yan, C. Kemere, A. Veeraraghavan, and J. Robinson, "In vivo fluorescence imaging with a flat, lensless microscope," in *Biorxiv*, 2020. doi: https://doi.org/10.1101/2020.06.04.135236

[92] L. Akbar, V. C. G. Castillo, J.P. Olorocisimo, Y. Ohta, M. Kawahara, H. Takehara, M. Haruta, H. Tashiro, K. Sasagawa, M. Ohsawa, and Y. M. Akay, "Multi-Region Microdialysis Imaging Platform Revealed Dorsal Raphe Nucleus Calcium Signaling and

Serotonin Dynamics during Nociceptive Pain," *International Journal of Molecular Science*, vol. 24, no. 7, 6654, 2023.

[93] R. Rebusi, J. P. Olorocisimo, J. Briones, Y. Ohta, M. Haruta, H. Takehara, H. Tashiro, K. Sasagawa, and J. Ohta, "Simultaneous CMOS-Based Imaging of Calcium Signaling of the 93 Central Amygdala and the Dorsal Raphe Nucleus During Nociception in Freely Moving Mice," *Frontiers in Neuroscience*, vol. 15, 667708, 2021.

[94] Y. Sunaga, Y. Ohta, Y. M. Akay, J. Ohta, and M. Akay, "Monitoring Neural Activities in the VTA in Response to Nicotine Intake Using a Novel Implantable Microimaging Device," *IEEE Access*, vol. 8, pp. 68013–68020, 2020.

[95] N. Antipa, G. Kuo, R. Heckel, B. Mildenhall, E. Bostan, R. Ng, and L. Waller, "DiffuserCam: lensless single-exposure 3D imaging," *Optica*, vol. 5, no. 1, pp. 1-9, 2018.

[96] J. K. Adams, V. Boominathan, B. W. Avants, D. G. Vercosa, F. Ye, R. G. Baraniuk, J. T. Robinson, and A. Veeraraghavan, "Single-frame 3D fluorescence microscopy with ultraminiature lensless FlatScope," *Science Advances*, vol. 3, no. 12, pp. 1–9, 2017.

[97] G. Kuo, F. Linda Liu, I. Grossrubatscher, R. Ng, and L. Waller, "On-chip fluorescence microscopy with a random microlens diffuser," *Optics Express*, vol. 28, no. 6, pp. 8384-8399, 2020.

[98] K. Yanny, N. Antipa, W. Liberti, S. Dehaeck, K. Monakhova, F. L. Liu, K. Shen, R. Ng, and L. Waller, "Miniscope3D: optimized single-shot miniature 3D fluorescence microscopy," *Light Science & Applications*, vol. 9, no. 1, 171, 2020.

[99] K. Tanaka, Y. J. Choi, Y. Moriwaki, T. Hizawa, T. Iwata, F. Dasai, Y. Kimura, K. Takahashi, and K. Sawada, "Improvements of low-detection-limit filter-free fluorescence sensor developed by charge accumulation operation," *Japanese Journal of Applied Physics*, vol. 56, no. 4S, 04CM09, 2017.

[100] K. Sugie, K. Sasagawa, M. C. Guinto, M. Haruta, T. Tokuda, and J. Ohta, "Implantable CMOS image sensor with incident-angle-selective pixels," *Electronics Letters*, vol. 55, no. 13, pp. 729–731, 2019.

[101] V. Boominathan, J. K. Adams, J. T. Robinson, and A. Veeraraghavan, "PhlatCam: Designed Phase-Mask Based Thin Lensless Camera," *IEEE Trans Pattern Anal Mach Intell*, vol. 42, no. 7, pp. 1618–1629, 2020.

[102] F. L. Liu, G. Kuo, N. Antipa, K. Yanny, and L. Waller, "Fourier DiffuserScope: single-shot 3D Fourier light field microscopy with a diffuser," *Optics Express*, vol. 28, no. 20, pp. 28969–28986, 2020.

[103] J. L. Collins, B. van Knippenberg, K. Ding, and A. V. Kofman, "Time-Lapse Microscopy," in *Cell Culture*, 2018. doi: 10.5772/intechopen.81199

[104] D. C. Worth, and M. Parsons, "Live Cell Imaging Analysis of Receptor Function," in *Live Cell Imaging: Methods and Protocols*, pp. 311–323, 2010.

[105] J. L. Roti, "Cellular responses to hyperthermia (40-46°C): Cell killing and molecular events," in *International Journal of Hyperthermia*, vol. 24, no. 1, pp. 3-15, 2008.

[106] J. Wang, Y. Wei, S. Zhao, Y. Zhou, W. He, Y. Zhang, and W. Deng, “The analysis of viability for mammalian cells treated at different temperatures and its application in cell shipment,” *PLoS One*, vol. 12, no. 4, e0176120, 2017.

[107] L. Hunt, D. L. Hacker, F. Grosjean, M. De Jesus, L. Uebersax, M. Jordan, and F. M. Wurm, “Low-temperature pausing of cultivated mammalian cells,” *Biotechnol Bioeng*, vol. 89, no. 2, pp. 157–163, 2005.

[108] I. R. Brown, “Induction of heat shock (stress) genes in the mammalian brain by hyperthermia and other traumatic events: A current perspective,” *Journal of neuroscience research*, vol. 27, no. 3, pp. 247–255, 1990.

[109] T. Tahara, Y. Kozawa, A. Ishii, K. Wakunami, Y. Ichihashi, and R. Oi, “Two-step phaseshifting interferometry for self-interference digital holography,” *Optics Letters*, vol. 46, no. 3, pp. 669–672, 2021.

[110] Y. Huang, D. Xie, C. Yan, and C. Wu, “Effect of Fiber Optic Plate on Centroid Locating Accuracy of Monocentric Imager,” *Applied Sciences*, vol. 11, no. 5, 1993, 2021.

[111] H. Photonics, “Application Data 62 Division of Ser,” 1996.

Appendix A: Fiber Optic Plate

A fiber optic plate (FOP) is an optical component consisting of a bundle of optical fibers with several micrometers in diameter. These fibers are aligned parallel to each other and tightly packed within a transparent substrate. The FOP acts as a light distributor, transmitting incident light from one end of the plate to the other through multiple internal reflections and total internal reflection principles. Every single fiber comprises a core glass that conveys light, a clad glass that covers the core glass, and an Extra Mural Absorption (E.M.A) layer that prevents light leakage from the core, as shown in Figure 50. When light enters at a specific angle, it can pass through the fiber and exit without reflection. The E.M.A. layer confines the absorbed light, ensuring clear images without crosstalk [110], [111]. This arrangement allows for efficient light transmission while preserving the spatial distribution and coherence of the original light source.

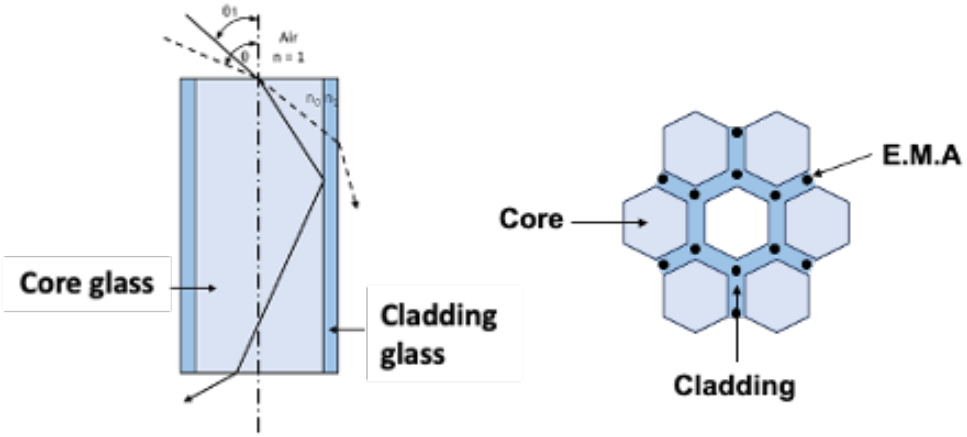

Figure 50 Concept of the light paths inside fiber optic plate.

The FOP provides advantages, including high spatial resolution, low image distortion, and high transfer efficiency. In addition, unlike an optical lens, it is unnecessary to consider the focal length between the image sensor and target sample, enabling the compactness of optical design, which is compatible with the lensless imaging system.

Appendix B: Procedures for removing the glass lid from the image sensor's package

A commercially available image sensor was utilized in this study. An image sensor is typically integrated with a lens, and the package is sealed with a glass lid. However, the glass lid was removed for lensless imaging purposes. The glass lid is glued, and peeling it off with a knife is difficult because it often leads to breakage. In a previous study, a burner was employed, but this approach sometimes resulted in damage to the solder and contamination of the sensor surface due to heating. In this study, the glass lid was successfully peeled off by irradiating a 266 nm of ultraviolet laser pulse to the interface between the adhesive and the glass. Furthermore, the remaining adhesive around the glass edge was carefully removed by cutting the peripheral edge of the glass lid with a utility knife. Consequently, the surface of the image sensor was easily peeled off with minimal damage or contamination to the pixel array.

Appendix C: Source code for imaging software control in time-lapse imaging system

- **Script for Arduino**

```
int camera = 8;
int led_red1 = 13;
int led_red2 = 12;
int led_red3 = 11;
int led_red4 = 10;

void setup() {
// put your setup code here, to run once:
        Serial.begin(9600);
        pinMode(led_red1, OUTPUT);
        pinMode(led_red2, OUTPUT);
        pinMode(led_red3, OUTPUT);
        pinMode(led_red4, OUTPUT);
        pinMode(camera, OUTPUT);
        digitalWrite(camera, HIGH); //camera is enable

}

void loop() {

// put your main code here, to run repeatedly:

if (Serial.available())

{

        int data = Serial.read();

        if (data == '1') //Camera

{

        digitalWrite(camera, HIGH);

        Serial.print("The camera is ON!\n");

}

        if (data == '2') //RED

{

        digitalWrite(led_red1, HIGH);
```

```
        digitalWrite(led_red2, HIGH);
         digitalWrite(led_red3, HIGH);
        digitalWrite(led_red4, HIGH);
        digitalWrite(camera, HIGH);
        Serial.print("The red LED is ON!\n");
}
        if (data == '0') //off
{
        digitalWrite(led_red1, LOW);
        digitalWrite(led_red2, LOW);
        digitalWrite(led_red3, LOW);
        digitalWrite(led_red4, LOW);
        digitalWrite(camera, LOW); //camera is disable
        Serial.print("The LEDs are OFF!\n");
        Serial.print("The cemera is OFF!\n");
}
}
}
```

- **Script for AutoIt**

```
#include <Date.au3> ;For date and time
#include <CommMG.au3> ;Serial communication with Arduino

#include <ButtonConstants.au3>
#include <GUIConstantsEx.au3>
#include <WindowsConstants.au3>

Global $CMPort = 4 ;Arduino COM port
Global $CmBoBaud = 9600
Global $sportSetError = ''
Global $CmboDataBits = 8
Global $CmBoParity = "none"
Global $CmBoStop = 1
Global $setflow = 2
Global $var = 1
```

```
_CommSetPort($CMPort, $sportSetError, $CmBoBaud, $CmboDataBits, $CmBoParity,
$CmBoStop, $setflow)

If @error Then
   MsgBox(16, "Error!", "Can't connect to Arduino on port - " & $CMPort)
   Exit
EndIf

_CommSetRTS(0)
_CommSetDTR(0)

        camera_ON()
        Sleep(5000)
        stviewer()
        camera_START()

        LED_RED()
        file_SAVE()
        ALL_OFF()

While 1
        camera_ON()
        open()
        camera_search()
        camera_START()

        LED_RED()
        file_SAVE()
        ALL_OFF()
WEnd

Func camera_ON()
   _CommSendString("1") ;Sends the Arduino a string of "1" to turn on yellow LED
   Local $ret = _CommGetLine(@CR, 100, 100) ; Waits for up to 100 for a carriage return
response from Arduino.
   ConsoleWrite($ret & @CRLF) ;Print to Console.
EndFunc

Func stviewer() ;Open StViewer
        $stviewer = "C:\Program
Files\OMRON_SENTECH\SentechSDK\v1_1\Application\StViewer_VC141_x64.exe"
                Run($stviewer)
                Sleep(3000)
                Send("{DOWN}")
                Sleep(500)
```

```
                Send("{DOWN}")
                Sleep(500)
                Send("{ENTER}")
                Sleep(3000)
EndFunc

Func camera_START()
$color_1 = PixelGetColor(89, 58) ;Define where the start button is
        $coord_1 = PixelSearch(89, 58, 89, 58, $color_1) ;Search for the start button
                If @error Then
                        ToolTip("Not found")
                        Sleep(2000)
                                ElseIf Not @error Then
                                        MouseClick("left", $coord_1[0], $coord_1[1], 1, 0)
                                        ToolTip("Start")
                        Sleep(2000)
                EndIf
EndFunc

Func LED_RED()
   _CommSendString("2") ;Sends the Arduino a string of "1" to turn on red LED
   Local $ret = _CommGetLine(@CR, 100, 100) ; Waits for up to 100 for a carriage return
response from Arduino.
   ConsoleWrite($ret & @CRLF) ;Print to Console.
EndFunc

Func LED_GREEN()
   _CommSendString("3") ;Sends Arduino string of "2" to turn on the green LED
   Local $ret = _CommGetLine(@CR, 100, 100) ; Waits for up to 100 for a carriage return
response from Arduino.
   ConsoleWrite($ret & @CRLF) ;Print to Console.
EndFunc

Func file_SAVE()
        $color_2 = PixelGetColor(139, 58) ;Define where the save button is
        $coord_2 = PixelSearch(139, 58, 139, 58, $color_2) ;Search for the save button
                If @error Then
                        ToolTip("Error")
                        Sleep(3000)
                ElseIf Not @error Then
                                $i = 1
                                MouseClick("left", $coord_2[0], $coord_2[1], 1, 0)
                                ToolTip("Save")

                                Local $sFolderPath = "D:\"& @YEAR & @MON & @MDAY
&"\" ;Check if the folder path exists
```

```
                                If FileExists($sFolderPath) = 0 Then
DirCreate($sFolderPath) ;Create full folder path
                                Local $iFileName = @YEAR & @MON & @MDAY & "_" &
"Image" & $var & "_" & @HOUR & "h" & @MIN & "m" & @SEC & "s" ;Create file name
                                Local $sFileName = $sFolderPath & $iFileName ;Create full
folder path and file name

                                WinWaitActive("Save Still Image File")
                                ControlFocus("Save Still Image File", "", "Edit1")
                                ControlSend("Save Still Image File", "", "Edit1", $sFileName)
                                Send("{ENTER}")
                                Sleep(1000)
                                $var += 1
                EndIf
EndFunc

Func ALL_OFF()
        _CommSendString("0") ;Sends Arduino string of "0" to turn off camera, yellow, and blue
LEDs
   Local $ret = _CommGetLine(@CR, 100, 100) ; Waits for up to 100 for a carriage return
response from Arduino.
   ConsoleWrite($ret & @CRLF) ;Print to Console.
        Sleep(3000)
        Send("{ENTER}")
        Sleep(240000)
EndFunc
Func open()
        Send("^o")
        Sleep(10000)
EndFunc

Func camera_search() ;Keystrokes control
        $color_3= PixelGetColor(314, 245) ;Define where the camera icon is
        $coord_3 = PixelSearch(314, 245,314, 245, $color_3) ;Search for the camera button
                MouseClick("left", $coord_3[0], $coord_3[1], 1, 0)
                Sleep(500)
                Send("{ENTER}")
                Sleep(3000)
EndFunc
```

Appendix D: Supplementary material

Movie 1: Movie time-lapse bright-field imaging in culture cells (HeLa) captured by the proposed lensless imaging device.

URL: https://www.dropbox.com/s/4hhxlzjpi1y0g1x/Timelapseimaging.gif?dl=0

List of Publication

• Journals:

[1] **N. Kulmala**, K. Sasagawa, T. Treepetchkul, H. Takehara, M. Haruta, H. Tashiro, and J. Ohta., “Lensless dual-color fluorescence imaging device using hybrid filter,” *Japanese Journal of Applied Physics*, vol. 61, no. SC, SC1020, 2022.

• International conferences:

[1] **Natcha Kulmala**, Thanaree Treepetchkul, Kiyotaka Sasagawa, Hironari Takehara, Makito Haruta, Hiroyuki Tashiro, Jun Ohta "A hybrid filter for lens-free dual-color fluorescence imaging," at *2021 International Conference on Solid State Devices and Materials (SSDM2021)* – Sep. 2021

[2] **Natcha Kulmala**, Thanaree Treepetchkul, Kiyotaka Sasagawa, Hironari Takehara, Makito Haruta, Hiroyuki Tashiro, Jun Ohta "Development of implantable lens-free CMOS image sensor for bioluminescence resonance energy transfer (BRET) observation," at *the 12th AMF-AMEC International Conference 2021* – Jul. 2021

[3] **Natcha Kulmala** and Jun Ohta, "CMOS image sensor for FRET imaging using hybrid emission filter," at *the 3rd International Workshop by the 174th Committee on Coexistence of Biology and Nanodevices* 2019 – Jun. 2019

[4] Thanaree Treepetchkul, **Natcha Kulmala**, Kiyotaka Sasagawa, Hironari Takehara, Makito Haruta, Hiroyuki Tashiro, and Jun Ohta, “Dual-color lensless fluorescence imaging by using a notch interference filter and absorption filters,” at *OSA Biophotonics Congress: Optics in the Life Sciences 2021* – Apr. 2021

[5] Thanaree Treepetchkul, **Natcha Kulmala**, Kiyotaka Sasagawa, Hironari Takehara, Makito Haruta, Hiroyuki Tashiro, Jun Ohta "Development of two excitation light rejection using hybrid filter for dual-color fluorescence lensless imaging device," at *the 12th AMF-AMEC International Conference 2021* – Jul. 2021

- **Domestic conferences:**

[1] **Natcha Kulmala**, Wan Shen Hee, Kiyotaka Sasagawa, Makito Haruta, and Jun Ohta, "CMOS Image Sensor for FRET Imaging Using Hybrid Emission Filter", at *the 80th Japan Society of Applied Physics Autumn Meeting 2019 (JSAP Autumn 2019)*, Hokkaido University, Sapporo Campus, Hokkaido – Sep. 2019

[2] **Natcha Kulmala**, Kiyotaka Sasagawa, Hironari Takehara, Makito Haruta, and Jun Ohta, "Lens-free Imaging Device with Hybrid Emission Filter for Dual-color Fluorescent Imaging", at *the 67th Japan Society of Applied Physics Spring Meeting 2020 (JSAP Autumn 2020)*, Sophia University, Yotsuya Campus, Tokyo – Mar. 2020

[3] **Natcha Kulmala**, Thanaree Treephetchkul, Kiyotaka Sasagawa, Hironari Takehara, Makito Haruta, Hiroyuki Tashiro, and Jun Ohta, "Development of Hybrid Filters for Dual-color Fluorescence Imaging Using Lens-free Device", at *the 37th sensor symposium on sersors, micromachines, and applied systems 2020*, Online – Oct. 2020

[4] **Natcha Kulmala**, Thanaree Treepetchkul, Hironari Takehara, Makito Haruta, Hiroyuki Tashiro, Kiyotaka Sasagawa, and Jun Ohta, "Lensless dual-color fluorescent imaging device with hybrid filter for cell imaging", at *the 69th Japan Society of Applied Physics Spring Meeting 2022 (JSAP Autumn 2022)*, Aoyama Gakuin University, Sagamihara Campus, Kanagawa – Mar. 2022

[5] **Natcha Kulmala**, Thanaree Treephetchkul, Hironari Takehara, Makito Haruta, Hiroyuki Tashiro, Kiyotaka Sasagawa, Jun Ohta, "Lensless fluorescence imaging device for cells observation with hybrid emission filter" at *the 39th sensor symposium on sersors, micromachines, and applied systems 2022*, ASTY Tokushima, Tokushima – Nov. 2022

- **Awards & Grants:**

[1] Recipient of NAIST (Nara Institute of Science and Technology) International Scholar Program from October 2020 until September 2023.